NASA-TT-20293 19880019516

NASA TT-20293

NASA TT-20293

NASA TECHNICAL TRANSLATION NASA TT - 20293

CONTRIBUTIONS TO THE MODELING OF WIND SHEAR FOR DANGER STUDIES

Manfred Swolinsky

Translation of "Beitraege zur Modellierung von Scherwind fuer Gefaehrdungsuntersuchungen", Technische Universitaet Carolo-Wilhelmina zu Braunschweig, April 1986, pp 200, ETN-87-90442
(Thesis - Ph.D. Technische Univ., Brunswick, (W.Ger.))

OCT 1 2 1988

NATIONAL AERONAUTICS AND SPACE ADMINISTRATION
WASHINGTON, D. C. 20546 SEPTEMBER 1988

NASA National Aeronautics and Space Administration

Report Documentation Page

1. Report No.	2. Government Accession No.	3. Recipient's Catalog No.
TT-20293		

4. Title and Subtitle	5. Report Date
CONTRIBUTIONS TO THE MODELING OF WIND SHEAR FOR DANGER STUDIES	SEPTEMBER 1988
	6. Performing Organization Code
7. Author(s)	8. Performing Organization Report No.
Manfred Swolinsky	10. Work Unit No.
9. Performing Organization Name and Address	11. Contract or Grant No.
National Aeronautics and Space Administration Washington, DC 20546	NASW-4307
	13. Type of Report and Period Covered
12. Sponsoring Agency Name and Address	translation
	14. Sponsoring Agency Code

15. Supplementary Notes

Transl. from GERMAN to ENGLISH of "Beitraege zur Modellierung von Scherwind fuer Gefaehrdungsuntersuchungen", Technischen Universitaet Carolo-Wilhelmina zu Braunschweig, April 1986, pp 200, ETN-87-90442

Transl. by SCITRAN, Santa Barbara, CA 93150.

16. Abstract

In this work we will describe how to approximate typical weather phenomena and wind relationships such as storm downdrafts, weather fronts, boundary layer laminar flow and boundary layer windshear with simple engineering models wherein known solutions and flow formulas from flow mechanics will be adapted. Good correlation between model and measurement will be demonstrated with the help of data measured in flight and with the help of measurement data from other experimenters. On the basis of wind models developed here, we will examine the danger situation existent during landing under differing wind conditions. Thus results an estimation of the extent of danger via consideration of danger criteria which were obtained from energy concepts.

17. Key Words (Suggested by Author(s))	18. Distribution Statement
	unclassified-unlimited

19. Security Classif. (of this report)	20. Security Classif. (of this page)	21. No. of pages	22. Price
unclassified	unclassified	193	

NASA FORM 1626 OCT 86

N88-10463#
N-157,526

Forword:

The present work originated during my activities as a scientific professional at the Institute for Flight Mechanics and at the Institute for Flight Navigation at Braunschweig Technical University.

I thank Prof. Dr.-Ing. Gunther Schänzer who encouraged me in this theme and always helped with the work with great interest.

I thank Dr. rer. nat. Rainer Roth from the Institute for Meterorology and Climatology at the University of Hannover for his helpful hints and information regarding meteorological questions and for sharing selected data.

All workers at the above named institutions helped with the experiments. I wish to thank them, especially Dipl.-Ing. R. König, Dr.-Ing. P. Krauspe, Dr.-Ing. R Luckner, Dr.-Ing. A Redeker and Dr.-Ing P. Vörsmann for their discussions with me as well as acknowledge the support of Dipl.-Ing. K.U. Hahn and Dipl.-Ing. B. Kaufmann for their help during numerous simulation calculations. I also wish to thank Ing. (grad) H.P. Kempter and students working with him for their help in preparation and evaluation of the comprehensive collection of flight data.

For their willingness to help me I wish to heartily thank all those interested colleagues who participated.

Synopsis

Problems of flight technology, for example, design and trial of flight controllers, flight-dynamics experiments and not the least systematic research into safety-endangering windshear phenomena require utilization of suitable wind models. These models should on the one hand describe flow relationships in dangerous situations with sufficient accuracy, and on the other hand should be structured simply enough that they are realizable on a real-time basis without great expense. Up to this point only a few models existed which met these requirements.

In the work at hand we will describe how to approximate typical weather phenomena and wind relationships such as storm downdrafts, weather fronts, boundary layer laminar flow and boundry layer windshear with simple engineering models wherein known solutions and flow formulas from flow mechanics will be adapted. Good correlation between model and measurement will be demonstrated with the help of data measured in flight and with the help of measurement data from other experimenters.

On the basis of wind models developed here we will examine the danger situation existent during landing under differing wind conditions. Thus results an estimation of the extent of danger via consideration of danger criteria which were obtained from energy concepts.

Table of Contents

		Page
0.	Abbreviations/Symbols	
1.	Introduction	1
1.1	Introduction	1
1.2	The State of Technology	14
1.2.1	Wind Models	14
1.2.2	Danger Criteria	17
1.3	Goals	19
2.	Windshear in the Lower Region of the Planetary Boundary Layer	21
2.1	Windshear Characterisation	21
2.1.1	Boundary Layer Windshear	22
2.1.2	Boundary Layer Laminar Flow	24
2.1.3	Windshear in Thunderstorms	26
2.1.4	Flow Relationships in Fronts	28
2.2	Statistical Research on Windshear in Terminal Control Areas (TMA)	34
2.2.1	Wind Speed and Stability in the Atmosphere	35
2.2.2	Statistics of Vertical Windshear Gradients	37
3.	Simple Windshear Models	44
3.1	Ground Boundary Layer Profiles	44
3.1.1	Logarithmic Laws	44
3.1.2	The Exponential Law	47
3.1.3	Relationships Between Exponential Law and Logarithmic Law	52
3.1.4	Description of Altitude-dependent Wind Rotation	55

3.2 Ground Boundary Layer Profile Variation via Atmospheric or Orographic Nonhomogeneity 62

3.3 Boundary Layer Beam Flow 70

3.4 Models for Windshear and Downdrafts in Thunderstorms 85

3.5 Windshear in the Flowfield of Fronts 93

4. Research on Criteria for the Strength of Windshears and for Endangerment of Flight Traffic 98

4.1 The Vertical Windshear Gradient 98

4.2 Wind Shear Severity Factor 99

4.3 Danger Criteria from Energy Considerations 101

4.3.1 The Energy-Altitude Error 101

4.3.2 The Ideal Thrust Control Law 103

4.4 Comparison of Danger Criteria 110

4.4.1 Comparison between Energy-Level Error and Energy Adjustment via Thrust Control 110

4.4.2 Comparison between Energy Fitting and Data for Describing Windshear Strength 117

4.4.3 Danger Statistics from Measured Results 121

5. Estimation of Aircraft Danger from Windshear during Landing 128

5.1 Landing under Normal Boundary Layer Conditions 128

5.2 Danger to Landing Aircraft by Boundary Layer Beam Flow 130

5.3 Landing in a Thunderstorm Downdraft 142

5.4 Landing in a Flow Field in a Front 147

6. Conclusion and Views 150

7. Literature 156

8. Appendices 162

A1 Defining equations for the LOG-LIN law model parameters

A2 Wind speed curves for various models of ground boundary layers

A3 Comparison of measured results and model description for boundary layer laminar flow

A4 Relationship between speed and temperature profiles in Free Jets

A5 Model parameters for the described examples

A6 Measured results from secondary squall fronts

A7 Derivation and simplification of the ideal thrust control law

A8 Measurement concepts, data treatment and error balancing for wind determinations in straight flight

0. Symbols/Abbreviations

a	general constant
A	lift
A_{tau}	exchange coefficient for impulse
A_q	exchange coefficient for heat
b	general constant
B	free jet width
C	general constant
C_A	lift coefficient
$C_{A\alpha}$	derivative of lift coefficient $\partial C_A/\partial\alpha$
C_q	cross-wind force coefficient
C_{qB}	derivative of the cross-wind coefficient $\partial C_q/\partial B$
C_W	resistance coefficient
C_S	form factor for free jet
C_p	specific heat for constant pressure
e	general constant
E	energy
f	general constant
F	thrust vector sum
ΔF	thrust change
g	Earth's gravitational acceleration
G	weight
H	flight altitude $H = -z_G$
H_o	roughness level
$\hat{H}$	turbulent heat flow
H_s	altitude of free jet maximum
H_E	energy level

ΔH_E energy level change

H_G altitude of uninfluenced altitude flow

k von Karmann's constant

K_H turbulent diffusion coefficient for heat

L_R Ramp length

L_* characteristic length

m mass, exponent of the potential rule

n load factor

q heat flow density

Q cross-wind force, general function

s semispan

S wing area

t time

Δt time interval

T temperature

T_o ground temperature

$\overline{T}$ average temperature

ΔT temperature change

u flow velocity

u_w, u_{wg} x_g component of wind velocity $\underline{V}_x$

u_{wx}, u_{wy}, u_{wz}, u_{wH} gradients of horizontal wind components

u_* thrust shear stress velocity

u_{*0} thrust shear stress velocity at ground level

$\dot{u}_{wg}$ time change of component u_{wg}

v_{wg} y_g components of wind velocity $\underline{v}_w$

$\dot{v}_{wg}$ time change of component v_{wg}

$\underline{V}_K$ velocity of flight

$\underline{V}$ airspeed

$\underline{V}_w$ wind speed

V sum of airspeed ("speed")

V_K sum of velocity of flight

V_G geostrophic wind

V_{GS} groundspeed

W resistance

u_{Wg} z_g component of wind velocity $\underline{v}_g$

w_{wx}, w_{wy}, w_{wz}, w_{wH} gradients of vertical wind components

X_K force in x-direction

x_g flight path

$\ddot{y}_g$ transverse acceleration

z_g flight elevation $z_g = -H$

$\ddot{z}_g$ vertical acceleration

α angle of incidence

α_w wind angle of incidence

α_0 empirical constant

β angle of sideslip

γ path angle of gradient

γ_w flight wind angle of gradient

Γ, Γ_0 circulation

$\dot{}$ time differential operator

δ boundary layer density/thickness

Δ change

η	dimensionless coordinate, elevator/stabiliser stop
θ	pitch position angle
$\dot{\theta}$	potential temperature
ν	kinematic ductility
ρ, ρ_0	air density at altitude H above ground
σ	standard deviation
Σ	summation
τ, τ_0	shear stress
$\Phi(x, y, z)$	velocity potential
$\Phi(H/L_g)$	dimensionless windshear
Φ	banking angle
ϕ	geographic latitude
ψ	path azimuth
ψ_0	wind azimuth
$\psi_{g,G}$	geostrophic wind azimuth
ψ	azimuth of course
ω	angular velocity
ω'	components of Ω_E in geostrophic latitude
Ω_E	Earth angular velocity vector

Indices

a, A	aerodynamic
b, baro	barometric
f	fixed in aircraft or body
g	geodetic
gr	boundary value
i	general counting index
k	oriented to flight axis
m, max	maximum

min	minimum
rel	relative
R, Ref	reference
soll	theoretical value
W	oriented to wind axis
K	oriented to flight axis

Abbreviations

CAT	Categories of Instrument Landing according to ICAO
ICAO	International Civil Aviation Organization
INS	Inertial Navigation System
METAR	Meteorological Air Report
MM	Middlemarker
NM	nautical miles
OM	Outermarker
WMO	World Meteorological Organization

Note: These symbols and abbreviations were selected with reference to Aviation Norm LN 9300; SI units are used.

1. Introduction /1*

1.1 Introduction

In aviation accidents and dangerous situations occur chiefly in close proximity to the airport. According to an analysis done in the USA of 79 aircraft accidents, about 25% occurred during takeoff and 50% occurred during landing /71/. In these stages of flight which are characterized by great pilot stress, meteorological phenomena and their effects such as low cloud ceiling, poor visibility, icing and variable wind situations represent further sources of danger. Especially impairment of flight safety by windshear and downdrafts has been returned to because of a series of accidents and dangerous situations in the last few years and has initiated a large number of research projects.

At the Technical University of Braunschweig, the problematics were taken up in 1977 in the framework of the special research area 58 "Flight-Mechanics" with the goal of physically detecting the windshear phenomenon, describing it and eliminating its effects on aircraft.

The fact that danger to an aircraft from windshear is dependent on a series of influences which have not been separated from each other and analysed makes research on windshear very complex. A truly clear description of windshear effects on an airplane offers consideration of the flight-mechanics energy balance /1, 13, 14/: wind changes along the aircraft lead to a deviation /2 between existing and required performance. If the performance difference is not balanced by corresponding thrust adjustment,

* Numbers in margin indicate pagination of foreign text

there form emergy deficits or surpluses which become apparent in deviations in existing flight and theoretical flight path.

A method can be derived to compensate for windshear which is especially good for landings, because here (in contrast to takeoff) there are reserves of thrust power and danger boundaries are easily definable /1/.

For realization of this method one must differentiate between automatic and manual flight. Although modern flight control systems used today consist of vector and positive drive controllers and can guarantee safe landings in windshear situations there is considerable room for improvement. Energy/performance control can contribute significantly here /1, 13/. For manual landings there exists the difficult task for the pilot of soliciting the correct information for handling wind situations, that is, adjusting thrust correctly. The craft commander who is very busy during landing can see energy errors from a weighted combination of several displays. Display concepts must be developed to give the pilot the necessary information in a suitable fashion. It has been shown that the energy/performance principle can lead to an increase in flight safety during windshear conditions /1, 85/. Further investigation is needed in this area.

/3

Because the aircraft operates in the boundary areas of flight performance during takeoffs and landings, windshear research tasks are performed with the help of a flight simulator for reasons of safety, above all dangerous windshear situations are /3

only reproducible here. For this windshear models are necessary in the design of flight controllers and filters as well as in the education of pilots. These windshear models must reproduce flow relationships in dangerous windshear situations and be usable in real-time conditions without great expense.

1.2 The State of Technology

1.2.1 Wind Models

Because of the high number of thunderstorm windshears and downdrafts blamed for windshear-related accidents, experiments performed throughout the world concentrate windshear modelling efforts on description of flow fields in thunderstorm downdrafts. There are three different procedures here: utilization of stored data, development of meteorological simulation models and approximative solutions with the help of simple flow-mechanics models.

As an example of the first-named method, comprehensive measurements made in the USA should be mentioned. They were made on masts with the help of Doppler RADAR apparatus during passage of thunderstorms and secondary squall fronts /42/. Data storage (screen dimensions: dH=50m, dX=100 - 200m) was done tabularly at determined support points so that wind data were available for use with the help of corresponding interpolation programs for simulation purposes. We find a compromise between the mass of data to be stored and resolution which is relatively small in the case at hand. /4

The second method originates in expensive dynamic simulation

models which describe the structure and time-space development of thunderstorms under consideration of thermodynamic processes and meteorological boundary conditions /68/. These models are characterized by comparably small horizontal and vertical resolution and considerable calculation time/expense and are hardly suitable for the task of flight simulation in a realtime situation.

For simulating takeoffs, pull-ups and landings it is sufficient in most cases to mathematically describe the courses of wind velocity components in a range at 500m elevation and 10km long. Furthermore one can often limit oneself to quasistationary flow for the range of application. These considerations have led to comparably simple flow mechanics models. KRAUSPE /36/ approximated flow relationships in a downburst with a planar stagnation point flow and performed a series of flight-dynamics experiments therewith. Because the model only describes core flow, an enhancement via ambient flow and transition areas had to be utilized for simulation of landings.

Considerably more expensive is the three-dimensional model of ZHU and ETKIN /40/ which is based on a vorticity field doublette. Here, a circular surface positioned 1000m above the ground and a corresponding mirrored circle on the ground with potential vortex are used whose circulation strengths vary across the circle radius. The velocity field induced by the vortexes between the upper vortex surface and the Earth's surface approximately corresponds to the wind velocity path in thunderstorm downdrafts. /5
As regards fitting this data to measured wind data, many

improvements are still possible. Other 3D models are described in /72/, /73/ and /16/.

In contrast to flow processes in thunderstorms, poorly suited models from existing literature are used to describe windshear reltaionships in warm and cold fronts. All that exists here are tables of values from measured wind situations if one disregards the simple statements of SINCLAIR /38/ which describe the courses of headwind and sidewind components in the shear layer along an inclined flight path.

A not-inconsiderable potential danger in aviation can occur via wind phenomena which are grouped under the heading "boundary layer laminar flow." According to research at the Institute for Meteorology and Climatology at the University of Hannover, night-time boundary layer laminar flow which can form between the evening hours and early morning in stable boundary layers in the North German Lower Plains at a comparably high rate is especially to be watched /32/. In meteorological technical literature one can find a series of model statements to mathematically describe this type of laminar flow /74, 75, 76, 77/.

In the simple cases it concerns analytic solutions, generally numeric solutions of the displacement equations. These methods are poorly suited for the present flight simulation task because of the generally very high computation cost and low resolution /33/. Because wind situation chronological development is only beginning in meteorological areas, simple quasistationary engineering models fulfill the requirements of flight-technical

experimental procedures in most cases.

/6

1.2.2 Danger Criteria

Experiments on the endangering effects of windshear to air safety were done in many forms during the last 10 to 15 years /36, 78, 79, 80, 81, 82/. Often, dynamic response behavior of aircraft or certain aircraft types in defined wind situations stands in the foreground.

One definition of danger criteria and danger boundaries for landings was formulated by KÖNIG /1/ as a result of experiments on flight-technical energy balances. It is thereby possible to estimate the danger to aircraft (in real or simulated landing situations) from the apparent energy errors. As an energy error we characterize a deviation of the sum of aerokinetic and potential energies from the theoretical value. This method led moreover to a conception of a windshear display and improvement of future flight controllers /1/.

To classify the dangerousness of certain windshear situations it is of interest to produce a relationship between characteristic, easily measured wind parameters and the extent of danger.

The wind vector can be a function of time and location. If time changes in the wind field are small enough to neglect so that it can be considered "frozen" in space, then changes in the three wind conponents along the three spatial coordinate axes can be expressed by a collective tensor from nine local gradients /36/. Previously, the headwind vertical gradient was considered the

essential characteristic for description of windshear intensity so that it has been considered since 1970 in license conditions for flight controllers. The 5th Air Navigation Conference of the WORLD METEOROLOGICAL ORGANIZATION (WMO) has assumed shear strength division according to the vertical windshear gradient /7 and has made suppositions about their effects on flights of transport aircraft /15, 16/. Thus it is easy to see that vertical windshear gradients alone are no direct measure for windshear-conditioned endangerment. The chronological change of wind components at the aircraft location has a considerable effect when the craft flies through a wind field. A relationship between time and location gradients results from the aircraft's flight path velocity. Here, a small horizontal gradient in the headwind can lead to a similarly large chronological change because ground speed during landing is about 20 times greater than the aircraft's vertical speed. Thus instantaneous values for chronological wind gradients provide little evidence if no information is available for the effective period. The aircraft reaction is thus influenced by spatial expansion of the shear layer.

The Wind Shear Severity Factor formulated by the ROYAL AIRCRAFT ESTABLISHMENT, RAE /16/ represents a significant development by considering spatial expansion of shear whenever vertical wind influences do not enter into consideration and thus limitation to certain wind situations is necessitated.

It is still to be examined whether the Severity Factor permits predictions beyond descriptions of windshear strength concerning

windshear endangerment of air traffic.

/8

1.3 Goals

The goal of this work is essentially to develop suitable wind models for tasks in flight simulation and application of these models in research on endangerment of aircraft landing in windshears.

The basis of these windshear situation models is formed by information from publications, measured data from the Institute for Meteorology and Climatiology at the University of Hannover and some data taken from aircraft.

Because models to describe typical ground boundary layer profiles exist in many forms and will thus be described in this work, development or at least enhancement of model hypotheses for the other typical windshear situations is necessary. This is especially valid for boundary layer laminar flow and flow processes in fronts. We make a special note here about the compass/extent and expense of models so that use in a flight simulation is possible in realtime conditions.

With the windshear models developed here, comparative research on danger criteria and characteristics for describing shear force will be done and endangerment to landing aircraft during windshear situations will be estimated.

In order to limit the scope of this work to a reasonable extent, various limitations will be assumed. For one, wind modes will be limited to the middle area of the wind current, without

consideration of atmospheric turbulence. Turbulent wind fluctuations can attain especially high intensity in thunderstorm and front situations. As opposed to windshear, aircraft reaction to turbulence is differentiated basically by response behavior /9 and will be reserved for special research.

During evaluation of measured wind profiles, separation of turbulent wind changes from the course of average wind is not unproblematic. If these measurements are made with fixed sensors (masts or towers) the turbulent portion is eliminated from the signal via average value forming over time (in meteorology, use of ten-minute average values is typical). If on the other hand there are instantaneous profiles as is the case for measurements made in an aircraft, separation in the frequency range is necessary, that is, separation into a low-frequency non-stationary trend portion and one as a stationary turbulence portion. To solve this problem, one uses a nonrecursive digital filter /87, 88, 89/.

The models considered here are universally usable for average wind in a number of technical applications. For the research being done for this report, only transport craft landings are being considered because for this stage of flight danger criteria are easily formulated and make sense /1/. A windshear effect compensation is possible via corresponding thrust adjustment. By contrast, there are no reserves of thrust at takeoff so that here solutions need to be found for developing suited takeoff procedures.

Likewise not a subject of this report is the influence of variable side wind on landing endangerment. Changes in sidewind components have almost no effect on the aircraft's energy balance and do not enter into danger criteria determinations. It should not be assumed that variable sidewinds are not dangerous. /10

During a manual landing one would expect there to be stress on the pilot. Corresponding research is being performed with the help of a flight simulator. This is certainly valid for a series of other influences and effects which enters pilot behavior in windshear situations. At the time of publication there was no suited simulator available for use. Because previously there was also no pilot model corresponding to our task, simulated landings were done primarily with the rudder fixed. On the basis of the named boundary conditions, one can limit aircraft longitudinal movement. /11

2. Windshear in the Lower Region of the Planetary Boundary Layer

2.1 Windshear Characterization

As windshear we generally classify a spatial or time change of a wind vector or its components. Turbulent fluctuations are not considered, that is, variations of average winds alone are considered (Figure 2.1).

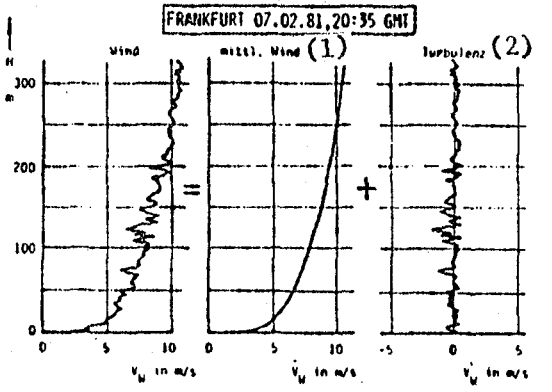

Figure 2.1: Dissociation of a turbulent wind profile into average wind and turbulent wind portions. 1-average wind, 2-turbulence

The causes of wind changes in the lower region of interest here (altitude 500m) are various: friction influences, temperature inversions, orographic influences, trailing vortexes, thunderstorms and frontal passage.

/12

For the appearing windshear forms and situations the basic types can be differentiated.

2.1.1 Boundary Layer Windshear

The planetary boundary layer is divided in meteorology into different regions (Figure 2.2). With sufficiently smooth surfaces one finds a very thin laminar underlayer (1mm).

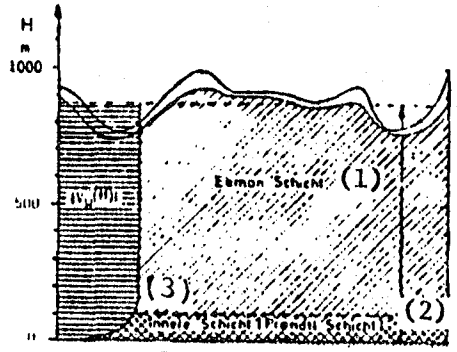

Figure 2.2: Layering of the planetary boundary layer according to /53/ 1-Eckmann layer, 2-inner layer, Prandtl layer, 3-laminar layer

In the upper, inner layer, flow is only dependent on distance to the ground, thrust stress on the ground, ground roughness and atmospheric stability. This layer near the ground boundary layer (also known as the Prandtl layer) grows about 10% of the total boundary layer height at an altitude between 30 and 100m, wherein flow velocity often attains 70 to 80% of the boundary layer upper limiting velocity.

As regards expansion, the outer layer forms (which together with the Prandtl layer enlarges from 250 to 1000m the Ekmann layer) the major portion of the boundary layer. While above the boundary layer, pressure and Coriolis forces are balanced and thus wind blows parallel to the isobar (geostrophic wind), friction force increases in the Ekmann layer with decreasing distance to ground. Flow is braked and there results a movement towards the direction of the geostrophic wind (in the Northern Hemisphere to the left).

Ground boundary layer profiles can be more or less influenced by orographic and atmospheric non-homogeneities. So along the flow direction the appearing changes in ground surface roughness affect the wind profile in that they gradually separate the flow /65/. Moreover considerable wind field disturbances caused by flow around/over hindrances (hills, high mountains, high buildings) arise. If these hindrances lie in the area of takeoff and landing strips (for example the Weidacher latitude at the Stuttgart airport), this situation can bring problems with it during takeoff and landings of twin-engined aircraft in case of powertrain failure. Certainly only the half value of headwind measured at 10m altitude at the airport is considered for reasons of safety in takeoff weight calculations, however wind velocities appearing alongside the flight path can vary substantially from the reference value. Even in the simplest case of an approximately contour-parallel flow, the downdraft for takeoff weight computations (for increases in safety) appearing in a lee-

region can dissipate in some circumstances /67/. Measurements with the research aircraft Dornier 28 in lee regions at the Weidacher altitude have indicated larger downdraft velocities than were assumed earlier /66/. This research is not yet concluded.

/14

2.1.2 Boundary Layer Laminar Flow (Low Level Jet)

The term low level jet is not uniformly used in technical literature because the formation of lower tropospheric wind maximus significant for low level jets can be caused by several different things. Some jets appear in certain wind directions for reasons of local topography (for example, chinooks) or in Alpine regions as a valley wind during the day and as a mountain wind during the night. Moreover, jets arise in connection with the approach of cold and warm fronts (prefrontal jet). In northern Germany, nightly low level jets are frequent. By this one understands a phenomenon which is found at an altitude of 100 to 300m in stable, nighttime planetary boundary layers during ground inversions. With weak ground winds there forms a layer a few decameters thick which is a laminar jet whose wind velocity maximum exceeds the 1.5x geostrophic wind defined by ROTH /31/. In a few cases one can observe large changes in wind direction (up to 90° at an altitude of 300m) (Figure 2.3). The jet turbulence is only weakly formed for reasons of stable layering.

If one considers chronological development of a nighttime low level jet one recognizes that one is dealing with a non-stationary process. As an explanation of this phenomenon, we use

the principle of inertial oscillation/vibration in stable nighttime boundary layers postulated by BLACKADAR /54/. As a result of thermal flow, especially on cloudless nights and with the associated temperature inversion, turbulent friction forces disappear. Equilibrium between pressure, friction forces and Coriolis forces is thereby disturbed and there occurs an acceleration of air particles. Figure 2.4 shows the difference vector inertial oscillation formed between geostrophic and actual wind. /15

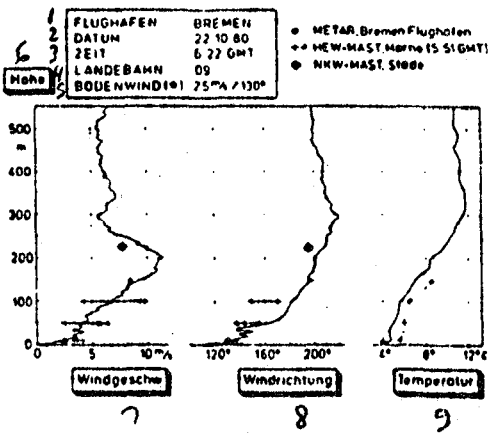

Figure 2.3 Example of a Low Level Jet
1-airport, 2-date, 3-time, 4-runway, 5-ground wind, 6-altitude, 7-wind velocity, 8-wind direction, 9-temperature

According to the theories and observations of KOTTMEIER /32/, the period is 14.5 hours in North Germany.

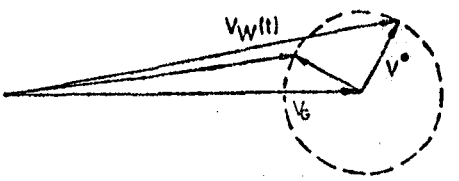

Figure 2.4 Inertial Oscillation of a Low Level Jet

/16

For windshear experiments in aviation, it is generally of less significance whence low level jets originate. Furthermore, this term is generally used for wind situations in which wind maxima appear in the lower troposphere. The relationship between wind velocity maximum and geostrophic wind has not yet been considered.

2.1.3 Windshear in Thunderstorms

Thunderstorms are known to be dangerous to aviation in consideration of their secondary effects, those being sleet, hail, electrical loading and discharge, downdrafts and turbulence. From the numerous phenomena related to thunderstorms two main forms can be derived from their bases of origin.

With the first main form designated as air-mass internal thunderstorm we are concerned with local appearances which form inside a unit air mass.

The second main form, the frontal thunderstorm develops as a result of labile rearrangement at the boundary surface between two differing air masses. Expansion of such thunderstorm fronts can sometimes encompass hundreds of kilometers. Basic conditions for formation of both thunderstorm types is humid-labile layering in the atmosphere.

Each thunderstorm cell proceeds through three stages of development after the initial step of formation /55/. This is depicted in Figure 2.5.

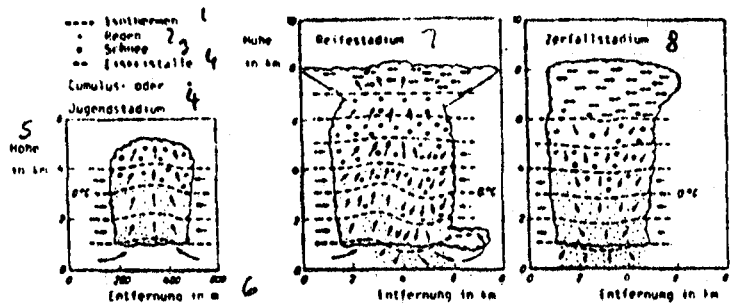

Figure 2.5, Development of a Thunderstorm Cell according to /55/
1-isotherm, 2-rain, 3-snow, 4-cumulus stage,
5-altitude, 6-distance in m, 7-mature stage,
8-decay stage

In the first stage (cumulus) there quickly arises a swelling cumulus cloud after initiation of convection or forced lifting of a front to attainment of the condensation level. In the total cloud air flow is directed upwards and is fed from above as well as below by the environment around the cloud. The updraft maximum is attained above the condensation level with velocities between 5 to 10 m/s.

The second stage is designated the mature stage and is initiated when the icing process has made great progress in the cloud. With the beginning of this stage the maximum updraft appears, whereby in European latitudes vertical velocities of 20 to 30 m/s and extremes of 50 m/s can form /55/. Precipitation falling from great elevations leads (by their low temperature and by melting and evaporation processes) to a cooling of environmental air. Therewith begins a reverse in flow relationships in the cloud. Along with updrafts there appear downdrafts of approximately the /18
same order of magnitude and thunderstorm cell structure is made

non-symmetrical. In the downdraft fields which become stronger and stronger, temperature drops compared to the environment. Updraft zones and downdraft vents exist together only in a confined state. At their mating faces there is tremendous turbulence.

In the last stage of a thunderstorm cell, the decay stage, downdrafts are constricted by constantly expanding downdraft channels. Cold air under the cloud hinders further axial energy thrust so that downdrafts are finally and completely exhausted. In the total thunderstorm cell, downdrafts control and precipitation falls to the Earth.

If in all thunderstorm clouds vertical velocity does not manifest itself in the mentioned extreme, it frequently remains in the range of 10 m/s. Wind velocities at and in the cloud deviate most strongly from values in the immediately surrounding area (more than 10 m/s or 50°). Moreover peak gusts of 25 to 37 m/s appear /56/.

Especially in the USA there are differing types of appearances of downdrafts observed. Along with the above-mentioned cases there are also "dry microbursts" in which precipitation does not reach the ground on account of evaporation in the air. There are also downdrafts from high cumulus formations (Virga) /6/. Figure 2.6 shows the time and space development of a microburst cell according to /57/ obtained with a Doppler radar unit. In this characteristic example the time period from first appearance of a downdraft on the ground to gradual initiation of decay is about

10 minutes. In this time the distance from the squall front to the core of the downdraft has increased from 2km to 8km.

/19

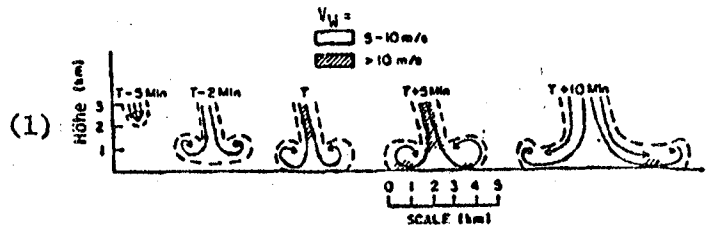

Figure 2.6, Time and space development of a microburst cell /57/
1-altitude

Lastly, via interaction of horizontal windshears with intensive downdrafts and strong turbulence, wind relationships in thunderstorms (as a rule) comprise the greatest danger for landing and ascending aircraft as regards wind influences.

2.1.4 Flow Relationships in Fronts

We designate the separating surface between two air masses with different properties as a weather front. A warm front is characterized by advancement of warm air which forces itself on an existing cold air mass and displaces it. In contrast, a cold front arises under the influence of a cold air advancement which forces itself under a warmer air mass in a wedge shape. Trends and form of both types of fronts are well differentiable. A warm front shows a definite and uniform trend (usually 1:50 to 1:200 /58/). In comparison the cold front profile is often drop-shaped. Figure 2.7 shows the curves of characteristic meteorological data for passage of a frontal system in connection with the effects of a low pressure vortex (cyclone).

/20

The diagram reproduces chronological changes for air pressure, temperature and wind velocity parameters for a front going East to West over an low pressure area observation point.

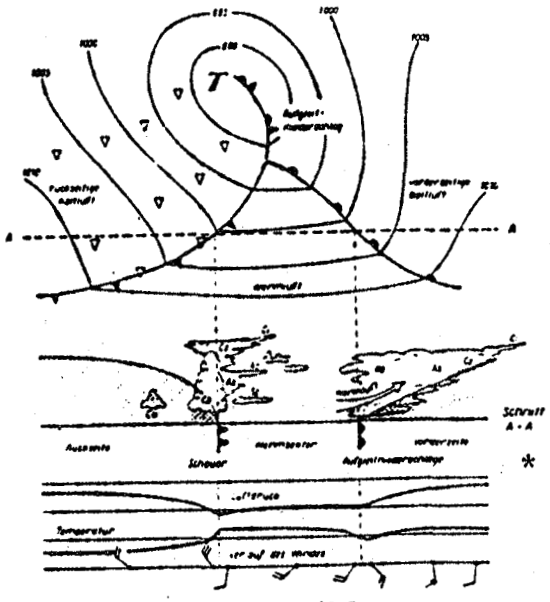

*Foreign text illegible

Figure 2.7, Passage of a frontal system according to /55/

The approaching warm front makes itself known by lowering air pressure and renewing the wind which is blowing transversely to the trajectory motion (from the South here). Clouds become more dense (on account of warm air rising from cold air underneath) and precipitation falls in the form of rain or snow. Immediately infront of the warm front there is often poor visibility or almost fog which moves with the front. As a result of /21 precipitation, temperature drops but after passage of the warm front. The wind turns to the right and can attain storm strength according to the air pressure gradient.

In front of the cold front air pressure begins to drop, the wind turns back and subsides. As an indicator of cold front passage

one sees swollen clouds, showers or thunderstorms with strong squalls. Other indicators are increasing air pressure, decreasing temperatures and increasing wind velocity. The wind turns in the example presented here from 90^{o} to 135^{o} to the right. As a whole there appear fluctuations in wind velocity between 5 and 15 m/s and directional changes of 180^{o}. These observations were confirmed by test data (Figure 2.8) which were recorded with the help of aircraft flying through warm and cold fronts /38/. There is unfortunately no data here for vertical wind velocity.

Stream line analyses as well as descriptions of wind velocity components and measured temperature data can be found in /42, 43 and 44/. The data given here which were obtained with the help of radar measurements, radiosonds and a 450m mast come chiefly from thunderstorm squall fronts. Flow processes correspond extensively to relationships in cold fronts, that is, cold air coming from the thunderstorm core forces itself under the warmer air. From the great number of appearance types, one can see in the example in Figure 2.9 that typical characteristics are well reproduced. The apparent updraft velocity attains values up to 4 m/s in the area of the frontal plane; the maximum horizontal velocity is somewhere between 6 and 20 m/s.

/22

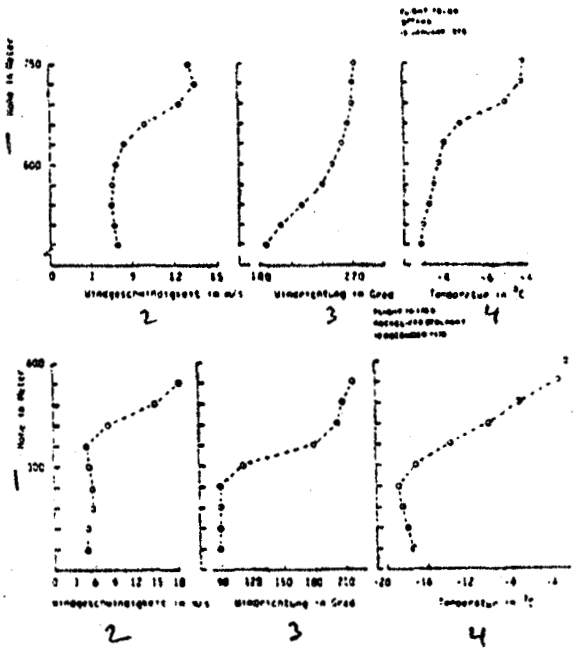

1-altitude in m

2-wind speed m/sec

3-wind direction, degree

4- temperature in deg C

Figure 2.8, wind and temperature curves at the flow field in a front (from /38/).

Weather fronts belong to phenomena which are by comparison well predictable on the basis of synoptic observations. Expected windshear parameters can be estimated from /59/ from the frontal draft velocity and apparent vertical temperature increase so that basic warnings are available to pilots.

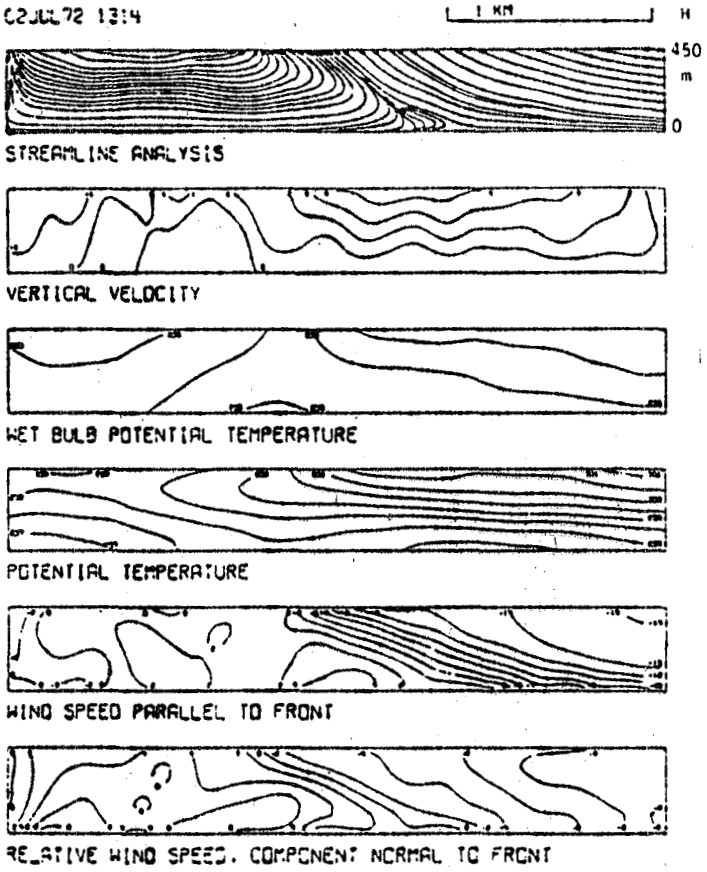

Figure 2.9, Test results from /44/.

2.2 Statistical Research on Windshear in Terminal Control Areas

A model description of windshear situations requires support from suited measurement data. Up to this point there existed only a bit of data from airport areas, especially in Europe. This is especially the case for precise, high-resolution aircraft measurements which are extremely expensive because of the demands placed on measurement technology /49/ and are thus seldom done by research institutes.

To enhance our description of type, strength and frequency of windshear in takeoff and landing areas at airports, in cooperation with DEUTSCHE LUFTHANSA an AIRBUS A 300 was equipped with a supplemental data recorder in order to record raw data during takeoffs and landings to be used in wind calculations. The recorder was so adjusted that data recording was performed during landings starting with extension of landing gear but at least 300m off the ground until the nose wheel touched the ground. For takeoffs the recorder remained on for four minutes after liftoff so that data could be recorded up to an altitude of about 3000m. Details concerning the measurement concept, data preparation and error balancing are given in Appendix A8 and in /7, 49/. These measurements were performed with a few interruptions in a time period between October 1980 and July 1981 in one region which is bounded by Copenhagen, London, Las Palmas and Cairo. Most of the data are from the Frankfurt airport (28% of all usable data) followed by Orly (18.7%) and Algiers (15%).

/25

Because of a previous charter arrangement in which the measurement plane (from LUFTHANSA) was leased to an Algerian airline there was a significantly smaller statistcal base (229 sets of evaluable data) than had been planned. Evaluation results can thus only give reference information and should be enhanced by other experimental data.

2.2.1 Wind Speed and Stability in the Atmosphere

In the vicinity of airports, ground-side wind measurement is done at a reference altitude of 10m. As an average value for the measured 229 on-board wind speeds at this altitude, v_x(10m)=4.85 m/sec and has a maximum value of 13.2 m/sec. The value of v_x = 7.5 m/sec is exceeded in 15.7% of all cases while the frequency of values exceeding v_x = 10 m/sec is about 3%. A value for comparison can be taken from resesarch at the NATIONAL LUCHT-EN RUIMTEVAART LABORATORIUM in Holland (NLR) whose results originate in 8000 large aircraft landings worldwide /19/. Here a probability for exceeding v_x>7.5 m/sec was calculated to be 12.3% which agrees in order of magnitude with measurements done on an AIRBUS.

If one considers frequency distribution of wind directions at 10m altitude (Figure 2.10) one recognizes frequency maxima in the areas NORTH to EAST-NORTHEAST as well as SOUTH to WEST. As an axis for the main wind direction we select 55 - 235°. (Stuttgart uses 60 - 240°).

It was further investigated how far the statistical parameters of wind speed had an effect via atmospheric stability. /26

Stability boundarys were set in accordance with PRITSCHARD et.al. /45/ as follows:

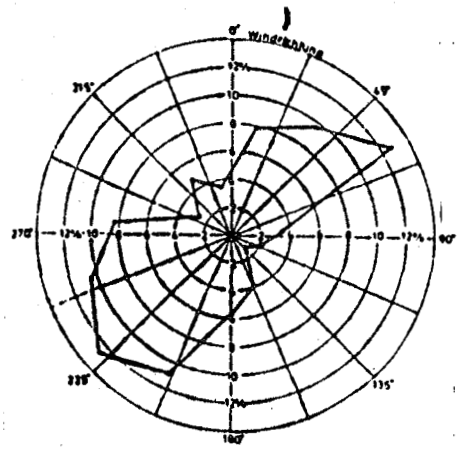

Figure 2.10: main wind directions, determined from 229 aircraft measurements. 1-wind direction

An evaluation of AIRBUS measurements of average vertical temperature gradients at altitudes between the ground and 300m showed neutral results in 38% of measurements. Stable relationships were observed 30% of the time and unstable relationships were observed 32% of the time. Figure 2.11 represents (at an altitude of 10m) the arithmetic average value of wind speeds as well as speed values of a 10% frequency for exceeding the average speed in dependence on atmospheric stability. One recognizes that even the smallest contributions /27 appear in a stable layer, in contrast the largest values during neutral conditions. An increase of v_w(50%) and v_w(10%) with decreasing stability would only be expected for an equally large geostrophic wind which apparently never appears here.

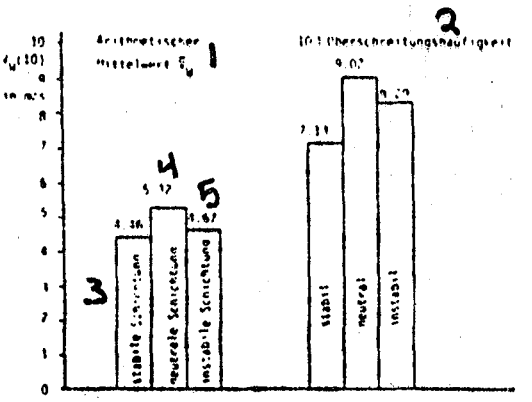

Figure 2.11: atmospheric stability influence on wind speed values at 50% and 10% "exceeding frequencies" 1-arithmetic average value v_w, 2-10% exceeding frequency, 3-stable layering, 4-neutral layering, 5-instable layering

2.2.2 Statistics of Vertical Windshear Gradients

As a measuring guide for windshear strength, one generally considers change in horizontal wind at an altitude interval of 30m (100ft). Squall fronts and wind fluctuations with smaller wave lengths rarely enter into windshear considerations. If determination of the altitude interval is desirably greater or less, it should be known that this reference value is used internationally in the definition of vertical windshear gradients, as for example in recommendations of the ICAO for classification of windshear strength and its influence on flight /28
path control and acceptance of flight controllers. Also, because usable data originate from the same definition of vertical windshear gradients it must be used for this research. Previously there existed very little statistical material concerning strength and frequency of windshears in middle Europe so that results for other geographic areas had to be referred back to, above all areas in the USA.

Figure 2.12 shows windshear distributions as they were determined

in the USA, Canada, Japan and Finnland, represented by frequency summations. With this graphing method one obtains information about the probability that a certain gradient will be exceeded or fallen short of. So for example, by exceeding a shear of 4 m/sec per 30 meters [which is classified as the boundary value between average and large shear values by the ICAO] (see Section 4) one is dealing with an "exceeding probability" between 2% (Helsinki) and 5% (Whiteshell, Canada). For the specification of automatic landing systems in the USA and England for this gradient an "exceeding probability" of 0.1% is assigned (Figure 2.12).

The results given here originated in mast measurements and relate to contributions of windshear gradients. For an aircraft which flies through the shear layer, the type of shear is of tremendous significance. A diminishing wind or an increasing tail wind works along the flight path to reduce performance. If wind speed is dependent only on altitude there results a negative gradient in this case $du_x/dH=u_{xH} < 0$. Correspondingly the NLR has performed statistical analyses on landing-direction-related wind components /19/ on the basis of the mentioned 8000 landings /29 worldwide. For wind change per 30 meters altitude difference an average value of 0.18 m/sec was determined (0.006 /sec) for a range of variation of +/-4.5 m/sec per 30 meters (0.15 /sec). With increasing gradient there appears an increasing deviation from normal distribution. Wind strength at 10m altitude barely influences the average value of u_{xH} but there is a stronger scattering of values for $u_x > 7.5$ m/sec.

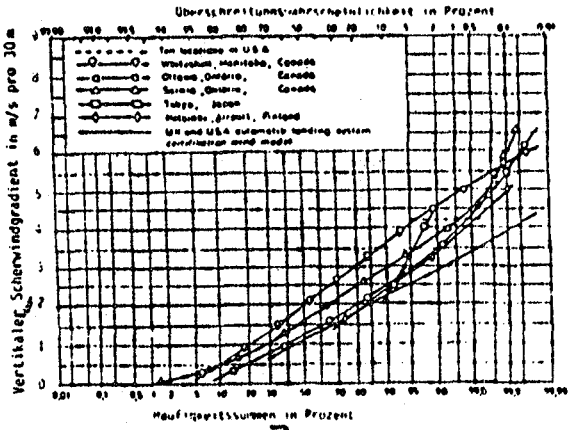

Figure 2.12: summation frequencies of vertical windshear gradients measured worldwide (from /56/)
1-"exceeding probability" in percent,
2-vertical windshear gradient in m/sec per 30m,
3-frequency summation in percent

For ground winds with u_x<7.5 m/sec, 89.5% fall into the category of light shear and the remaining 10.5% fall into the category of medium shear. For greater wind speeds (u_x>7.5 m/sec) values shift to 95.5% light shear and 4.5% medium shear (Figure 2.13). /30

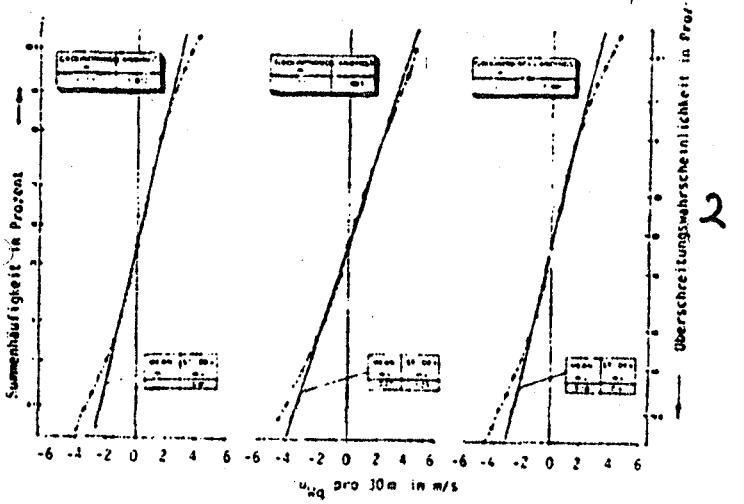

Figure 2.13: frequency of windshears in dependence on ground wind speed (from /19/)
1-summation frequency in percent, 2-"exceeding probability" in percent

For the airports used most frequently a statistical view was made of the most unfavorable windshear conditions at JFK (New York) followed by Houston (Texas), Montreal, Schiphol, Dubai, Singapore and Bangkok.

Data about windshear conditions in European regions are given by

an evaluation of intermediate distances made with an AIRBUS /7/. About 82% of the 229 usable landings and a few takeoffs took place in Europe, of those two-thirds at airports in the Federal Republic of Germany (West Germany). Evaluation of windshear /31
gradients encompasses along with the direction-of-landing component "u" (du_x per 30m) side wind components (dv_x per 30m altitude) and change in the vertical wind per 600m path interval DELTA X (which corresponds in a 3-degree glide path to an altitude interval of about 30m). Figure 2.14 shows the frequency summation for the three gradients. Maximum u-component change per 30m altitude interval is on the average -1.5 m/sec (=0.05 /sec) for a standard deviation of +/-1.49 m/sec (=0.048 /sec) and a range of variation between -3.9 m/sec and +1.1 m/sec (-0.13/sec and 0.037 /sec). In comparison with the WMO/ICAO classification (Table 4.1) 65% of values fall into the range of light windshear (0-2 m/sec per 30m) while the remaining 35% are classified as windshears of medium strength. For side wind components the average value of maximum gradient u_{xH} is 1.38 m/sec per 30m (0.046 /sec). As regards windshear strength, the order of magnitude is the same as for u-components.

In Figure 2.15 we show a subdivision of atmospheric stability wherein the above-named stability classification finds application according to /45/. Frequency summations of maximum gradients $u_{WH'}$ v_{WH} and w_{Wx} are plotted (related to a 30m altitude interval and/or 600m path interval) for stable, unstable and neutral layers.

For a better comparision, values for 50% (average value) and 5%

"exceeding frequency" are given as a bar graph in Figure 2.16. For vertical gradients of the headwind components there result in both cases the largest values for neutral conditions, the smallest for stable conditions. Vertical gradients of the side wind components show increasing average values for decreasing atmospheric stability, above all an opposing tendency for values of 5% "exceeding frequency." Figure 2.17 presents relative frequency of appearance of weak, medium and strong shears for the differing stability conditions. /32

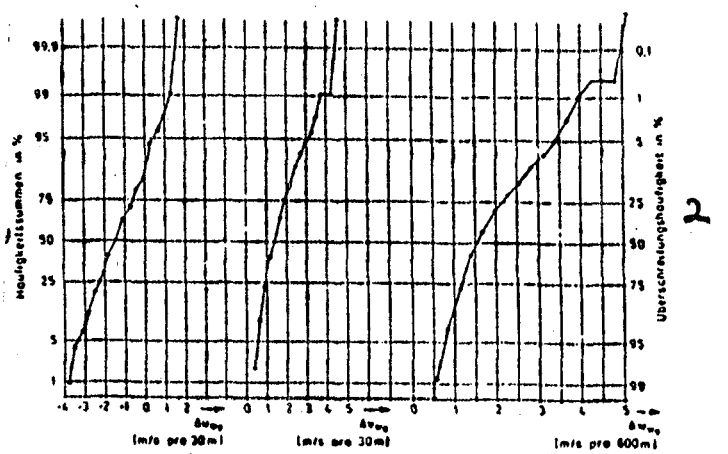

Figure 2.14: frequency summation of wind gradients from AIRBUS measurements, 1-frequency summation in percent, 2-"exceeding frequency" in percent

The results confirm the tendency determined and expected from the above that appearances of larger windshear gradients are probably fewer in stable conditions than in neutral and unstable conditions. In contrast, an accumulation of larger gradients would be presumed on account of more intense impulse transferral during strong mixing in unstable conditions than during neutral conditions. Here the smallest statistical basis per stability group could play a role in certain circumstances in that most values fall into the range of neutral layering.

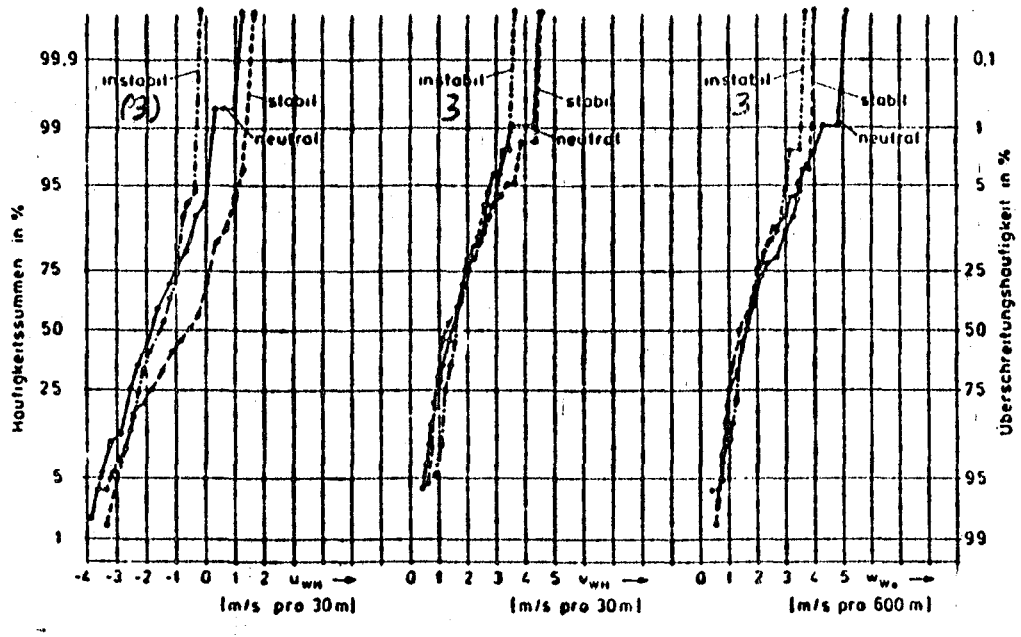

1

2

Figure 2.15: frequency summation for vertical windshear gradients in dependence on atmospheric stability 1-frequency summation in percent, 2-"exceeding frequency" in percent; 3 - unstable

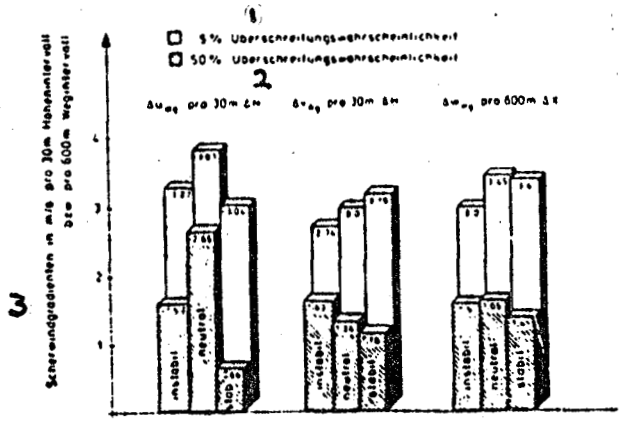

Figure 2.16: "exceeding frequency" in dependence on atmospheric stability 1-5% exceeding probability, 2-50% exceeding probability, 3-windshear in m/sec per 30m altitude interval or per 600m path interval

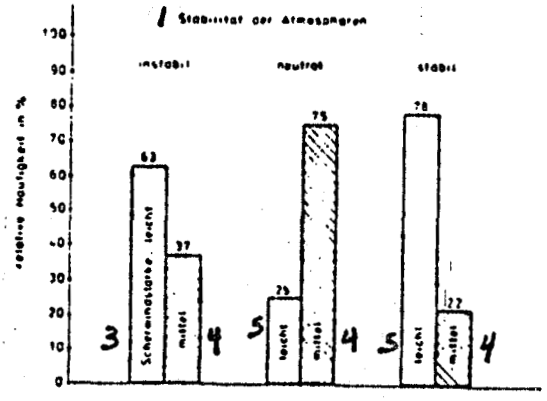

Figure 2.17: frequency of appearance of windshears of light, medium and great strength, 1-atmospheric stability, 2-relative frequency in percent, 3-windshear, light, 4-medium, 5-light

3. Simple Windshear Models

3.1 Ground Boundary Layer Profiles

3.1.1 Logarithmic Laws

To mathematically describe windshears which appear most frequently in nature, ground boundary layer shears (Fiugre 3.1), there are a series of models in the meteorological literature which are well suited for application in flight simulation. Greatly distant from those is the logarithmic law (Eqn. 3.1) developed by PRANDTL /22/ in 1924 for adiabatic conditions in the atmosphere (neutral layering).

$$V_g = u_{*0}/k \cdot \ln(H/H_0) \qquad (3.1)$$

U_{*o} is tangential stress velocity on the ground which is formed here by tangential stress tau_o and air density rho_o on the ground.

$$u_{*0} = \sqrt{\tau_0/\rho_0} \qquad (3.2)$$

The parameter H_o expresses the influence of surface roughness and is designated as the roughness height. It contributes about 1/30th to 1/10th of the actual height of ground hindrances. The number calculated by PRANDTL for the value of k was later known as the KARMAN constant (k = 0.4).

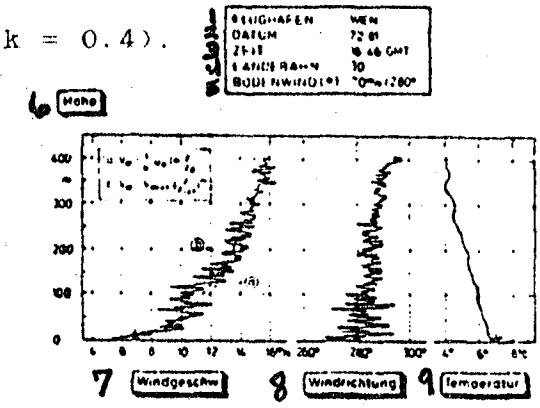

/36

Figure 3.1: example of a ground boundary layer profile
1-airport, 2-date, 3-time, 4-runway, 5-ground wind, 6-altitude, 7-wind speed, 8-wind direction, 9-temperature

Validity of this law is limited to the PRANDTL layer, that is to an altitude region of 30 to 100m. In this region tangential stress and air density change so little as a rule that the simplified assumption is good here. Likewise change in wind direction in the PRANDTL layer can be considered as being negligibly small.

If the atmosphere shows labile or stable conditions, the wind profile deviates more and more strongly from an adiabatic path with increasing altitude.

Predictions about wind profile structures for **adiabatic** cases are basically supported by work of MONIN and OBUCHOW /23/. Thus the following general model is developed with help of similarity hypotheses.

$$k\, H/u_{*0}\, (\partial v_g/\partial H) = \phi(H/L_*) \qquad (3.3)$$

The normalization value L_* represents a longitudinal measure which is formed from values of tangential stress velocity u_{*0}, heat flux H, specific heat at constant pressure c_p, air density rho_0, temperature T_0 and earth's acceleration g as follows:

$$L_* = -\frac{u_{*0}}{k}\,\frac{c_p \cdot T_0 \cdot \rho_0}{g \cdot H} \qquad (3.4a)$$

with heat flux

$$H = -\rho_0 \cdot c_p \cdot k_w \cdot \partial\theta/\partial H \qquad (3.4b)$$

and potental temperature change at altitude

$$\partial\theta/\partial H = dT/dH + g/c_p \qquad (3.4c)$$

The phi function is not given by similarity hypotheses and must be determined empirically. For small values of the argument (H/L_*) the function can be approximated by a linear function /20/:

$$\phi(H/L_*) = 1 + \alpha_\phi\, H/L_* \qquad (3.5)$$

It thus represents a further development of the adiabatic case described by PRANDTL (Eqn. 3.1) for which phi=1 is valid. After insertion into Eqn. 3.3 and integration over the altitude H there results the so-called Log-Lin law for wind speed:

$$V_g(H) = \frac{u_{*0}}{k}\left(\ln(H/H_0) + \alpha_\phi \frac{H - H_0}{L_*}\right), \qquad (3.6)$$

with $alpha_{phi}$ being an empirical constant. Wind profile from a logarithmic adiabatic portion (corresponding to the PRANDTL model) and a stability-dependent term linear with altitude are put together. This is depicted in Figure 3.2.

/38

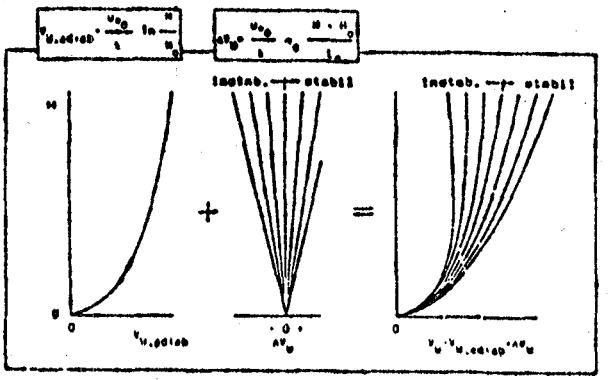

Figure 3.2: relationship of the Log-Lin profile (from /47/)

With this model law measured wind profiles can frequently be approximated to several hundred meters. For smoothed profiles as a rule three representative measurement points are sufficient for determining model parameters u_{*o}, H_o and $alpha_o/L_*$. The associated calculation equations are listed in Appendix A1.

Further empirically determined phi-functions were described in /20/ and /47/ (DYER-BUSINGER relationships):

$$\phi(H/L_*) = 1+4.7\ H/L_* \qquad \text{for } H/L_*>0 \qquad (3.7a)$$

$$\phi(H/L_*) = (1-15\ H/L_*)^{-1/4} \qquad \text{for } H/L_*<0 \qquad (3.7b)$$

They lead to the following wind profile /91/:

$$V_W = \frac{u_*}{k}\left(\ln\left(\frac{H}{H_0}\right) + 4.7\,\frac{H - H_0}{L_*}\right) \qquad (3.8a)$$

and /39

$$V_W = \frac{u_{*0}}{k}\left(\ln\frac{H}{H_0} - 2\ln\left(\tfrac{1}{2}\left(1+f(H/L_*)\right)\right) - \ln\left(\tfrac{1}{2}\left(1+f^2(H/L_*)\right)\right) + 2\,\mathrm{atan}(f(H/L_*)) - \pi/2\right) \qquad (3.8b)$$

$$\text{mit } f(H/L_*) = \left(1 - 15\,\frac{H}{L_*}\right)^{\frac{1}{4}}$$

The vertical profile of wind speed is shown in a few examples in Appendix A2.

3.1.2 The Exponential Law

Very good results are given by the simply applied and frequently used exponential laws for approximating measured ground boundary layer profiles.

$$V_x = V_{x,Ref}\,(H/H_{Ref})^m \qquad (3.9)$$

Herein, $V_{x,ref}$ is measured wind speed at the reference altitude. The first theorems for an exponential law were published before the turn of the century by ARCHIBALD /61/ (see also /52/). In the following years through today numerous measurements and experiments were done to determine the exponents m for differing terrain types. Ground surface roughness and atmospheric stability show themselves to be significant influences.

COUNIHAM /52/ analysed in 1972 neutral conditions for data existing then and plotted the determined exponents versus roughness height and/or main terrain type (Figure 3.3). Definitions can be had from Table 3.1. One recognizes an increase in the exponents with ground surface roughness wherein a not inconsiderable scattering is observed.

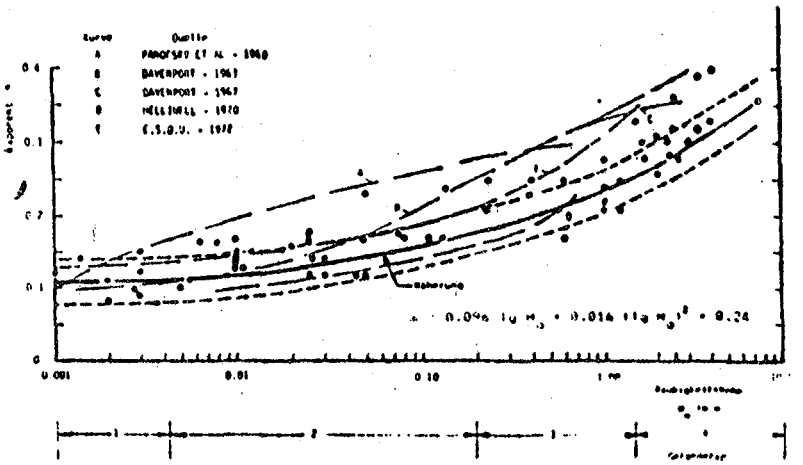

/40

Figure 3.3: dependence of exponents m on roughness height (from /52/)

This is valid for individual measurement values as well as for the plotted curves from other sources. The approximation relationships given by COUNIHAM from Eqn 3.10 were calculated with regression analysis which above all only considered the most precise and reliable data from his research:

$$m = 0.096 \lg H_0 + 0.016 (\lg H_0)^2 + 0.24 \qquad (3.10)$$

Reference values for different terrain types and roughness heights are shown in Table 3.1.

/41

Table 3.1: Definitions of Terrain Types

Terrain Type	1 flat ice, snow lakes	2 med. rough short grass meadows	3 rough fields forrests	4 very rough cities
H_0 in M	$10^{-4} \cdot 4 \cdot 10^{-4} \cdot 10^{-3} = 0.02$	0.001 · 0.03 · 0.07 · 0.2	1.0 · · · · · 1.5	1.0 · 3.0 · 6.0
Exponent m	0.08 · 0.11 · 0.12	0.13 · 0.143 · 0.16	0.2 · · · · · 0.23	0.25 · 0.4

For Eqn. 3.10 dry adiabatic atmospheric conditions are presumed, that is, a temperature gradient of $dT/dH = -0.0098$ K/m.

Research on the effects of vertical temperature gradients on the value of the "m" exponents was done by FROST /25/ and others.

Results show in a good approximationa linearly increasing (with increasing stability) exponent (Figure 3.4). If one relates roughness and stability influences , then the following approximation is formed for m (H_o, dT/dH):

$$m = k_1 + k_2 \lg(H_o/c) + k_3 (\lg(H_o/c))^2 + k_T \, dT/dH \qquad (3.11)$$

mit:

$k_1 = 0.345$ $\quad c = 1.0$ m

$k_2 = 0.096$ $\quad k_T = 10.7$ m/K

$k_3 = 0.016$

For comparison with AIRBUS results, model parameters for the exponential law were fitted to 39 measured wind profiles. The determined exponents are plotted in Figure 3.5 over average temperature gradient (altitude interval DELTA H=300meter). In addition lines from Eqn. 3.11 for four roughness heights are plotted (H_o = 10m, 1m, 0.1m and 0.01m) because no information exists concerning surface roughness in the measurement region at the associated airport. /42

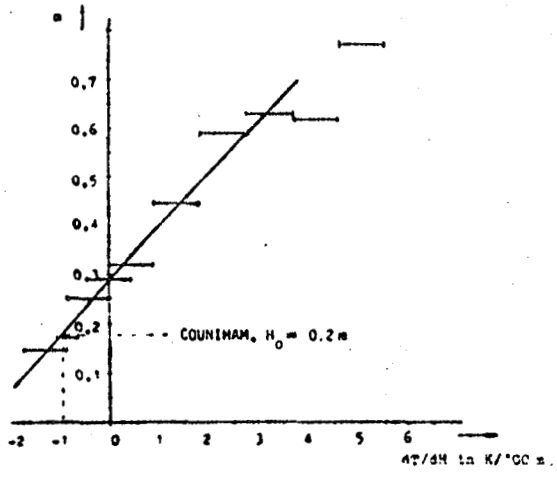

Figure 3.4: influence of temperature gradient on exponents from measurements /25/

Strong value scattering is probably not caused alone by differing surface roughness for respective airports and wind directions. Other causes are:

-Application of instantaneous values in place of wind profiles made over a 3 to 10 minute period usually used in meteorology.

-Influences from horizontal non-homogeneities, because meaurements along flight paths took place over a 6-10km path.

-Deviation of local vertical temperature gradient from the value determined above 300m altitude. /43

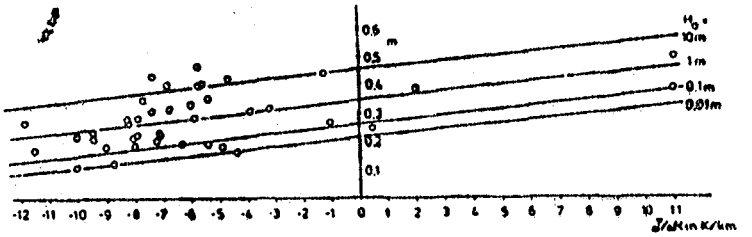

Figure 3.5: relationship between exponent m and average temperature gradient from AIRBUS experiments

Along with influences of surface roughness and atmospheric stability some authors (see also N.M. BARR et al /47/) also mention exponent dependence on ground wind speed. In contradiction to /63/, /62/ postulated an exponent decrease with increasing ground wind and gives the following relationship as a result of research at KENNEDY SPACE CENTER (Figure 3.6):

$$m = \frac{b}{(V_g(H=18\ m))^{3/4}} \qquad |V_g(18)| = m/s \qquad (3.12)$$

The parameter b scatters to an average value of 0.52 $(m/sec)^{3/4}$ for the most different weather conditions and can be viewed in a good approximation as being normally distributed.

$$b = 0.52 \pm 0.36 \quad (m/s)^{3/4}$$

The tendency expressed by Eqn. 3.12 to decrease the exponent for increasing wind speed at ground level can be clearly

demonstrated. If the wind speed is above the boundary layer for different boundary layer profiles of the same order of magnitude there results a constrained decrease in ground reference speed with increasing exponents (see Figure 5.1). /44

If one starts with equally large wind speeds at a reference altitude of 500m and compares the described wind profiles described by exponents $m=0.4$ and $m=0.2$, one obtains for the smaller exponent at an altitude of 10m a more-than-doubled wind speed than for the one with $m=0.4$

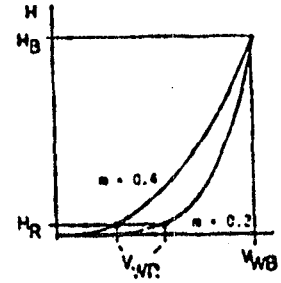

Thus even with large variances in geostrophic wind speed one would expect the tendency of decreasing value of m with increasing reference wind speed. Here we are apparently concerned with an effect of the selected reference altitude which becomes smaller with increasing measurement altitude.

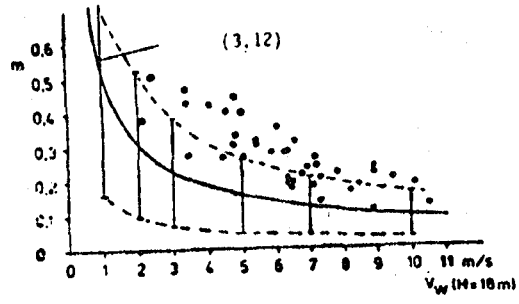

Figure 3.6: dependence of exponents on ground wind

For comparison with Eqn. 3.12, the determined exponents from the 39 measured wind profiles (AIRBUS measurements) are plotted versus wind speed at the selected /62/ reference altitude of 18m. One recognizes that AIRBUS measurements on the average produce larger exponents than those calculated in /62/. The data trend can be approximated with Eqn. 3.12 if the parameter b is given a value of 0.9 $(m/sec)^{3/4}$. Data scatter is considerable so that only a rough exponent approximation is possible from individual ground wind measurements.

3.1.3 Relationships between Exponential Laws and Logarithmic Laws

SKELTON /64/ showed that the exponential law can be used under certain circumstances with the logarithmic law. By using Eqns. 3.1 and 3.9 one obtains the following relationship:

$$\frac{u_H - u_{H,R}}{u_{H,R}} = \frac{\ln(H/H_R)}{\ln(H/H_0)} = \left(\frac{H}{H_R}\right)^p - 1 \qquad 3.13$$

The right side of the equation can be described by a series summation of a logarithmic expression:

$$\frac{H^m}{H_R} = 1 + m \ln\left(\frac{H}{H_R}\right) + \frac{m^2(\ln(H/H_R))^2}{2} + \ldots \qquad (3.14)$$

Under the condition that the considered altitude region does not considerably deviate from the reference altitude (there is an error of about 3%) one obtains the following relationship: /45

$$m(H_0) = \frac{1}{\ln(H_R/H_0)} \qquad 3.15$$

$$m(u_{H0}) = \frac{u_{H0}}{k\, u_{HR}} \qquad 3.16$$

Results are thus dependent on selection of reference altitude H_R. To determine a suitable value of H_R comparative data are

necessary for individual cases for tangential stress velocity and roughness height. Because these data are not directly extant there resulted a comparison between Log-Lin law and/or exponential law and 39 measured ground boundary layer profiles. Model parameters were so fitted such that correlation was attained in the altitude region of interest between 10 and 300m. Figure 3.7 shows the relationship between exponents m and parameters u_{*o}, H_o and $alpha_{phi}/L_*$ as a result of the comparison calculation. The curves of $m(u_{*o})$ and $m(H_o)$ were well described by Eqns. 3.15 and 3.16 whenever the reference altitude was set at H_R = 14m. In comparison to the relationship represented in Section 3.1.3 between m and H_o (Eqn. 3.8) the exponent increases more strongly with increasing roughness height. Figure 3.3 indicated strong scattering of results originating from different authors. The cause of this is basically the differing altitude regions which were selected for fitting model parameters to measurements.

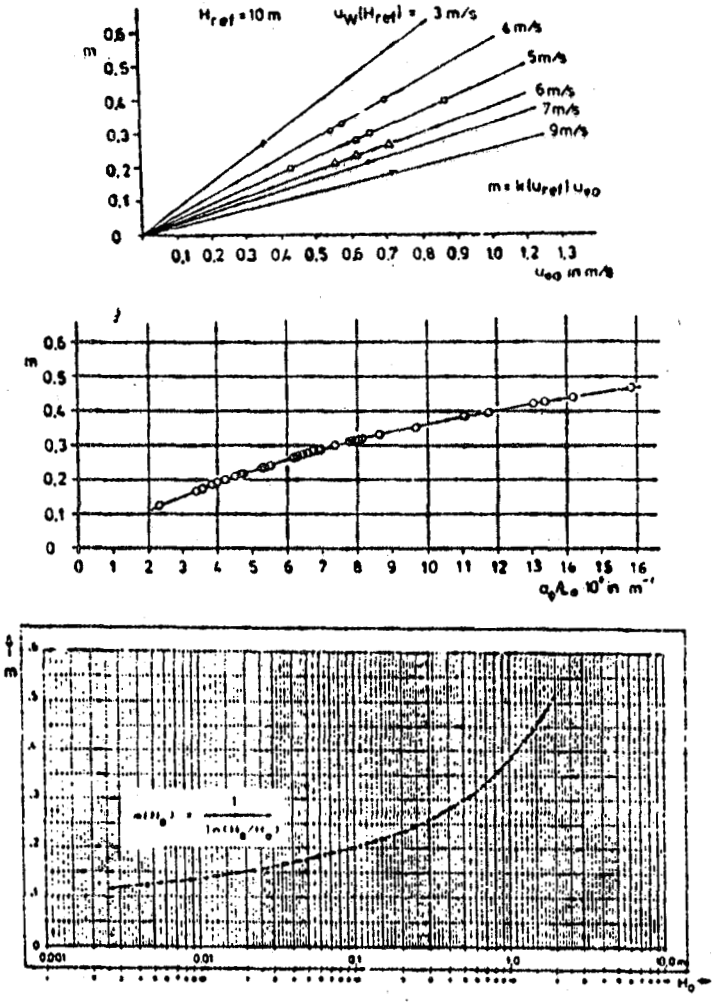

Figure 3.7: comparison between exponent law model parameters and Log-Lin law parameters

3.1.4 Description of Altitude-dependent Wind Rotation /48

In the previous consideration wind direction changes with altitude were considered permissibly small. A few of the named model equations reproduce the appearing wind profile pretty well to a few hundred meters altitude where this assumption is not allowable. Above this altitude range, directional changes of 30 to 40 degrees are not uncommon. Model laws must be correspondingly expanded or models must be used for componential description of wind speed with altitude.

One of the first theoretical studies of wind rotation with altitude was done by W. EKMAN /27/. The point of departure for his solution is the displacement equation for laminar, horizontal flow under neutral atmospheric conditions. Further simplifying assumptions include altitude independence, straight, parallel isobars as well as constant air viscosity and density with altitude. This solution is the so-called EKMAN spiral which is depicted in Figure 3.8.

The upper diagram shows wind speed components in the direction of geostrohic wind and transverse to that in the lower diagram both components are plotted as a hodograph. A value of exactly 45^{o} is given as the deviation of the ground wind from the direction of the geostrophic wind. Under consideration of the simplified assumptions met with, it is not surprising that this model only qualitatively describes relationships in the atmospheric boundary layer. PRANDTL /28/ also looked at representing wind vectors as a function of altitude, above all for the case of interest here of turbulent frictional flow. His approximating solutions start

from an exponential function for components in the direction of the geostrophic wind (see Figure 3.9). /49

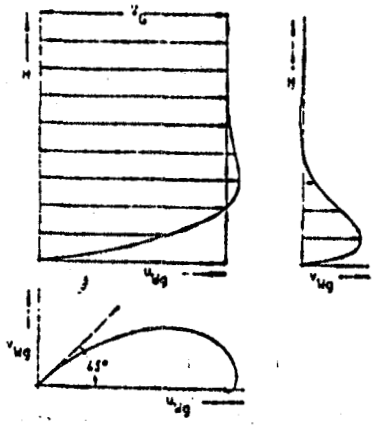

Figure 3.8: laminar ground flow from EKMAN /28/

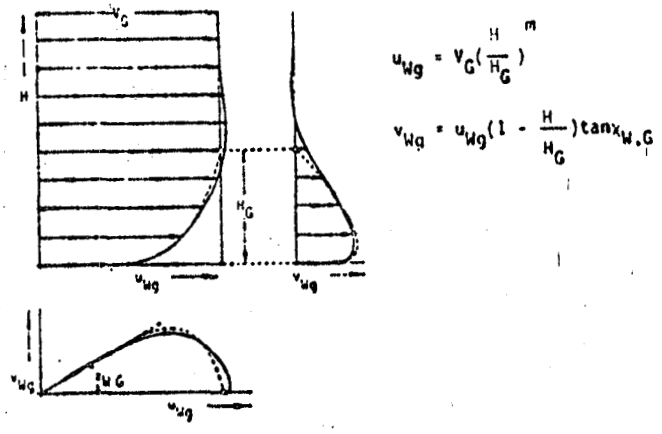

Figure 3.9: turbulent ground flow from PRANDTL /28/

From the relationship obtained from Eqn. 3.18a there results for the deflection angle opposed to the geostrophic wind angle:

$$\tan\alpha_g = (1-H/H_G)\ \tan\alpha_{g,G} \qquad (3.18b)$$

Along with geostrophic wind V_G and boundary layer thickness H_G the rotational angle $\alpha_{W,G}$ between the geostrophic wind and the ground wind must be determined. This appears to be a problem persistently unsolved in meteorology about which FORTAK /70/ makes the following comment:

"None of the almost uncountable number of experiments based on theory as well as measurement has been able to explain using easily measureable parameters the great variability of the angle between the wind at the upper boundary of the planetary boundary layer and that at ground level as well as the thus-related structure of the wind spiral."

A significant disturbing influence is the coming together of cells of air with differing temperatures, large chronological variability of metoerological parameters and nonhomogeneities in ground form (terrain).

From the differing mathematical relationships for angle of deflection $\alpha_{W,G}$ which can be read in the literature we will mention two estimating formulas.

From Eqn. 3.19 from PLATE /24/ the angle of deflection between geostrophic and ground wind can be calculated from shear stress speed and geostrophic wind:

$$\sin\alpha_{g,G} = 10.7\ u_*/V_G \qquad (3.19)$$

PRANDTL /28/ gives an approximation with which the angle of deflection can be determined as a function of the exponent m of /51
the exponential law (Eqn. 3.18a):

$$\tan x_{W,G} = +(m(m+2))^{1/2} \qquad (3.20)$$

This relationship is represented in Figure 3.10 as a diagram.

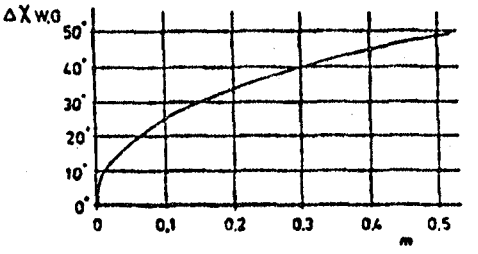

Figure 3.10: dependence of wind deflection angle from exponents of the exponential law (from PRANDTL)

For the typical range of variation for exponents m between 0.1 and 0.4 the angle of deflection is between 24 and 45 degrees. Often significantly smaller values are observed. From Eqn. 3.20 very small values for $x_{W,G}$ appear in connection with the exponent m=0 which corresponds to almost constant wind at elevation. This certainly has a theoretical basis but cannot be verified with physical observations as are present for AIRBUS measurements (for example). These measurement results were obtained among other things for forming a correlation between angle of deflection and easily measurable meteorological parameters. Because maximum measurement altitude was limited during landings to 300 to 500 meters , it seemed sensible to consider wind deflection at elevation H in contrast with flow at a reference altitude H_o so /52
that knowledge of geostrophic wind and boundary layer thickness is not necessary. PRANDTL's supposition from Eqn. 3.18 allows a retransformation under the following boundary conditions (see Figure 3.11):

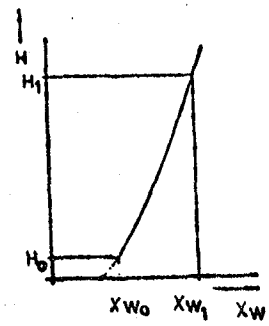

$$x_w = x_{w0} + \arctan\left(\frac{H - H_0}{H_1 - H_0}\right) \tan(x_{w1} - x_{w0})$$

Figure 3.11: angle of deflection as a function of altitude

In Figure 3.12 the tangent of the angle of deflection between the altitude H_0 = 10m and H_1 = 300m as regards an altitude interval $H-H_0$ = 290m (and/or the angle of deflection) is plotted with average temperature gradient DELTA T/(H_1 - H_0). Especially in the range between 0 and 30 degrees in which the majority of measurement points lie, there is great scattering of values. Including the few large angles of deflection and negative values one can presume (as a basic tendency) an increase in angle of deflection with increasing atmospheric stability. Comparison experiments with other meteorological parameters show even greater scatter so that in correlation with the above-mentioned predictions of FORTAK an estimation of wind direction from meteorological boundary conditions must be viewed as being very uncertain.

For further windshear experiments and simulation calculations, /53
models based on Eqns. 3.7 and 3.21 were selected to describe ground boundary layer profiles. A few selected examples in Figure 3.13 for a comparison between model and measurement show that a good approximation is possible from instantaneous value profiles from aircraft measurements.

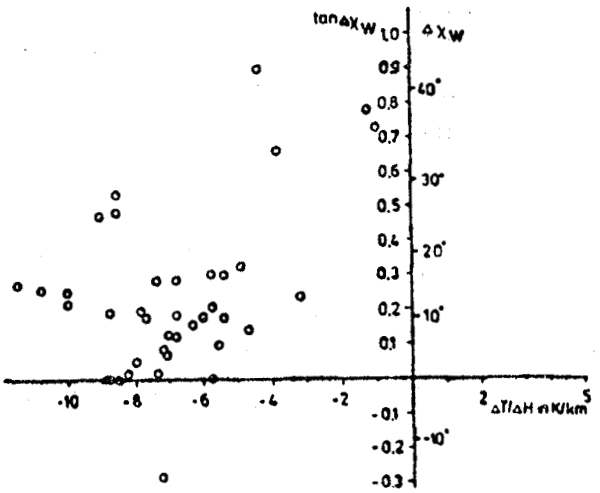

Figure 3.12: relationship between angle of deflection and temperature gradient

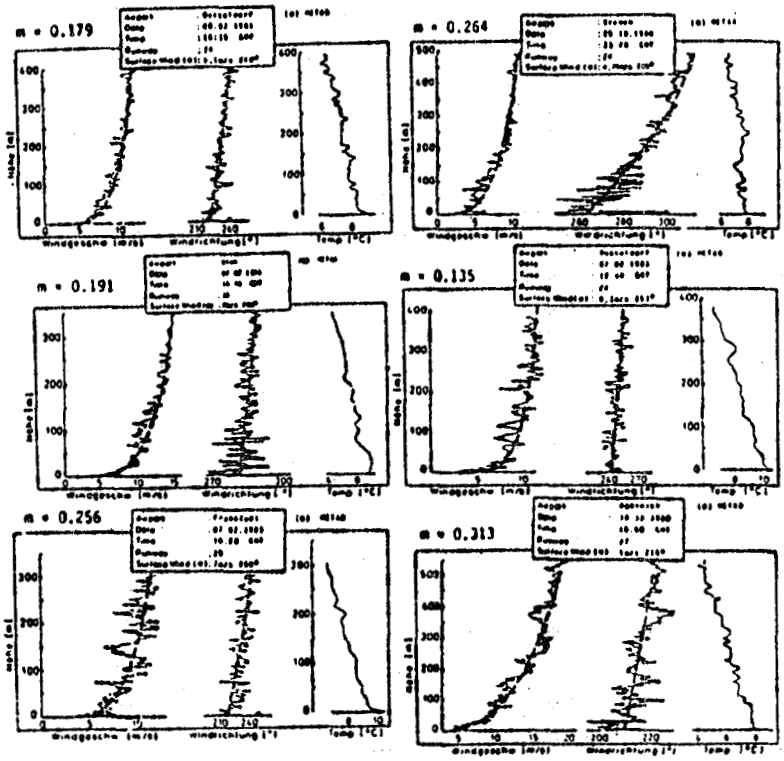

Figure 3.13: comparision of the ground boundary layer model with measurements. (print is small but I think the key reads as follows: airport, date, time, runway, surface wind - translator.)

3.2 Ground Boundary Layer Profile Variation via Atmospheric or Orographic Nonhomogeneity

Ground boundary layer profiles do not always appear in the above-described ideal form, even if one neglects special wind situations such as weather fronts, thunderstorms and boundary layer beam currents. Wind profile form can be considerably influenced by atmospheric and orographic nonhomogeneities. With this we see a relationship with vertical temperature gradient changes. The examples in Figure 3.14a show that especially with appearance of temperature inversions, deviations in wind direction as well as wind speed come into play. Likewise the expected decrease in turbulence intensity for increasing atmospheric stability above the temperature inversion becomes clearly recognizable. A modeled description of the wind process appearing here can be dealt with using a first-order approximation by section-wise variation of model parameters as is depicted in Figure 3.14b. For strong temperature inversions, marked wind speed and wind direction events can form which indicate similarities to boundary layer beam currents. This will be considered in Section 3.3.

Special orographic conditions can also affect flow in the ground boundary layer in many ways. We name here changes in surface roughness in the direction of flow as well as flow over and around hindrances (high buildings, hills). In the model equations (Eqns. 3.1, 3.6, 3.9) surface roughness will be considered via the roughness height parameter H_o. A change in surface roughness along the path would correspondingly vary

according to the total wind profile. In contrast, research has shown that roughness jumps become part of the wind profile from below [65], [86]

/56

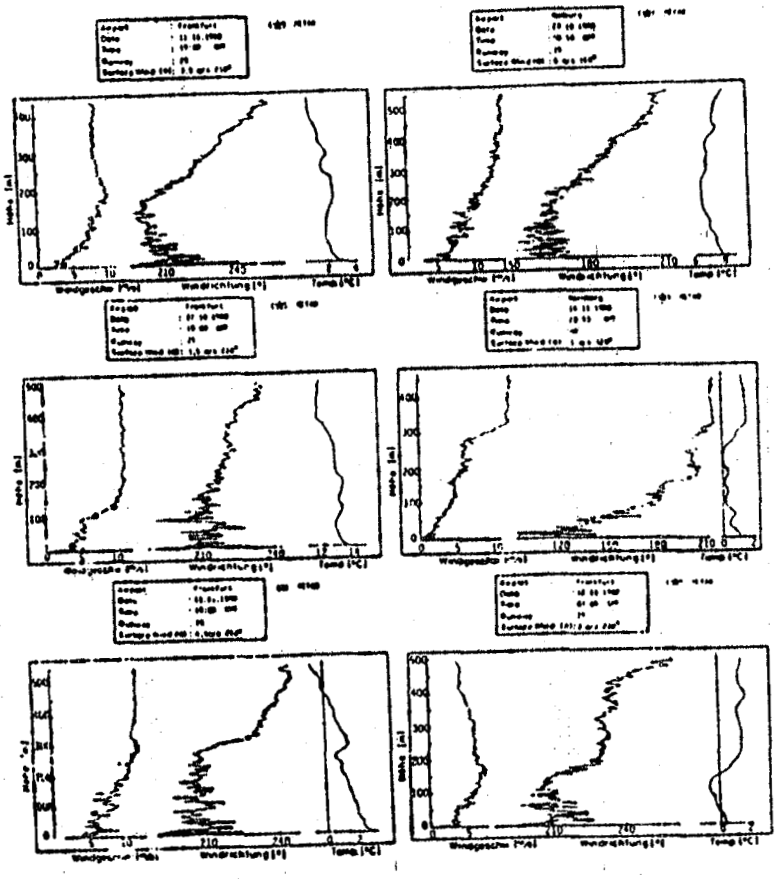

Figure 3.14a: wind profiles for changing temperature gradients

/57

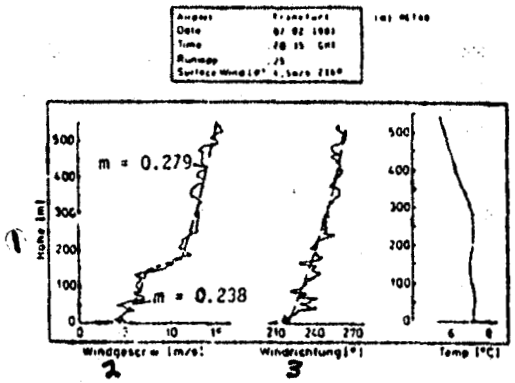

Figure 3.14b: sectional variation of model parameters
1-altitude (m), 2-wind speed, 3-wind direction

This is well recognizable from a logarithmic plot (Figure 3.15). For this a step in roughness height (in a countercurrent direction) from H_{01} to H_{02} was considered. A simple solution is described in /65/ which involves a superposition of the co-current wind profile $u(H/H_{01})$ with a disturbance speed DELTAu (X,H) resulting in:

$$\Delta u = -\frac{u_*}{k}\ln(H_{01}/H_{02}) + \frac{\Delta u_*(X)}{k}\ln(H/H_{02}). \qquad (3.22)$$

One might also consider the exponential law in which one expresses the exponents m and u_{ref} in suitable form as a function of H and X. The relationship between m and the function $u_*(X)$ or $H_0(X)$ to be determined can be produced via the relationships presented in Section 3.14.

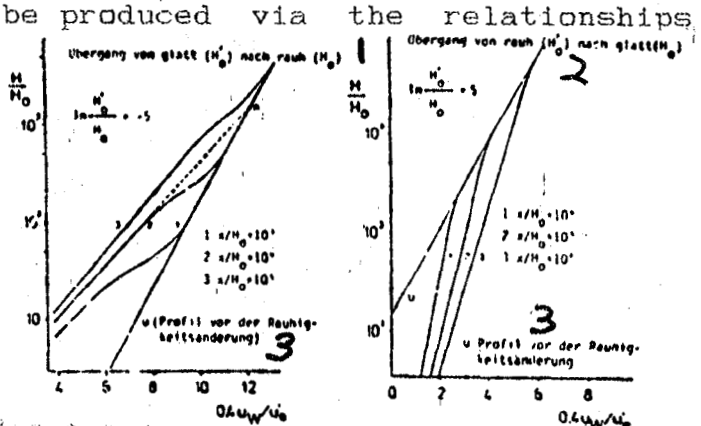

Figure 3.15: influence of changes in ground surface roughness on wind profile (from /86/), 1-transition from smooth (H'_0) to rough (H_0), 2-transition from rough (H_0) to smooth (H'_0), 3-u(profile in front of the roughness change)

Far greater influences affecting flow in the boundary layer can appear via "over flow" of ground hindrances, especially flow relationships on lee sides. Hills around airports can enter into safety considerations and research is currently being done in this area /66/. In the case of contour-parallel flow, negative effects on performance during takeoffs and landings are possible because of downcurrent components /67/.

In flow path research in the lee areas of hills appearances of flow separation are of special interest because they can be connected with considerable vertical wind changes. The basic separation mechanism here is described in /65/. The pressure disturbance generated by the hindrance affects in the windward side (luff) a flow acceleration, on the lee side a deceleration which can lead (in connection with a basic decrease of surface /59
flow speed) in certain areas to reverse flow. Outer flow separates from the surface and in the area between outer and reverse flow, fixed-location vortex can occur.

According to results chiefly from experimental research, separation behavior was influenced by certain conditions /65, 29/. Accordingly flow separation was forced by large luff- and lee-sided slope tendencies, small surface roughness or a roughness change from smooth to rough, stable atospheric layering and by the FROUDE number F:

$$F = \frac{u_0}{N L_1} \quad \text{with} \quad N = \sqrt{\frac{g\,(\partial\rho/\partial H)_\xi}{\rho_0\,(H = H_h)}} \qquad (3.23)$$

In this equation u_o is flow speed, L_1 is a characteristic length and d rho/dH is the vertical air density gradient for rho_o at the

upper end of the boundary layer (H=delta). Figure 3.16 shows flow forms at hills of smaller and average slopes in dependence on the FROUDE number (from /29/). The critical value F_{krit} is characterized here as the highest FROUDE number for which separation in the lee area is exactly suppressed.

The mentioned mountain range "Weidacher Höhe", west of the Stuttgart airport shows with values of 0.04 (East side) and 0.1 (West side) comparatively small average slope tendencies. From existing data fixed-location lee rotors were previously not determinable. In contrast measurement results give data about large, free vortexes which "swim" with the flow. Figure 3.18a shows an example from AIRBUS measurements which were made during a landing in a Weidacher Höhe lee at the Stuttgart airport. Above all the distance from the mountain range ridge being from 5 to 15 kilometers was comparatively large. Special resesarch on windshear situations in the Weidacher Höhe is being done at this time with a research aircraft by the Technical University at Braunschweig under contract to the Federal Minister for Transportation /66/. /60

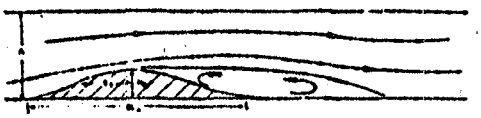

over-critical $F>F_{crit}$, no wave formation possible, controlled boundary layer separation

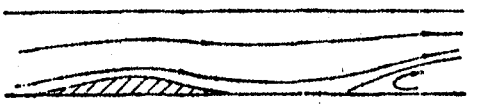

Hills with small slopes, undercritical Froude number, $F<F_{crit}$; no lee-side separation, countercurrent separation caused by lee waves

Hills with medium slopes, overcritical Froude number $F>F_{crit}$; boundary layer separation on the lee side

Undercritical Froude number for medium slopes, lee waves induced by separation on the lee side

Figure 3.16: (above and p.p.) flow forms above hills with smaller and medium slopes (from /29/)

For this, wind measurements take place along a defined flight path between runway 26 and the mountain range. Previously existing data indicated lee-side downcurrent areas with average values between 0.2 m/sec and 0.6 m/sec wherein wind relationships were subjected to significant changes in the time frame of one hour. Further, in a few cases typical vortex effects were indicated in wind components. In Figure 3.19a a corresponding example is depicted with a comparison to simulation results /61 (Figure 3.19b). One recognizes in both cases for the speed components induced by vortexes an extreme value in the headwind components and a null passage in the vertical wind component.

Similar effects in wind component patterns were also observed in the lee regions near the city of Frankfurt (Figure 3.18b). These effects could also have been generated by vortex created by large aircraft.

A model description of this influence for application in flight simulation is made possible by superposition of ground boundary layer profiles with viscous turbulence. The procedure thus

corresponds to the method described in the following for boundary layer flow. Tangential speed of a viscous vortex can be described with the following relationship /69/:

$$v_T(r,t) = \frac{\Gamma_0}{2\pi r}\left(1 - e^{\frac{-r^2}{4\sigma t}}\right)$$

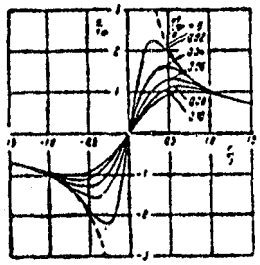

Figure 3.17: mathematical representation of a viscous vortex (from /69/)

For this relationship $GAMMA_0$ is vortex circulation at time t=0, r- the distance from the vortex core and σ the kinematic viscosity (Figure 3.17). Componential description of induced speed is further explained in Appendix A 5.3.2.

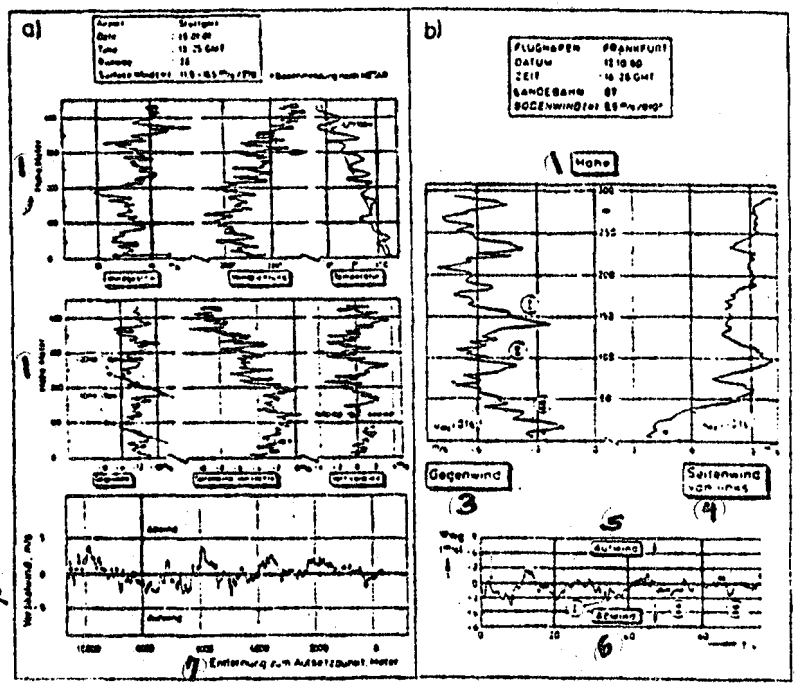

/62

Figure 3.18: vortex influence on wind component signals
1-altitude, 2-vertical wind, 3-headwind, 4-sidewind
6-upcurrent, 7-downcurrent

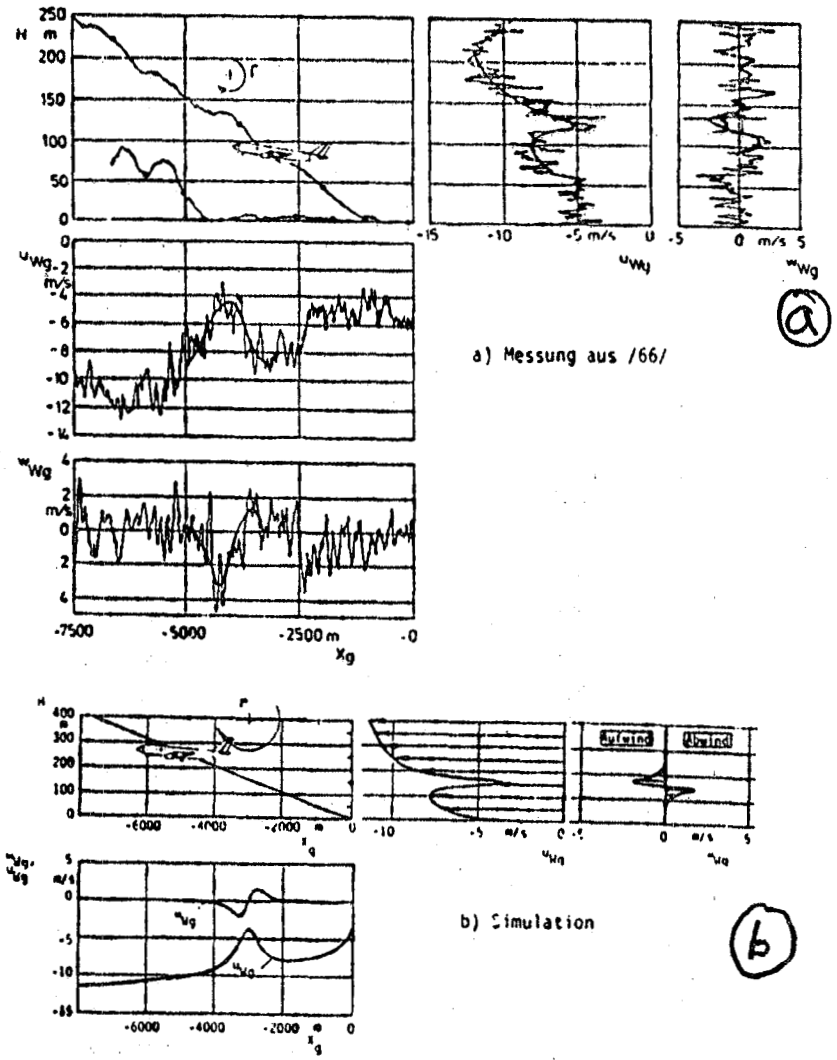

Figure 3.19: characteristic wind pattern for underflying a vortex, a) measurements from /66/, b) simulation

3.3 Boundary Layer "Beam" Current

In Section 2 it was already explained that the term "boundary layer beam current" (in regard to aviation applications) had wide interpretation and thus included wind speed profiles as they are generally observed in weather situations with pronounced temperature inversions (Figure 3.20).

Russian research /35/ differentiates between two basic types of boundary layer beam currents. The corresponding wind speed patterns with altitude are depicted in Figure 3.21 on the basis of 71 or 78 observations in the form of average values and standard deviations at five measurement altitudes (0, 100, 200, 300, 500 meter). Even if vertical separation is very small and the actual wind maximum is coincidentally detected, significant differences in profile form come to light. While for Type I a pronounced wind speed maximum occurs, Type II shows a continuously increasing wind speed, wherein from one determined altitude further speed increases are very small. There is no data concerning wind direction patterns.

Both basic forms were observed in the AIRBUS measurements as the examples in Figure 3.22 show. For reasons of appearing inertial oscillation the nightly boundary layer beam current represents an unstationary phenomenon. Because the significant windshear region is flown through in one to two minutes when landing and the period of inertial oscillation is of the order of magnitude of 15 hours, one can limit oneself to a quasistatic model for mathematically describing this wind situation in aviation

technology.

A similar speed distribution appears for a flow mechanics problem which is labeled a "planar wall beam" in the literature and is the subject of much research.

/65

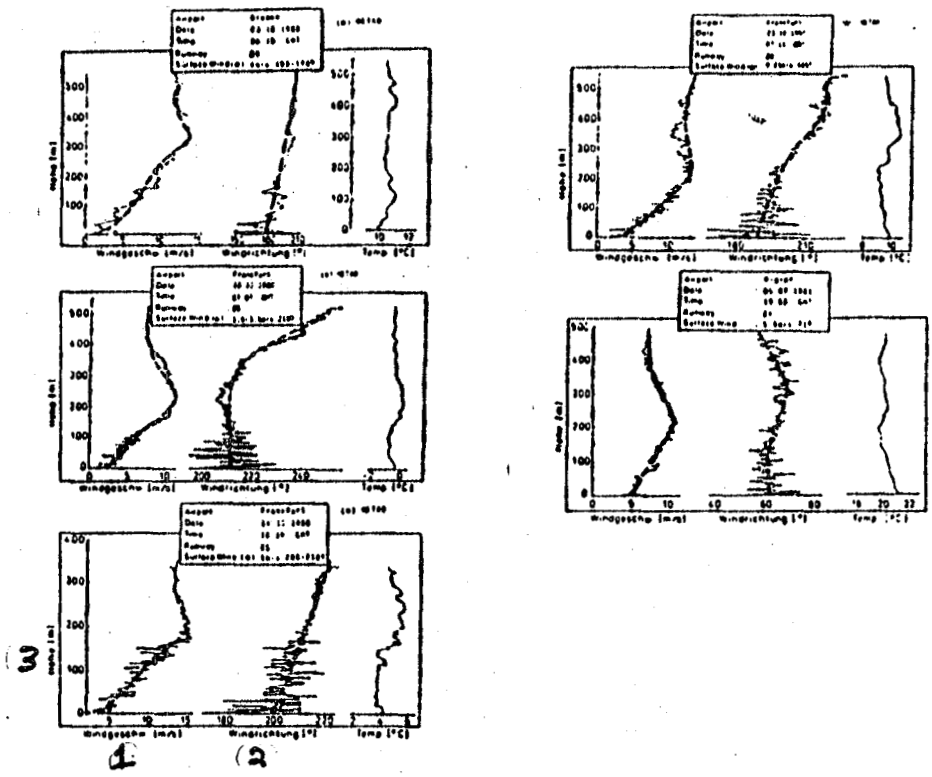

Illustration 3.20: wind profiles with "beam flow" characters (small keys read in English: airport, date, time, runway, surface wind) 1-wind speed, 2-wind direction, 3-altitude

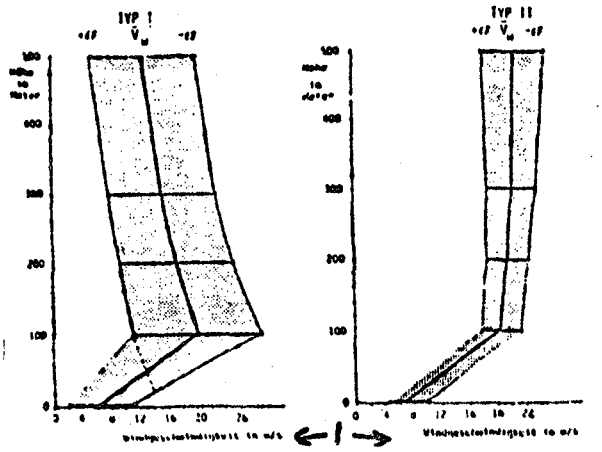

Figure 3.21: Basic types of boundary layer beam flows from /35/
1-wind speed in m/sec

Herein we are concerned with a planar free flow of great width which emanates from a narrow opening and flows along one side of a wall while on the upper side mixing takes place with stable or displaced air (Figure 3.23). In proximity to the wall, speed distribution has the character of boundary layer flow and has at great distance from the wall the appearances of a free "beam." Figure 3.23 shows speed profiles from measurement results /21/ for differing distances from the exit opening. Boundary layer thickness height and flow speed are related to the value u_1 above the boundary layer. One recognizes a decrease in the velocity maximum and an increase in flow strength and height of the maximum with increasing distance from the flow exit.

Thus a basic difference in boundary layer flow becomes clear, being conditioned by excitation of wall flow as, for example, exit through an opening directly above the wall. Through this there result speed maxima at comparatively small distances from the wall (3 to 35% of the boundary layer thickness).

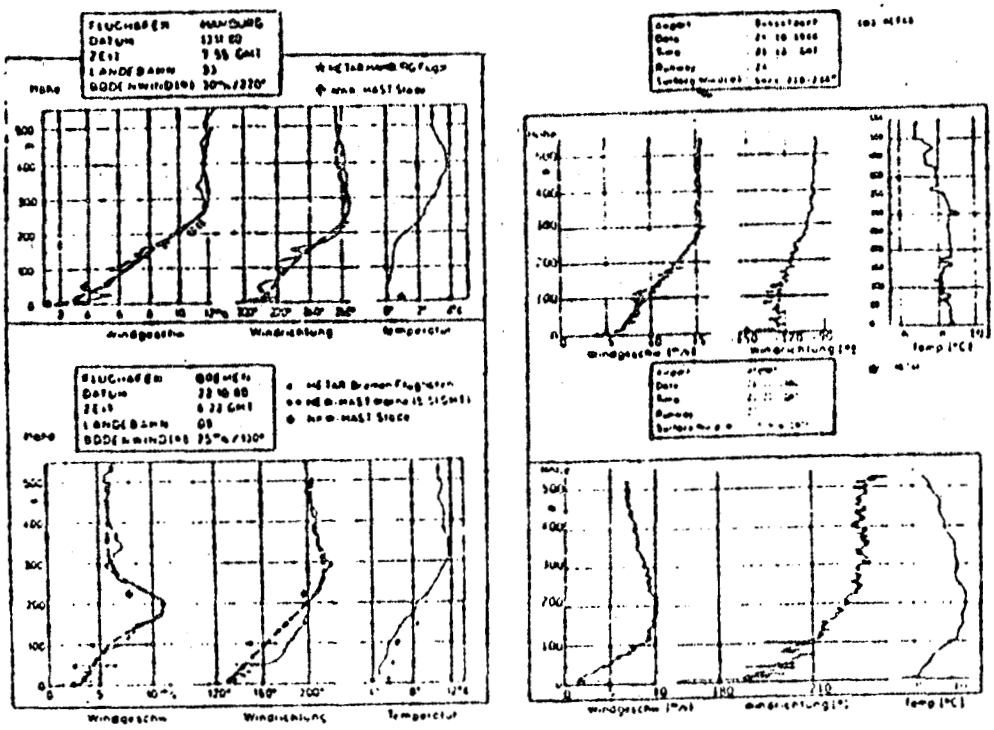

Figure 3.22: examples of aircraft measurements
1-airport, 2-date, 3-time, 4-runway, 5-surface wind
6-altitude, 7-wind speed, 8-wind direction
9-temperature

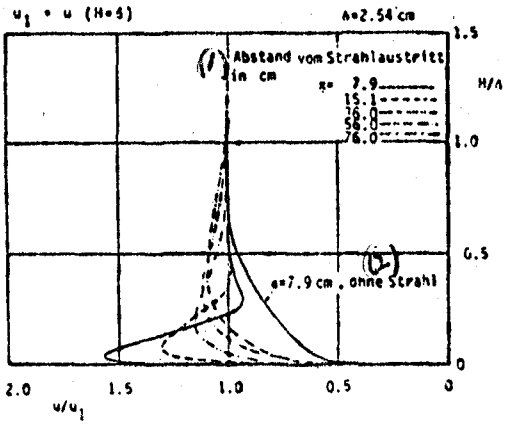

/68

Figure 3.23: speed distrubutions in a wall flow from measurements /21/, 1-distance from flow exit in cm, 2-without flow

Measured beam flows show by contrast maxima at 25 to 75% of boundary layer height. Moreover, nightly boundary layer flow can be far from horizontally homogeneous so that for the distances considered here the values u and $H(u_{max})$ must be considered as dependent on the coordinate X. Theoretical solutions for wall flow essentially relate to flow in the contacted environmental air and originate in a dissection of the boundary layer at the altitude of the flow maximum /11, 12/. For wall flow in moving boundary layer flow there are no analytical solutions extant. There are however a few numerical solutions mentioned in /72/. A simple approximation for describing speed patterns in the boundary layer flow is obtained by superposing a surface boundary layer profile onto the vertical speed profile for a planar free flow jet. This works because there are analytical solutions for /69
both portions. Speed distribution in turbulent flow was determined by REICHARDT /9/ and GOERTLER /10/ and is described in several technical texts /69, 34/ (see Figure 3.24). As regards speed of the flow maximum there results the following for the horizontal components:

$$\frac{u(X,H)}{u_e(X)} = 1 - \tanh^2\left(k\frac{H}{X}\right) \qquad (3.24)$$

Because for the mentioned reasons there is no dependance on path, Eqn. 3.24 simplifies to:

$$\frac{u(H)}{u_e} = 1 - \tanh^2\left(C_e \frac{H - H_e}{H_e}\right) \qquad (3.25)$$

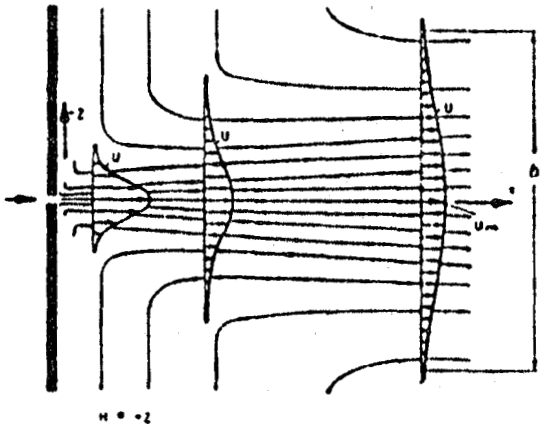

Figure 3.24: flow lines and speed distribution in free flow from /69/

/70

By introduction of altitude H_s into the argument of Eqn. 3.25 it is considered that the flow lies symmetrical to surface distance of the speed maximum. If one superposes a boundary layer profile onto the flow portion corresponding to Figure 3.25 , one obtains the characteristic vertical speed profile of a boundary layer flow:

$$V_W(H) = V_{W,R}\left(\frac{H}{H_R}\right)^m + V_{W,s}\left(1 - \tanh^2\left(C_s\frac{H - H_s}{H_s}\right)\right) \qquad (3.26)$$

The parameter C_s represents a norm factor determined empirically which will be described later.

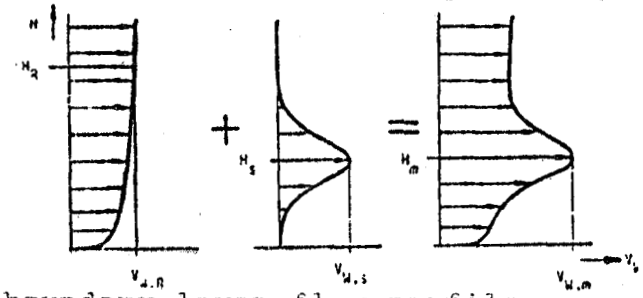

Figure 3.25: composition of the boundary layer flow profile

To describe wind rotation with altitude we will proceed in a similar fashion as was used for wind speed. The point of origin is formed by the directional course of the surface boundary layer profile from Eqn. 3.18b upon which a suited function is superposed. Even if the range of variation of directional profile is comparatively large, a function is indicated which describes the flow portion according to Eqn. 3.25 - in most cases as a usable equation (Figure 3.26). /71

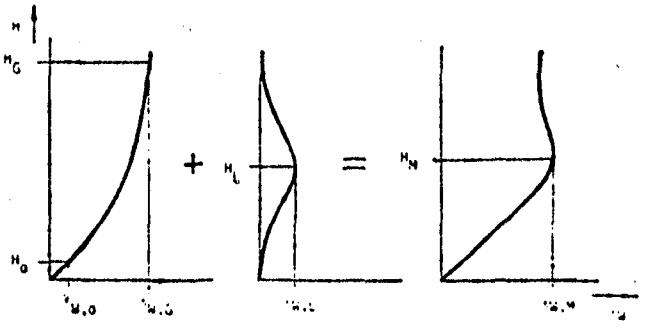

Figure 3.26: composition of the directional profile

Thus wind direction deviation is expressed at altitude H compared to altitude H_o in a first order approximation using the following relationship:

$$\chi_W(H) = \chi_{Wo} + \arctan\left(\frac{H - H_o}{H_G - H_o} \tan(\chi_{W,G} - \chi_{Wo})\right) + \\ + \chi_{W,L}\left(1 - \tanh^2\left(C_L \frac{H - H_L}{H_L}\right)\right) \qquad 3.27$$

Convenient model parameter fitting into a measured wind pattern is possible as a rule with a few iterations. Figure 3.27 shows two such examples. To simplify the procedure there are optimization methods based on least squares. In Appendix A3 the principle is explained and examples are given to compare model and measurement wherein model parameters are determined with the optimization method 'EXTREM' from JACOB /8/.

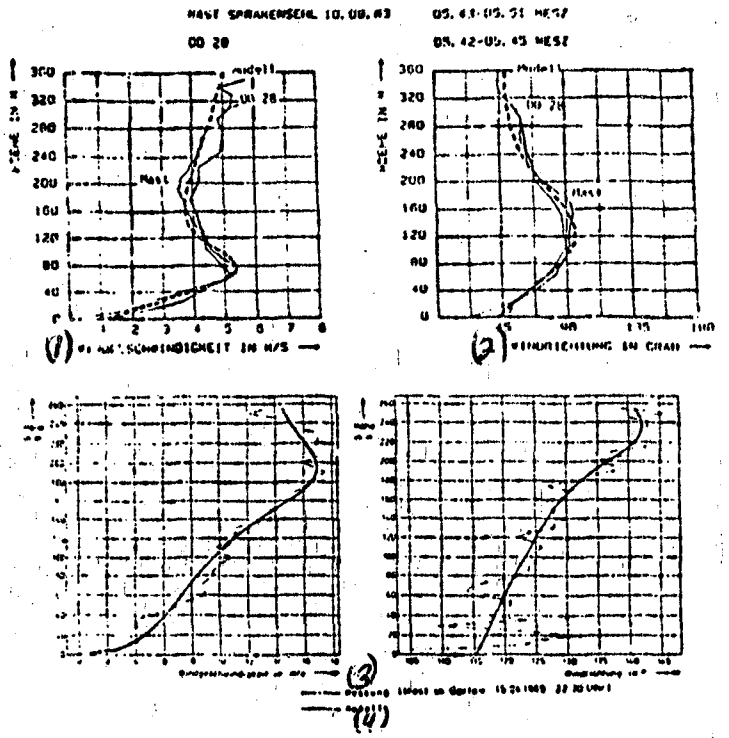

Figure 3.27: comparison of model and measurement
1-wind speed in m/sec, 2-wind direction in degrees
3-measurement, 4-model

In a few cases in which the speed maximum appears at several altitudes or the speed curve is described by a few sharp decreases above the maximum (Figure 3.28) a positive variation of the model laws is indicated. Herein the flow portion is superposed with a constant wind speed and multiplied with the surface boundary layer form function $(H/H_R)^*$ (Eqn. 3.28),

$$V_x(H) \quad (V_{G,R} - V_{x,s}(1 - \tanh^2(C_s \frac{H - H_s}{H_s}))) (\frac{H}{H_R})^m \qquad (3.28)$$

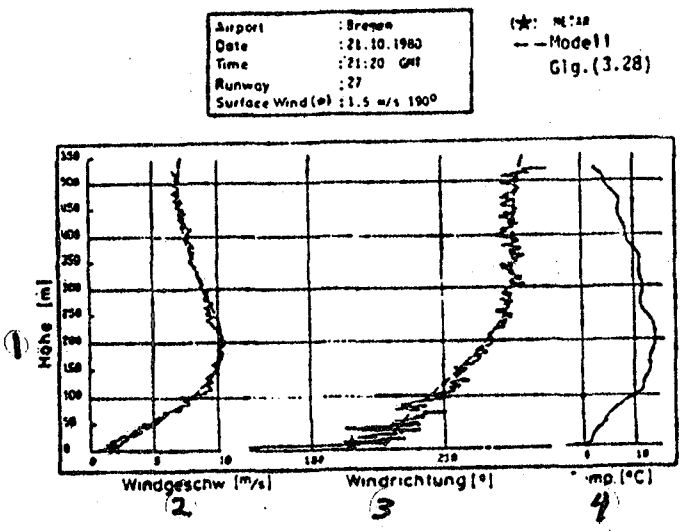

/73

Figure 3.28: comparison of measured profile with model eqn. 3.28
1-altitude, 2-wind speed, 3-wind direction, 4-temp

This means that the flow portion - especially below the speed maximum - indicates a boundary layer influence.

Efforts to determine model parameter dependencies on meteorological data and boundary conditions have been somewhat less than successful up til now,so it would be expected that temperature inversion strength or inversion layer thickness would have an effect on wind speed maxima. However there is so much data scatter that no functional dependency can be derived. From free-flow resesarch REICHARDT /4/ related speed and temperature distribution in turbulent free-flow in the following:

$$T/T_e = (u/u_e)^{A_T/A_q} \qquad (3.29a)$$ /74

Herein A_{tau} and A_q represent the appearing exchange values for impulse and heat during turbulent intimate mixing (for details see Appendix A4). From measurements /4/ a value of 0.5 was calculated for the relationship of both these values so that the following relationship is valid:

$$T/T_e = (u/u_e)^{1/2} \qquad |T| = °C \qquad (3.29b)$$

The temperature pattern was empirically approximated by REICHARDT

/4/ using:

$$T/T_s = e^{f(H)}$$

$$\text{with } f(H) = -\tfrac{1}{4}(H/H_R)^2 \qquad (3.30)$$

wherein the temperature maximum likewise appeared at the flow maximum altitude, the temperature profile is broader than the speed profile. From Eqn. 3.25 results the flow portion according to Eqn. 3.29b as a function of the form:

$$T/T_s = 1 / \cosh\left(C \frac{H - H_s}{H_s}\right) \qquad (3.31)$$

If one compares speed and temperature profiles for measured boundary layer flows (see also Appendix A3) similar relationships between both profiles can be found in a series of measurements if one considers the temperature profile to be made up of a portion which changes linearly with altitude and a flow portion from Eqn. 3.31. In this case the corresponding portions of speed and temperature profiles stand together (surface boundary layer and linear temperature pattern as well as the flow portion) in a relationship. Figure 3.29 shows a few examples for this. It is above all to be remembered that analogies between free flow and boundary layer flow must be restrained for reasons of differing /75
mechanisms of origin, influences and boundary conditions (e.g. temperature inversions via surface heating, flow across the rotating Earth). It is thus no wonder that in a few cases the flow portion temperature maximum lies above the speed maximum, somewhere in the range of maximum wind rotation or thereabouts (see Appendix A3).

Dependences between basic parameters like wind speed maxima, maximum wind rotation and attendant altitude on the one side and

absolute temperature change, inversion layer strength on the other side could not be uniquely determined until this time.

Via statistical evaluation of a series of measurement results there are at least reference values for the order of magnitude of essential values. For the AIRBUS measurements and mast measurements in Northern Germany, wind maxima were usually observed in the upper half of the inversion layer between 70 and 340 meters altitude whereby the wind speed maximum value attained values of up to 17 m/sec. Wind speeds at the reference altitude of 10m lay between 1.5 and 4.0 m/sec and thus characterized weak wind position. We have already **reported** about the great range of variation in wind direction patterns in contrast to wind direction at 10m altitude. Maximum wind rotation in contrast to wind direction at 10m altitude lay between 3 and 90 degrees with maxima in the altitude range between 130 and 450 meter (mostly at the upper boundary of the inversion layer). In the upper line of Table 3.1 there are basic data based on 26 measured wind profiles in the form of average values and standard deviations.

One can learn from the data of SHELKOVNIKOV /35/ that in the Soviet Union high wind speeds were observed in boundary layer flows (see Figure 3.18 and Table 3.1, lower line).

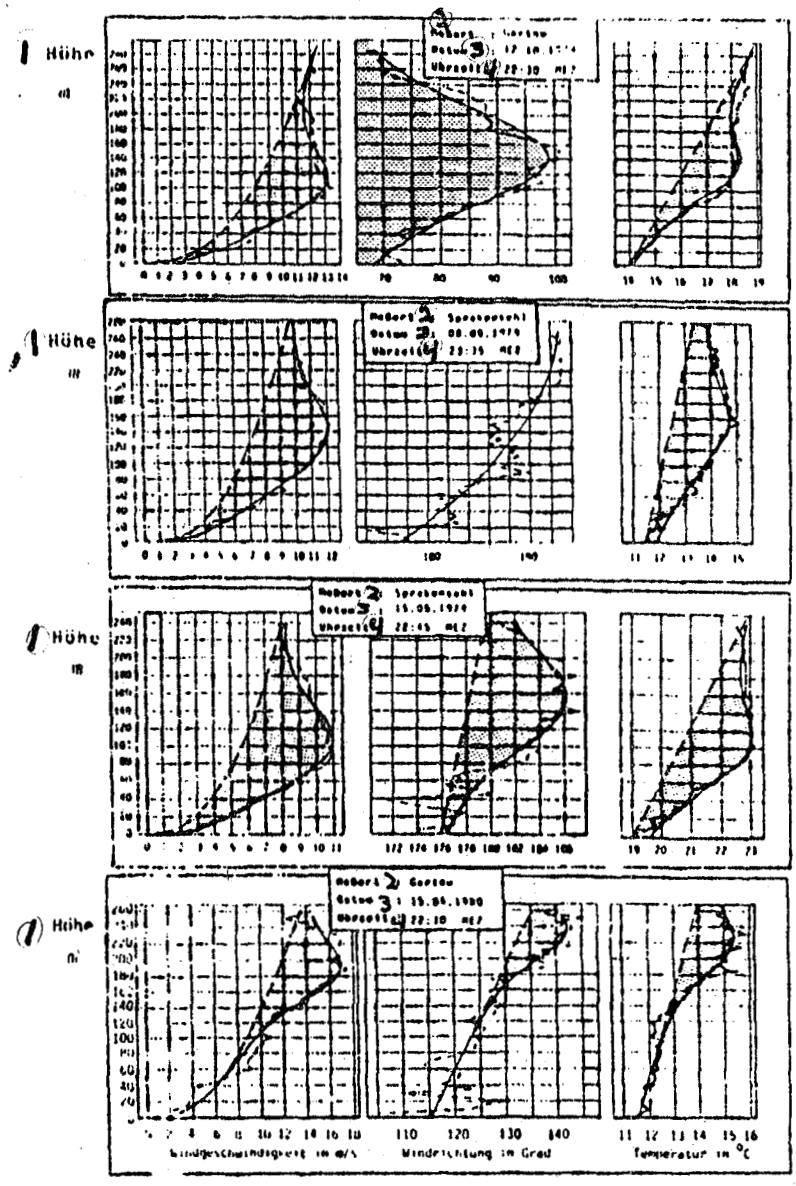

Figure 3.xx: relationship between wind speed and temperature profile, 1-altitude, 2-measurement location, 3-date, 4-time

	$V_W(10\,m)\pm\sigma$ in m/s	$V_{W_S}\pm\sigma$ in m/s	$V_{W,max}\pm\sigma$ in m/s	$C_s\pm\sigma$	m_s
(1) Messungen in Norddeutschland	3.17±0.89	4.27±1.56	9.34±4.0	2.12±0.9	0.33±0.11
(2) Sowjetunion /35/	7.0±5.0		20.3±9.2		

	$H_m\pm\sigma$ in m	$\alpha_{W,m}=\alpha_{W,L}\pm\sigma$ in Grad (4)	$C_L\pm\sigma$	ΔT_m pro $\Delta H=0$	Dicke der Inversionsschicht(en) (3)
(1) Messungen in Norddeutschland	123.0±82.7	47.1±40.2	2.19±1.97	4.1±1.92	166±98
(2) Sowjetunion /35/	150±50				

Table 3.1: typical GS parameters from aircraft and mast measurements, 1-measurements in Northern Germany, 2-Soviet Union, 3-inversion layer thickness, 4-in degrees

An increase in wind speed of 7 m/sec in 10m altitude to a maximum value of 20 m/sec is taken as a determined plot/course. In 67% of 175 cases wind speed maxima were observed in the region between 100 and 200m. Herein there appeared vertical windshear gradients inside the lower 100m thick layer of 4 m/sec and 10 m/sec per 30 meters altitude interval. The "worst case" scenario for a boundary layer flow is likewise to be learned from /35/. For Type I (distinct wind maximum) the result is given for a mast measurement in Khabarovsk (Figure 3.30a). Also plotted are measurement points for wind speed and temperature over altitude. Information for wind direction patterns was not given.

Conditioned by small altitude dissociation (5 measurement points at 180m altitude difference), model parameters cannot be uniquely determined. Under consideration of the typical model values listed in Table 3.1, especially the form factor C_s, localization of realistic values is easily possible. The factor C_s represents the relationship between altitude H_m (wind speed maximum) and the vertical strength B of the flow portion wherein the limit is

defined as 7 percent of the wind speed maximum (see illustration). In this case the approximation listed below is valid:

$$B = 4 * H_s / c_s \qquad /78$$

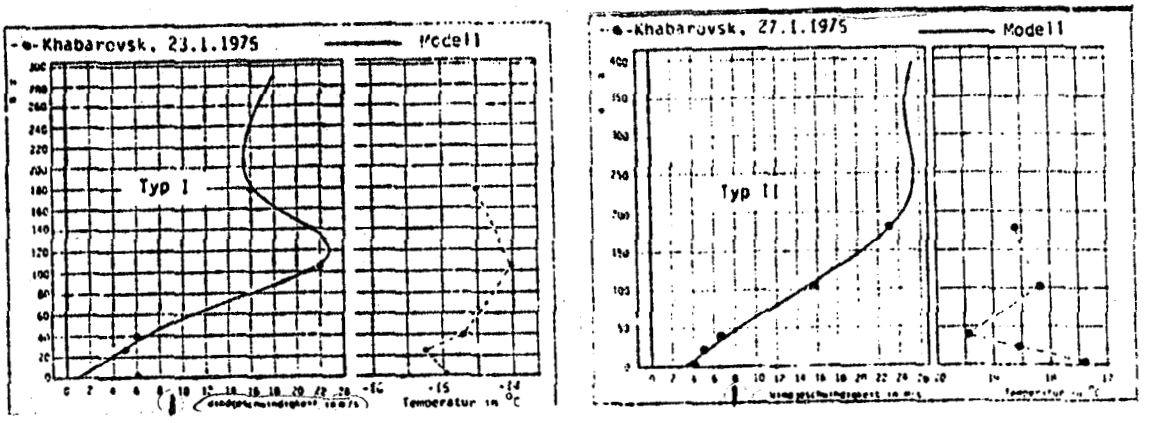

Figure 3.30: worst case GS profiles from /35/ and models
1-wind speed in m/sec

With the model parameters combined in Appendix A5, measurement points at 25m altitude are well approximated. Above all the decrease in wind speed cannot be formed in the lowest 25 meter section using the model.

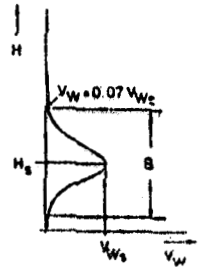

/79

In the same manner (however with the same limitations as regards high altitude measurement resolution) flow Type II can be approximated by models (see Figure 3.3b or Appendix A5).

In conclusion it could be said that via simple half-empirical rules, simple models can be won for determining vertical wind speed profiles and wind direction profiles with which measured wind patterns can be well described. Exponents determined for the boundary layer portion (exponential law) (average value m= 0.33 +/- 0.11) stand principally in correlation with research results as depends on atmospheric stability (see Section 3.1).

3.4 Models for Windshear and Downdrafts in Thunderstorms

The fact that of 15 windshear-caused accidents occurring since 1970 which have been analysed by the U.S. Safety Board, and in which 12 cases thunderstorm influences played a role indicates that there is a significant danger to air traffic from this type of dangerous situation. Thus research activities focused early on modeling description of this phenomenon. Generally three different methods are used to simulate thunderstorm downdrafts. In the first case determination of wind data is done from wind data which are obtained above all from mast measurements. Many thunderstorms were studied with the help of a 481m mast at the NATIONAL SEVERE STORMS LABORATORY in Oklahoma /43/ and certainly in the form of three wind components in specified time and altitude intervals. For a known thunderstorm suction speed, time dependence can be carried over into path dependence. In order to obtain usable wind speed at every point in the measurement region for simulation calculations, suited interpolation methods are used. The adantage of this procedure lies above all in the existence of realistic data for flow fields for simulation purposes. In contrast there are no possibilities for variation in thunderstorm contour and speed distribution. The second method uses mathematical models for typical thunderstorm situations on the basis of the NAVIER-STOKES equation of motion. Here in the scope of meteorology, very expensive dynamic models were developed (e.g. THORPE et. al. /68/) which were however not used here because of high computation cost and low resolution for

the tasks considered here.

/81

Better suited are simple models for describing the flow field which refer back to known solutions from flow mechanics. Figure 3.31 shows as an example the speed curve of a viscous stagnant flow which arises if a rotation-symmetrical free flow appears on a planar surface. The Downburst model of KRAUSPE /36/ originates in a simplified stagnation flow which omits ground surface friction (potential flow).

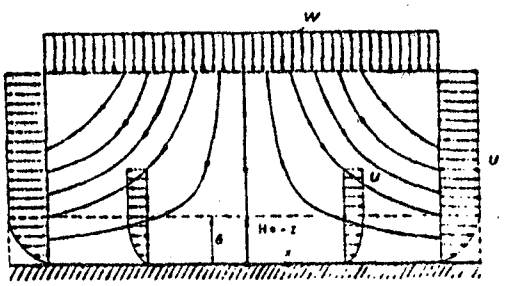

Figure 3.31: flow line figure for stagnant flow from /69/

Planar stagnation flow is a solution for the potential equation and must fulfill the boundary conditions for rotational freedom (rot(V)=0) and continuity (div(V)=0) under the condition of frictionless as well as source and sink-free flow. Wind speed can be expressed as a gradient of a speed potential phi to be determined:

$$\underline{V}_g = \text{grad}\ \Phi\ (x,y,z) \qquad (3.32)$$

Combination of the locations of equivalent gradients grad phi and thus equivalent wind speeds gives the flow line psi = constant, whose direction correlates at every flow point with the direction /82
of the associated speed. As an arrangement for the speed potential KRAUSPE selected the following relationship:

$$\Phi(x,y,z) = 1/2\,(ax^2 + by^2 + cz^2) \qquad (3.33)$$

Thus one obtains wind components which change linearly with the corresponding coordinates:

$$\begin{aligned} u_g &= d\Phi/dx = a\,x, \\ v_g &= d\Phi/dy = b\,y, \\ w_g &= d\Phi/dz = c\,z \end{aligned} \qquad (3.34)$$

and the corresponding constant wind gradients:

$$\begin{aligned} u_{gx} &= du_g/dx = a \\ v_{gy} &= dv_g/dy = b \\ w_{gz} &= dw_g/dz = c \end{aligned} \qquad (3.35)$$

This is basically verified with observations but is only valid for tightly limited core region flow. According to research in /36/ a linear relationship between the gradients u_{Wx} and w_W can be utilized in a comparison with measurement for a first approximation, that is c = -5a. To fulfill the continuity conditions, the following must be valid:

$$\begin{aligned} u_{gx} + v_{gy} + w_{gz} &= 0 \\ \text{bzw.} \quad a + b + c &= 0, \end{aligned} \qquad (3.36)$$

so that a value of b = 4a is attained for the gradient u_{Wy}.

Other relationships for speed potential were studied in /39/ however the relationships mentioned above give the best results for fitting measured wind patterns.

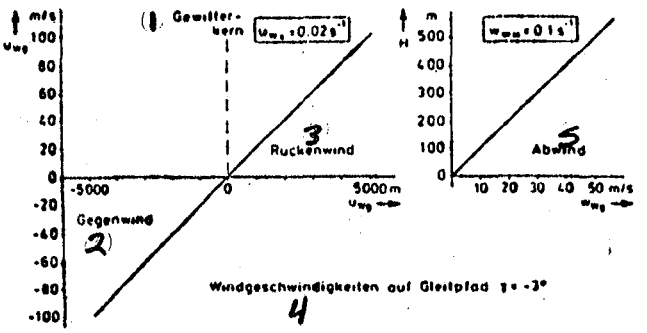

Figure 3.32: speed patterns for stagnation point models /36/
1-thunderstorm core, 2-headwind, 3-tailwind
4-wind speed on glide path gamma = -3°, 5-downdraft

It is easy to see that the range of validity for the stagnation point model is limited to thunderstorm cores. Speed components steadily grow with increasing distance from the ground or the axis of symmetry of the core and attain almost unrealistically high values. For simulation of takeoffs and landings through a thunderstorm flow field the model had to be expanded via surrounding air flow and transition regions between surrounding flow and core flow /39/. Figure 3.33 shows speed distribution for the expanded stagnation point model in a region at about 6000x500 meters. The darts in the individual points represent magnitude and direction of the local wind vector wherein for reasons of increased clarity the ordinate was extended. Surrounding air flow behind the core is formed in front of the core by a viscous vortex by a translation flow (Figure 3.33). In the place of a vortex, warm air can also be considered via inverse stagnation point flow /39/.

/84

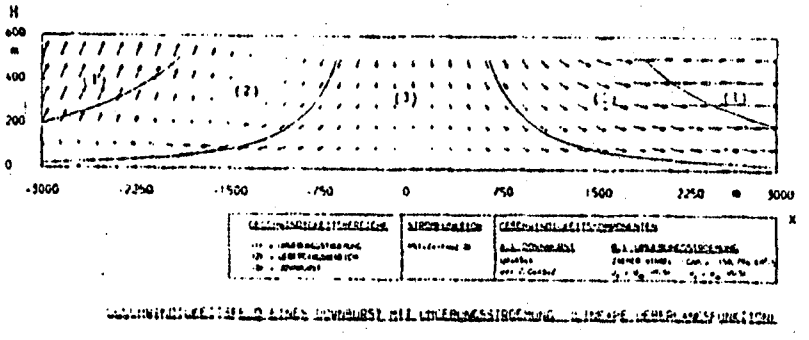

Figure 3.33: speed field for an expanded stagnation model (key illegible)

A further possibility for modeling wind fields in thunderstorms is offered by superposition of a number of vortexes or their induced flow speeds wherein the surface influence is generally considered by "reflection," thus by virtual vortex cores in the area of negative surface distances. Rules for three-dimensional downburst models are mentioned and better described in /40/ and /16/. Figure 3.34 shows the principle of a ring vortex model, Figure 3.35 shows a flow line curve for a vortex surface method.

With the model illustrated in Figure 3.35 we are concerned with a vortex surface doublet in which the two opposing horizontal circular surfaces at altitudes H_x and $-H_x$ are activated with potential vortexes of differing circulation distribution. In this way updraft regions appear at comparatively small distances from the flow core as they were observed in several measurements in /40/. Fitting the model to results obtained from mast measurements in thunderstorm squalls appears to have limited possibilities. /85

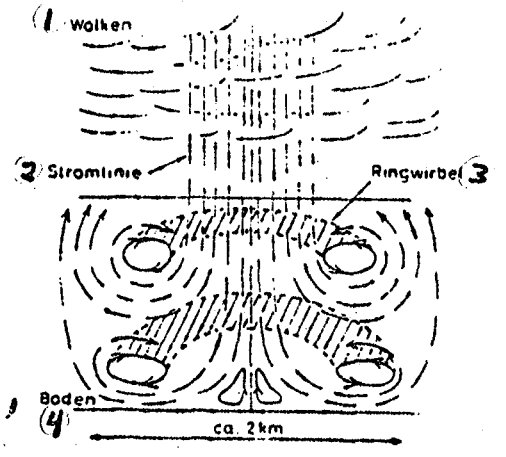

Figure 3.34: the principle of ring vortex models from /16/
1-clouds, 2-flow line, 3-ring vortex, 4-ground

If one selects superposition of discrete vortexes with variable local coordinates instead of the vortex surface doublet for the vortex core, then greater possibilities for variation are attainable for representing the flow field. Thus instead of potential vortexes, viscous vortexes are utilized in order to obtain finally induced speeds in the region of the vortex core. If one considers the gathered equations in /40/ for wind components for a three-dimensional vortex surface doublet model then the not inconsiderable computation expense drops out. Thus a limitation to the two-dimensional case should be undertaken. Figure 3.36 shows the flow field which results from superposition of induced speeds of 9 vortex pairs (see Appendix A5).

/86

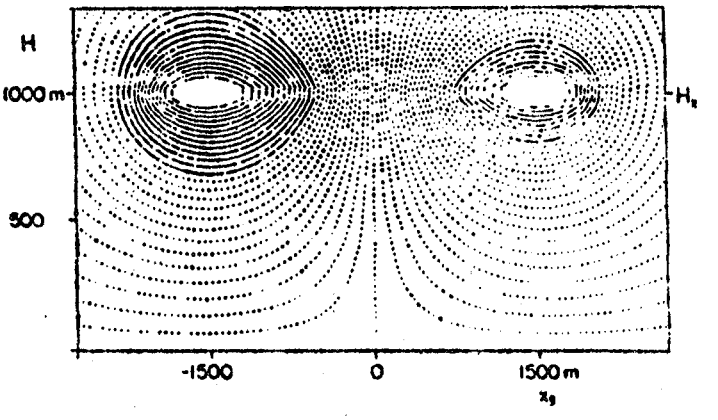

Figure 3.35: flow line curve for a downburst model cross section from /40/

The order of magnitude of appearing wind speed can be taken from the three following diagrams where the wind components are plotted along a glide path (gamma = -3°) through a downburst. This representation permits good possibilities for comparison with wind curves reconstructed from accident investigations and permits fitting model parameters. Fitting takes place essentially via selection of number and position of the vortex

and its circulation strength. The advantage to this method consists chiefly in that one can obtain a continual, cohesive flow curve without having to define special regions or sections (transition zones, surrounding flow). So it is possible to model a downburst including a squall front in closed form as is shown in Figure 3.37.

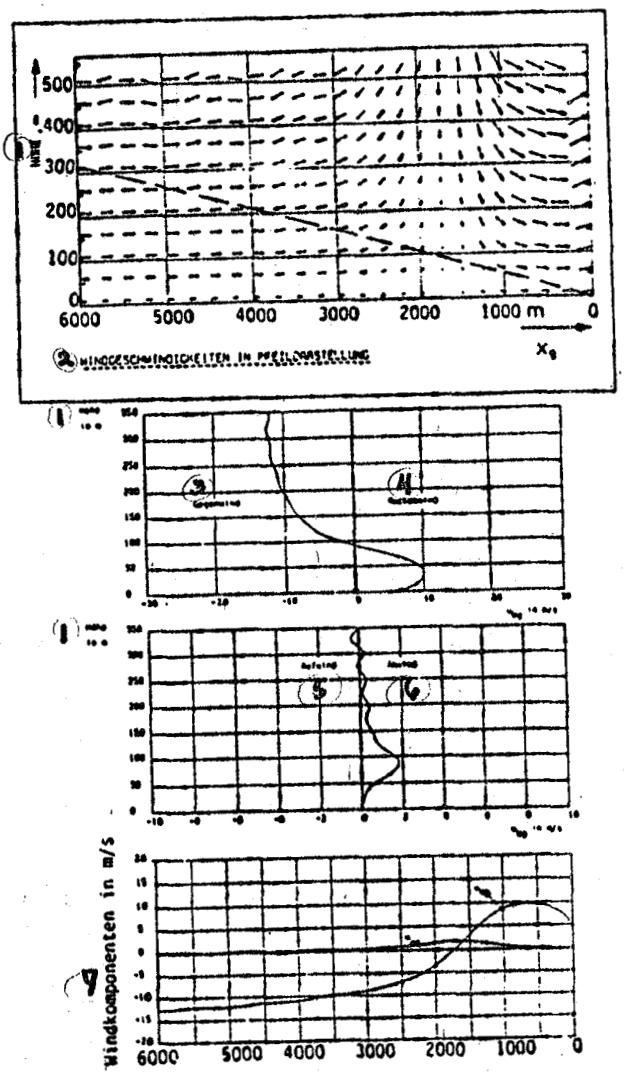

Figure 3.36: flow field and curves for wind components along a glide path of gamma = -3^{o} (vortex model)
1-altitude, 2-wind speed in dashed form,
3-headwind, 4-tailwind, 5-updraft, 6-downdraft,
7-wind components in m/sec

/88

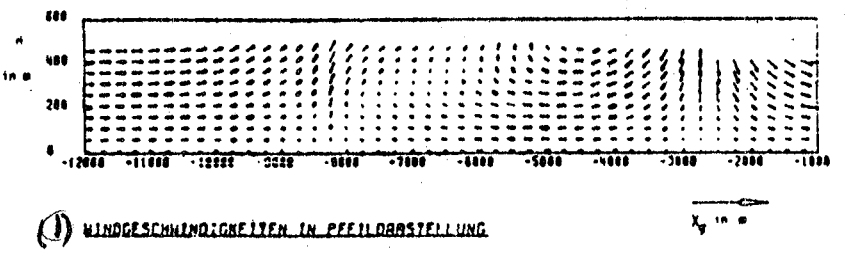

Figure 3.37: representation of a downburst and squall front with the vortex model
1-wind speed in dashed form

An enhancement of this model to a three-dimensional case can be realized by application of ring vortexes in place of planar vortexes. A mathematical description can be found in /83/ where components of the induced speeds are placed in tabular form.

/89

3.5 Windshear in the Flowfield of Fronts

Flow processes in warm, cold and thunderstorm squall fronts can assume differing and complicated forms as mast measurements of flow line diagrams in Appendix A6 show. SINCLAIR /38/ was able to record wind curves in fronts during steep angle landings with helicopters (Figure 2.8). As a typical characteristic one would recognize distinct temperature inversions, wind rotations of up to 130 degrees and an increase in wind speed inside the inversion layer. SINCLAIR gives for the horizontal wind component curve in the shear layer along the flight path a simple model:

$$u_{Wg} = V_{Wo} \cos x_{Wo} \left(\frac{H - H_o}{H_D}\right) \left(V_{W,H} \cos x_{W,H} - V_{Wo} \cos x_{Wo}\right)$$

$$v_{Wg} = V_{Wo} \sin x_{Wo} \left(\frac{H - H_o}{H_D}\right) \left(V_{W,H} \sin x_{W,H} - V_{Wo} \cos x_{Wo}\right) \qquad (3.37)$$

wherein the shear layer thickness is expressed by H_o and the lower shear layer boundary through altitude H_o. V_{Wo} and x_{wo} are the associated wind speeds or wind directions. Accordingly

horizontal wind components can be described inside the shear layer by approximation with constant wind gradients u_{WH} and v_{WH} which under certain boundary conditions agrees with the special stationary solution of the NAVIER-STOKES equation for planar flow in a narrow layer between two boundary surfaces in motion.

On account of horizontal nonhomogeneity in frontal flow fields, the above model which describes wind components along a completely determined flight path is only usable for simulation in special cases. It is aggravating that vertical components are not existent which according to experience have a pronounced effect on the aircraft energy balance. Thus there are solutions /90 to be sought which realistically describe the curves of all three wind components as a function of location.

In flow mechanics, solutions for flow surface branching are given which can be adapted for the problem at hand. Flow relationships given in Figure 3.38 can be described by the following equation system from /30/:

$$u = b \cdot x \cdot H + c \cdot H^2$$

$$v = -b \cdot H^2/2 \qquad (3.38)$$

For the front plane slope angle the following is valid:

$$\tan \vartheta = -3/2 \cdot b/c \; . \qquad (3.39)$$

If one superposes a linear flow with transverse flow which changes with altitude:

$$v = k \cdot H \qquad (3.40)$$

one obtains a three-dimensional flow like that depicted in Figure 3.38b.

In both cases the NAVIER-STOKES and continuity equations were satisfied. Because u and w components increase with the square of altitude, unrealistically high speeds are reached very quickly. There are thus - like the thunderstorm model - different regions for core, transition and surrounding flows to be defined or equations to be modified (3.38). If one reduces the exponents of H to 1, this describes the arising equation system in the flow form represented in Figure 3.39. u and w components only increase linearly here with altitude.

/91

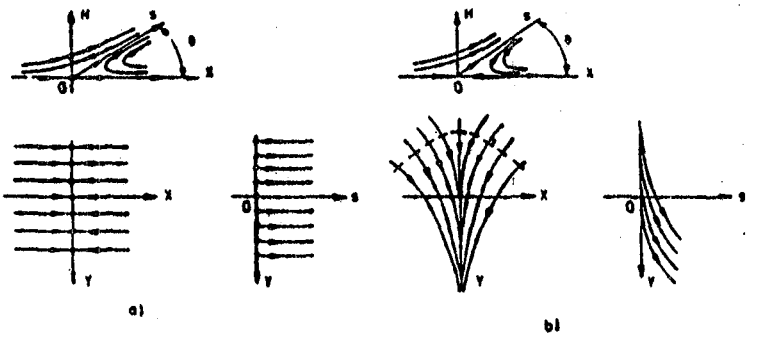

Figure 3.38: two and three-dimensional flow surface branching from /30/

From /30/ one obtains the solution for this case:

$$u = e \cdot x + f \cdot H$$

$$w = -e \cdot H \qquad (3.41)$$

$$\tan \theta = -2 \cdot e/f$$

For the task at hand only the positive altitude range will be considered. Here the flow curve corresponds in principle (from Eqn. 3.41) to the relationships which were found for squall fronts. As was already shown from Eqn. 3.39, by selection of relationship e/f one can obtain an arbitrary slope angle in the plane of the front. According to size of the simulation area it is sensible to undertake a limitation of wind component

magnitude, for example, such that it is set constant outside the region to be defined. /92

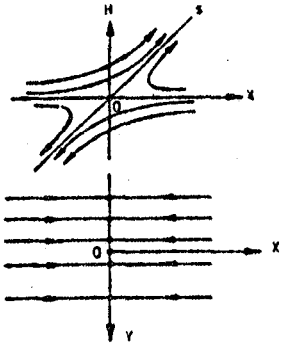

Figure 3.39: free flow surface branching from /30/

Figure 3.40 shows the result of a modelled description of slow relationships in a front using Eqn. 3.41. The speed field is represented in a region of 6000x1000m. One of the u-components obeying the exponential law can be superposed for transverse flow.

If one compares magnitude and direction of wind speed along a glide path (gamma = -3^{o}) with measurement results from /37/ one can see a fairly good correlation in principle (Figure 3.41).

In Section 3.4 it was demonstrated that squall fronts in thunderstorms can be modelled similarly to flow in downbursts by superposition of induced vortex speeds. This method offers further possibilities for description of flow relationships in fronts. /93

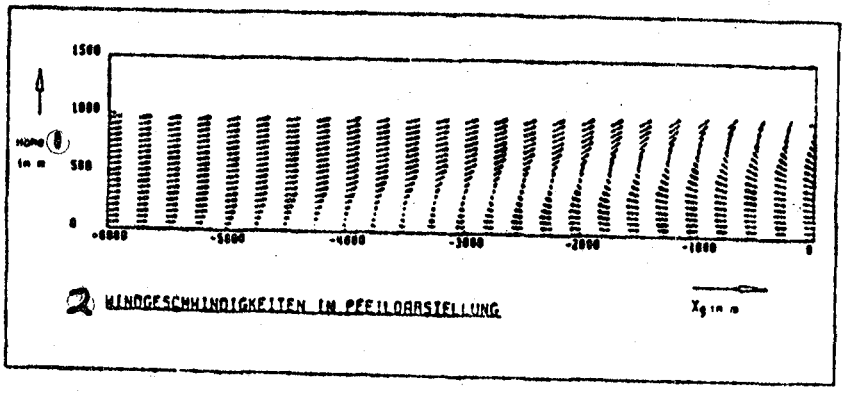

Figure 3.40: simulated frontal flow from Eqn. 3.41
1-altitude, 2-wind speed in dashed form

Figure 3.42 shows a corresponding example which was produced with 9 vortex pairs. Because wind speed did not decrease on the ground here, wind components will be multiplied with a boundary layer form function. In comparison to the method described above, transitions in the front plane are not so sharply defined as in vortex methods.

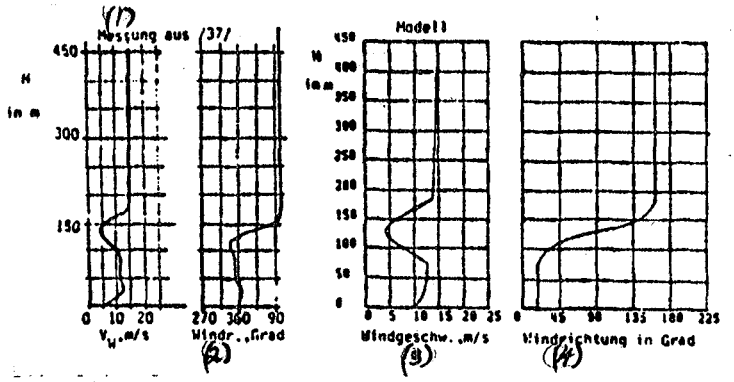

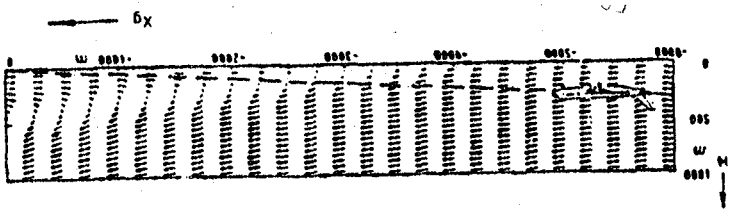

Figure 3.41: measured and modelled wind curves from sloped flight paths in a front, 1-measurement from /37/, 2-wind direction in degrees, 3-wind speed in m/s, 4-wind direction in degrees

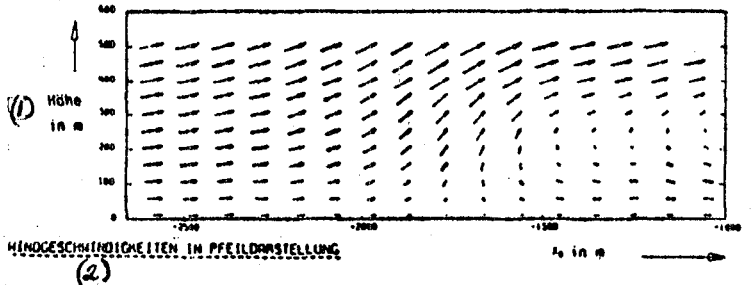

Figure 3.42: front flow according to the vortex method
1-altitude in m, 2-wind speed in dashed form

4. Resesarch on Critria for the Strength of Windshears and for Endangerment of Flight Traffic

4.1 The Vertical Windshear Gradient

To describe windshear strength, local wind gradients are generally the basis. In aviation technology and aviation meteorology researchers have concentrated above all on change in wind speed or wind components at an altitude interval of DELTA X =100 feet. For path dependent shear the relationship is shifted to a path interval of 600m which corresponds to a glide path of gamma = -3^{o}. According to recommendations of the WORLD METEOROLOGICAL ORGANIZATION, WMO the INTERNATIONAL CIVIL AVIATION ORGANIZATION, ICAO has undertaken a classification of vertical windshear gradients /15, 16/ as they are depicted in Table 4.1.

Intensity of Shear	Influence on Flight Path	Change in Windspeed in DELTA H = 30m	u_{WH} [sec-1]
light	none	0 - 2 m/sec	0.0 - 0.07
average	significant	2 - 4 m/sec	0.07 - 0.13
strong	large	4 - 6 m/sec	0.13 - 0.20
very strong	dangerous	> 6 m/sec	> 0.20

Table 4.1: Classification of Windshear Strengths (ICAO)

Corresponding to this, boundary values for vertical windshear gradients were found from 1970 on in legal documents, as for example acceptance of flight controllers. The WMO continues from there, in that changes in horizontal wind of more than 10 knots per 100 ft altitude interval impair landing procedures under CAT I conditions while for CAT II and CAT III conditions a gradient of 5 knots per 100 feet is named as the critical value /62/. /96

It is easily understandable that vertical windshear gradient alone is no measure of windshear-conditioned aircraft endangerment because equally large gradients can work in different flight altitudes and during throughflight with differing duration. Thus shear layer thickness, shear altitude and the question as to how much the maximum gradient represents the wind profile all play a significant role in aviation.

4.2 Wind Shear Severity Factor

The ROYAL AIRCRAFT ESTABLISHEMENT, RAE developed a method for analysing wind shear which uses the so-called "Discrete Gust Analysis" for evaluation of measurements made in aircraft /16, 17/. For this one traces certain windshear patterns in time plots of measured wind signals. By combination with smoothing filters with difference quotients one obtains information about strength, form and period or wavelength of the shear. Simple ramps and double ramps are used for patterns (Figure 4.1a) where the characteristic time intervals 4, 8, and 16 seconds are chosen which under typical conditions correspond to ramp lengths during landings in the order of magnitude of 300, 600 and 1200m. Figure 4.1b shows typical input and output signals for the analyser program for the appearance of ramps and double ramps in the windshear process.

In connection with this method there exists a definition for standard windshear strength which is labeled in /17/ the "Wind Shear Severity Factor."

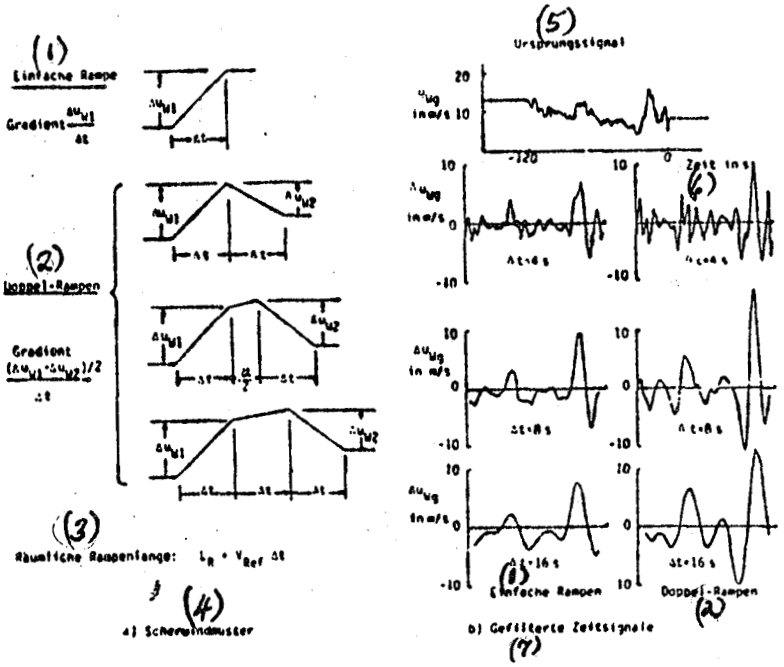

Figure 4.1: method for tracing windshears from /16/
1-simple ramp, 2-double ramp, 3-spatial ramp length, 4-windshear pattern, 5-original signal, 6-time, 7-filtered signal

$$s = \dot{u}_w \, (\Delta u_w / V_{Ref})^2 \qquad (4.1)$$

Herein V_{Ref} is the theoretical aircraft speed. The value DELTAu_w represents absolute change in headwind component. Wind acceleration is again a measure for required aircraft acceleration with the wind in order to hold flight steady. As will be shown later, these values enter into thrust equations for constant values of course and path angle.

The factor s is expressed with the spatial ramp length L_R instead of the chronological wind change whenever L_R is defined by the /98 theoretical flight speed and chronological ramp length, $L_R = V_{Ref} \cdot \Delta t$.

and chronological change in headwind is replaced by the difference quotient DELTAu/DELTAt. In this case one obtains the following relationship /17/:

$$s = \frac{\Delta u_g^3}{L_g \, V_{Ref}} \qquad (4.2)$$

The Wind Shear Severity Factor s has the dimensions of acceleration and represents a normed windshear quantity.

4.3 Danger Criteria from Energy Considerations

4.3.1 The Energy-Altitude Error

Research on aviation energy balances have shown that a danger criteria for landings can be expressed by energy and performance errors /1, 2, 13/.

While omitting rotational energy the total aircraft energy consists of kinetic and potential energy /3/. For the task at hand it is sensible to define kinetic energy as relates to the surrounding air (aerokinetic energy). Divided into flight weight one obtains the corresponding energy level:

$$H_{E_a} = \frac{V^2}{2g} + H, \qquad (4.3)$$

whose aerokinetic portion is composed of aircraft speed V and Earth's gravitational acceleration g. The potential energy level /99
portion is flight altitude H.

If an aircraft deviates from the glide path and theoretical value for speed during landing an energy error occurs which is expressed as a difference between actual value and theoretical value of energy level:

$$\Delta H_{E_a} = \frac{V^2 - V^2_{Soll}}{2g} + H - H_{Soll} \qquad (4.4)$$

In order to use the occuring energy error as a direct endangerment criteria, a definition of endangerment boundaries is required. KONIG /1/ determined a boundary value for the smallest allowable flight speed which is 1.1x the stall speed V_s so that for a landing with V_{theo} of $1.3V_s$ the relative danger is $-0.24/g\ V^2$. The critical altitude error (relative danger "altitude") was so selected such that it corresponded to the smallest pursued glide path (= 0.6* nominal glide path minus 30meter during CAT I approach). In Figure 4.2 these relationships are depicted in dependence on distance from the theoretical set point.

If both boundary values are reached simultaneously, the state of absolute danger appears, in that an energy redistribution altitude-to-speed has no problem solution. The absent energy must be replaced by thrust increase. If in contrast the state of absolute danger is not attained, an energy redistribution is possible in principle so that neither the relative danger "altitude" nor the relative danger "speed" is attained /1/. Accident investigations from manual landings as well as research with flight simulators have shown that flight deviations generated by windshear in many cases are relatively slight. In certain wind situations pilots have apparent problems in recognizing in a timely manner slowly building flight path /100
deviations, especially if additional disturbances such as poor visibility, strong turbulence and transition from instrument to visual flight are occuring. There thus results the requirement for suited information for the pilot which he can solicit under windshear conditions to correctly control the plane (command display).

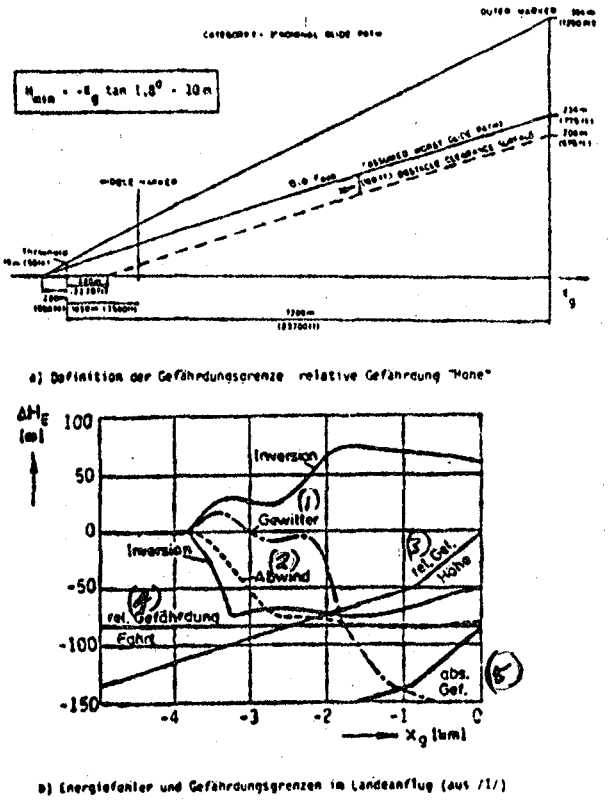

Figure 4.2: energy-altitude error as an endangerment criteria 1-thunderstorm, 2-downdraft, 3-relative danger in altitude, 4-relative danger in course/speed, 5-absolute danger

Research within the framework of the SFB special research project 5B at the Technical Unversity at Braunschweig has shown that the energy error behavior described in Eqn. 4.4 and its time derivative, the performance error, are well suited for realising /101 a windshear display and improving future flight controllers as regards compensation for windshear effects /1, 14, 85/. Furthermore the possibility is offered by this method for analysing flight data from real and simulated landings as regards windshear-conditioned flight endangerment.

4.3.2 The Ideal Thrust Control Law

In order to avoid energy errors in aircraft, energy corresponding to wind changes along the flight path must be corrected with the

help of thrust adjustments. If one prescribes that for a safe landing the glide path (constant path angle) and aerodynamic state must be maintained as constant, this means above all aircraft acceleration with the wind. This is easily explainable because the wind vector is formed from the difference between course and flight speed and there results a time derivation of wind components from the equation:

$$\dot{\underline{V}}_W = \dot{\underline{V}}_K - \dot{\underline{V}}$$

Under the condition $\underline{V} = \underline{0}$ the following is valid:

$$\dot{\underline{V}}_W = \dot{\underline{V}}_K .$$

The criteria for required thrust adjustment is obtained from lift and resistance equations as the aircraft moves /1/. In a fixed-aircraft coordinate system the equation system is expressed as follows from /3/:

$$\begin{aligned} x_K: \quad & G(\dot{V}_K/g + \sin\gamma) = F\cos(\alpha - \alpha_W) + A\sin\alpha_W - U\cos\alpha_W \\ z_K: \quad & n\,G = F\sin(\alpha - \alpha_W) + A\cos\alpha_W + U\sin\alpha_W \end{aligned} \qquad (4.5)$$

/102

Herein it was already prescribed that the thrust adjustment angle is zero, that is, the line of effective thrust is parallel to the aircraft's longitudinal axis.

With the requirements and simplifications described in Appendix A7 (small angles alpha, $alpha_W$, gamma as well as V = const and C_W/C_A = const) one obtains the approximative solution for the required thrust change DELTA F_{theo} after performing a linearization as opposed to the stationary approach thrust F_o which relates to flight weight G:

$$\Delta F/G = \frac{\dot{v}_{WK}}{g} - \Delta\alpha_W \qquad (4.6)$$

For wind angle of incidence alpha$_W$ compared with the value of the reference point alpha$_{W,0}$ the following is valid:

$$\Delta\alpha_W = -\frac{u_{Wg} - u_{Wg,0}}{V}\gamma - \frac{w_{Wg} - w_{Wg,0}}{V} \cdot$$
$$= -\frac{\Delta u_{Wg}}{V}\gamma - \frac{\Delta w_{Wg}}{V} \cdot \qquad (4.7)$$

Equation 4.6 is considered an ideal thrust control law and is a function of wind speed components u_{wg} and w_{wg} as well as their time derivations. As aircraft-specific values, only path angle gamma and flight speed V are considered.

From the required thrust change one obtains the corresponding energy or energy level change by integration of DELTA F/G along the flight path:

$$\Delta H_E = \int_{x_1}^{x_2} \Delta F/G \, dx_k$$

/103

or with $dx_k/\sin(\text{gamma}) \sim dH/\text{gamma}$:

$$\Delta H_E = \int_{H_1}^{H_2} \Delta F/G \; 1/\gamma \; dH \qquad (4.8)$$

If thrust is corrected for changing wind relationships along the flight path acrding to the thrust control law in Eqn. 4.7 and energy is added to or subtracted from the aircraft, under these ideal conditions no energy errors appear as relate to requirements for safe landings (V=0, gamma=0).

A correlation for the definition of danger as it is represented in Figure 4.2 can be made with the simplifying assumption that omission of thrust or energy correction leads to equally large energy errors. This is practically never the case because under these conditions flight deviations would occur and the

requirement that V=const, C_W/C_A=const is no longer satisfied and deviations from the planned route occur (gamma=0). The magnitude of speed and path deviations depends strongly on wind situation and will be the topic of later research.

Next we will attend to the question of the influence of individual portions (horizontal wind, vertical wind and their time derivatives) on required energy adjustment. Because this is different for certain wind processes the problem will only be qualitatively examined for a landing through a downburst thunderstorm wind field. The flow process in a thunderstorm is simulated by a model described in Section 3.4, Figure 3.35 (2D case). Figure 4.3 shows the curve of speed components on a glide path (gamma = -3°). The u_W component varies between -12.8 m/sec (headwind) and 10 m/sec (tailwind) after thunderstorm through-flight.

/104

The downdraft reaches a maximum value of 1.84 m/sec in the nucleus/core.

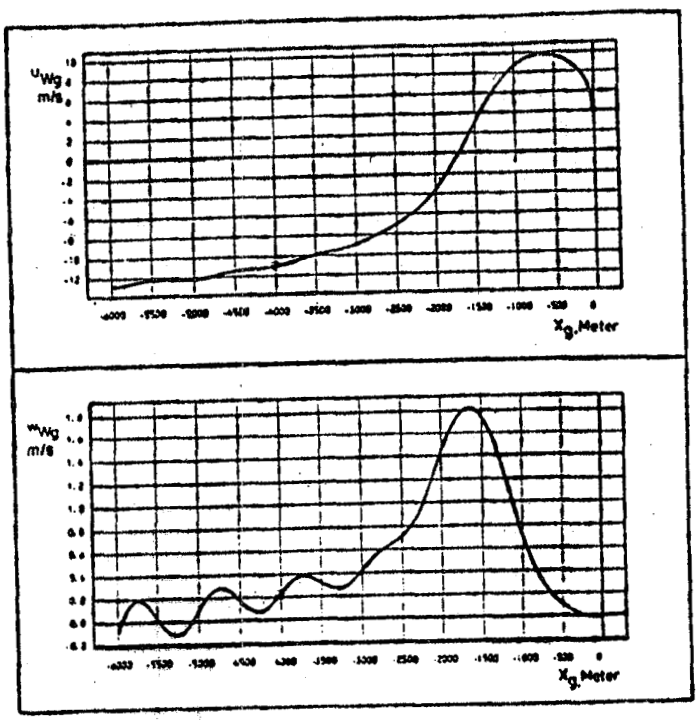

Figure 4.3: wind components in the glide path

In Figure 4.4 the individual portions of the total required suplemental energy are plotted over the distance to theoretical set point. One recognizes that the greatest influence originates in the headwind time change ($-\Delta H_z(u_w)_{max}$ = 150 meter). This energy level is necessary in order to accelerate the aircraft with the wind.

The headwind component u_{Wg} which is coupled with the wind incidence angle via the above-described approximation $alpha_w(u_{wg}) = u_{wg}$ gamma/V deviates more and more strongly from the reference value $u_{wg,o}$ with approach to the landing threshold /105 at the point X_o = -6000m, H_o = 314m. Headwind change DELTA $u = u_{Wg} - u_{Wg,o}$ is positive throughout the distance and thus also the associated portion of wind incidence angle change DELTA $alpha_W(DELTAu_{Wg})$. Through this an energy level overadjustment is made and must be corrected by a corresponding thrust reduction.

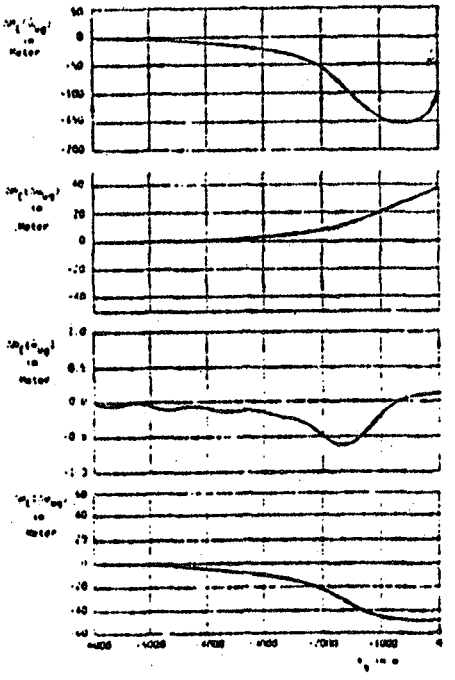

Figure 4.4: individual portions of energy level requirements

This only adds up to about a quarter of the portion which is affected by wind acceleration u_{Wg}. The physical relationships are clearly explained by the sketch in Figure 4.5 and Equation /106
4.5. At the reference point (Index 0) the term A sine($alpha_{Wo}$) (which is formed from lift and wind incidence angle) gives one of the forces opposed to flight direction X_k which is associated with a certain energy use. This was already considered when setting the stationary takeoff thrust for the point O. At point 1 the headwind u_{Wo} has changed into tailwind u_{W1}. Under the condition that aircraft speed and path angle remain constant, the direction of flight changes which inclines forwards from its perpendicularly positioned lift vector and produces the following force in the direction of flight.

$$A \cdot \sin(\alpha_{W1}).$$

An integration of the difference A*DELTA$alpha_W$ along the flight path gives the energy excess (DELTAalpha ≥ 0) which must be compensated for by thrust reduction.

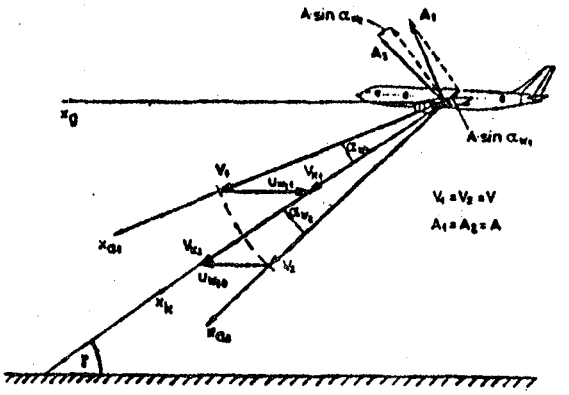

Figure 4.5: influence of change in DELTAu_{Wg} or DELTA$alpha_W$

For the component conditioned by downdrafts, deviation from the reference value $DELTAu_{Wg}$ leads to negative values for $DELTAalpha_{g}$ and thus to additional thrust requirements.

/107

The thus associated energy level requirement $-DELTA\ H_E\ (DELTAu_{Wg})$ reaches a maximum value of 50 meters which contributes about one third of the u_W component.

Research on surface boundary layer windshear and boundary layer "beam flow" in which the wind u-component alone is of significance has shown that the magnitude of $DELTA\ H_E(u_{Wg})$ is at least six times larger than that of the $DELTA\ H_E(DELTAu_{Wg})$ component. In most cases the relationship is significantly greater so that one can generally attribute the time derivation of headwind with having the greatest influence. Similar orders of magnitude are possible for vertical wind components $DELTA\ H_E(DELTAu_{Wg})$ in extreme thunderstorms or frontal situations in which vertical winds of more than +/- 5 m/sec have an effect on the aircraft. Figure 4.4 shows the component affected by time change in vertical winds. One recognizes that this contribution is many orders of magnitude smaller than the remaining components so that the assumed simplifications in the derivation in Appendix A7 can be justified.

4.4 Comparison of Danger Criteria

4.4.1 Comparison Between Energy Level Errors and Energy Adjustment via Thrust Control

As described in previous sections, energy adjustment to wind changes appearing along the glide path is based on the ideal thrust control law. Herein path angle and flight speed are held constant. As a result, the relationship between lift and resistance does not change. In contrast to that, these values become variable in flight with a fixed rudder (nu=const.). Simulated landings show that deviations in path and in the relationship of lift to resistance are often relatively small. The maximum decrease in flight speed compared to the reference value is (averaged over 25 cases, boundary layer flow, fronts, downbursts) DELTA V = -2.85 m/sec with a standard deviation of +/- 1.8 m/sec. This corresponds to an energy level error of about 19 m +/- 12m. The greatest deviations appeared for a sharp decrease in headwind (large wind maximum at low altitude), affected by aircraft inertia and strong pygoid oscillation. In the least favorable case researched, a maximum speed decrease of -8.5 m/sec was attained so that flight speed was reduced from 1.3x to 1.14x stall speed.

For the relationship C_W/C_A [lift/resistance] there results as an average value of the maximum deviation 0.59% of the reference value and a standard deviation of +/- 0.33%. The thus affected difference between simulation with rigid rudder and energy adjustment according to the thrust control law may thus be

comparatively small. Moreover it should be considered that during takeoff with fixed rudder greater or lesser deviations from theoretical flight path occur, generally associated with an /109
increase in descent speed during approach to the surface. Basically we have to differentiate here between wind situations with considerable horizontal homogeneity where wind speed can be considered to change only with altitude (surface boundary layer profile, boundary layer "beam flow") and wind processes which change with path and altitude coordinates. In the first case the same wind speed range is flown through independent of flight path and aircraft set-down point; however for steep flight paths there are large descent speeds and thus large per unit time changes in wind components (Figure 4.6).

As already mentioned, the parameter U_{Wg} enters the thrust control law as a significant factor and affects the resulting energy level adjustment. If one replaces the integration variable x_k by the altitude H (see Eqn. 4.8) there result the same integration boundaries for differing courses of flight:

$$\Delta H_E(u_{Wg}) = 1/g \int_{H_1}^{H_2} \dot{u}_{Wg}(H)/\gamma \, dH \qquad (4.9)$$

The per unit time change in headwind component can be described by limiting oneself to the longitudinal plane as follows:

$$\dot{u}_{Wg} = \partial u_{Wg}/\partial t + u_{Wx} \dot{x}_g + u_{Wh} \dot{z}_g$$
$$\text{mit } \dot{z}_g = -\dot{H} \qquad (4.10)$$

Because in the case considered here u_{Wg} is zero and a stationary state is presumed ($du_{Wg}/dt = 0$), u_{Wg} is expressed by the relationship:

$$\dot{u}_{Wg}(H) = u_{Wh} \dot{H}$$

Using groundspeed V_{GS} the following is valid: /111

$$\dot{H} = V_{GS} \tan \gamma = (u_{Hg}+V)\,\gamma\,, \qquad (4.11)$$

/110

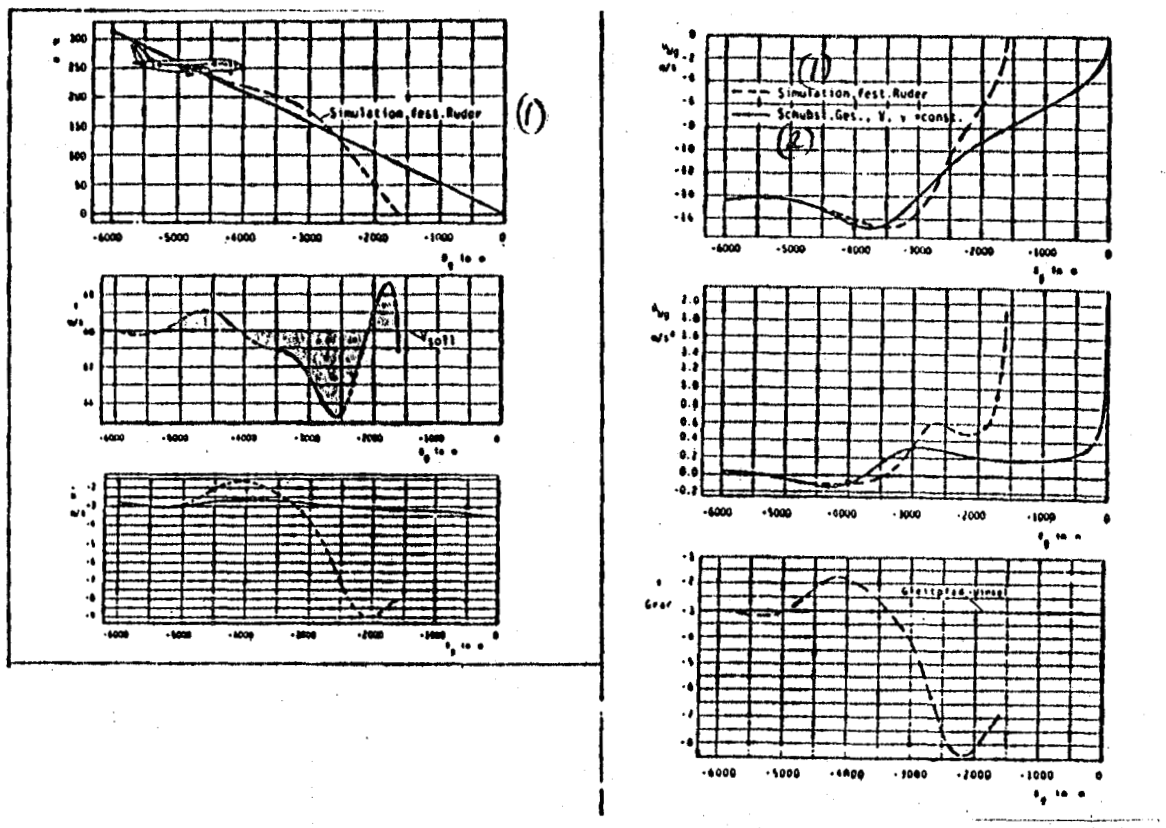

Figure 4.6: state of flight and wind magnitudes in a comparison between simulation (fixed rudder) and thrust control law (V. , const.) 1-simulation with fixed rudder, 2-thrust control law, V const

Inserted in Eqn. 4.9 one obtains:

$$\Delta H_E(\dot{u}_{Wg}) = 1/g \int_{H_1}^{H_2} (V+u_{Wg})\, u_{gH}\, dH \qquad (4.12)$$

This shows that the quotient u_{Wg}/gamma and as a result the energy level error to be balanced by thrust adjustment for an altitude-dependent wind process are independant of path angle (angle of position). The second term in the thrust control law for energy adjustment is dependent on the difference between the headwind component on the glide path and the reference point DELTA u_{Wg} $u_{Wg}(H)-u_{Wg}(H_R)$. After replacing the integration variables X_k with H one obtains for the energy requirements:

$$\Delta H_E(\Delta u_{Wg}) = \int_{H_1}^{H_2} \Delta u_{Wg}(H)/V\, dH \; . \qquad (4.13)$$

This component is also independent of angle of position.

The recognizable differences in energy error curves in Figure 4.7 or 4.8 from simulation and energy fitting/adjustment basically refer back to deviations in flight (aerodynamical changes). We see in the simulated case with fixed rudder the appearing maximum energy overcompensation as well as energy defecit are larger than the case in which V and gamma are constant for the required energy adjustment, because in the selected landing configuration the relationship C_W/C_A (resistance/lift) decreases and reverses during flight speed increases. Results from a statistical evaluation of 28 simulated landings under boundary layer "beam flow" as concerns energy erros in comparison with corresponding /112
values from the thrust control law are plotted in Figures 4.9 and 4.10.

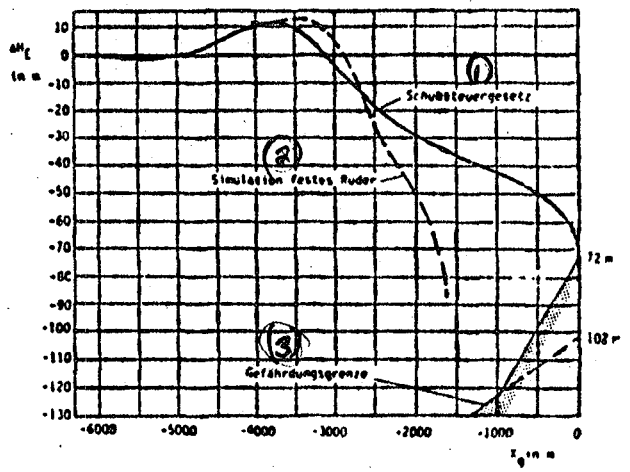

Figure 4.7: comparison between simulation and energy adjustment 1-thrust control law, 2-simulation, fixed rudder, 3-danger boundary

One recognizes that the simulation gives values about 15% higher (Figure 4.9). Even if the values from both methods do not exactly coincide, the possibility exists for estimating the maximum energy error (from the simulation with fixed rudder) using results from energy adjustment via the thrust control law.

In order to compare curves of relative energy errors from danger boundaries with values of relative energy adjustment, a representation with respect to altitude is necessary (Figure 4.8) because flight paths end at different points X. One /113 recognizes in this case an almost offsetting curve for relative values at points under H=50m, X=954m. At this point the danger boundary deviates (Figure 4.7) so that below this region the appearing relative energy level curve assumes larger values from the thrust control law than in the case of simulation. This region is generally never reached because of early ground contact during landing with constant rudder. If one extrapolates the danger boundary curve from the range x<-954m to the theoretical landing point (x=0) one obtains a boundary value of

DELTA $H_{Eboundary}$ = 102 meters instead of

72 meters

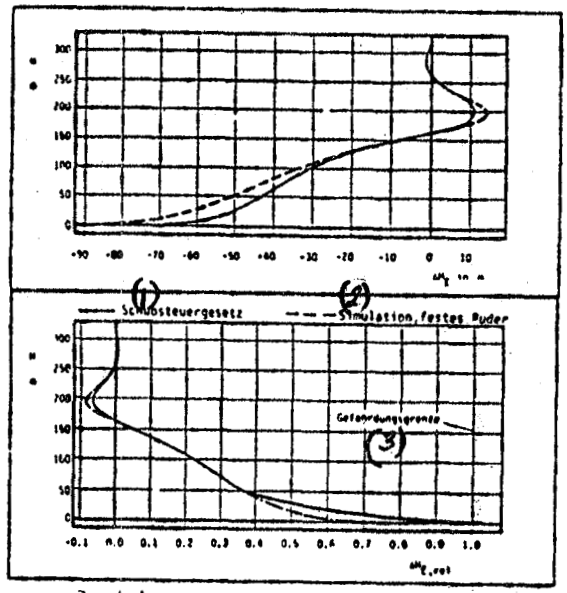

Figure 4.8: comparison of absolute and/or relative energy errors with relative energy use, 1-thrust control law, 2-simulation, fixed rudder, 3-danger boundary

Statistical evaluation of 28 simulated landings (Figure 4.10) gave an average value of 0.7 for the ratio of relative energy error (simulation) to relative energy use (thrust control law) which closely approximates the quotient of the boundary values /104 72m/102m = 0.704.

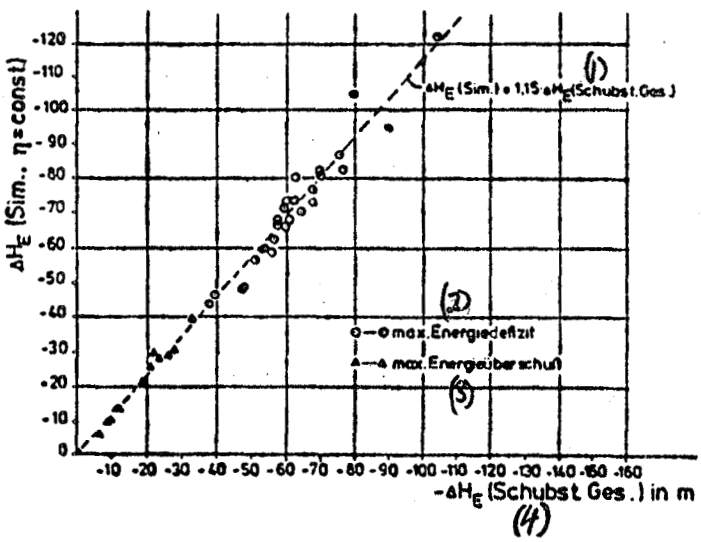

Figure 4.9: comparison of statistical results from simulation and thrust control law, 1-thrust control law, 2-maximum energy defecit, 3-maximum energy excess, 4-thrust control law

In this way the relative energy use resulting from the thrust

control law is transferred into the extent of danger in the simulation with fixed rudder. Also the expected touchdown point for a simulated landing can be estimated from the results of the thrust control law. If one goes forth with the simplifications that deviations from theoretical values of flight are small and that total energy level use for missing energy adjustment is effective in a first order approximation, as an altitude error one obtains the X-coordinate for the touchdown point:

$$X(H=0) \approx \Delta H_{E_{ges}} / \tan 3^{\circ} \qquad (4.14)$$

In the example above for boundary layer "beam flow" there results from this approximation formula x(H=0) ~ -1200m as compared to a value of -1300m calculated from simulation. /115

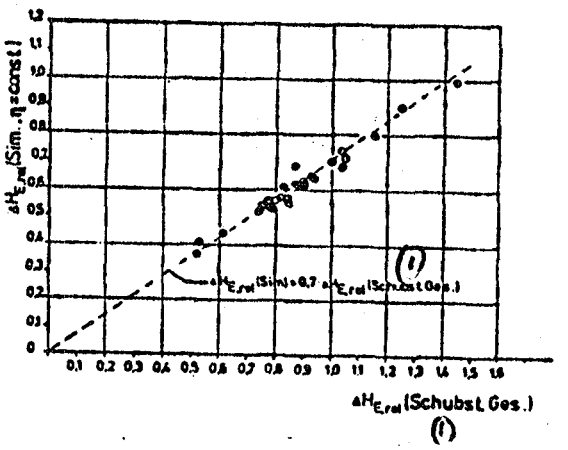

Figure 4.10: relationship between relative energy errors and and relative energy use, 1-thrust control law

Imprecision increases with increasing deviation from theoretical flight value V_0 becasue the kinetic energy component can no longer be omitted.

For altitude-dependent wind speed profiles the thrust control law and the thus calculated energy adjustment represents a simple mathematic procedure for approximating appearing energy level

errors during landings with fixed rudder, the extent of danger and the touchdown point. Wind components and their per unit time derivatives as well as the given values for glide path and aircraft speed alone are input values. Special comprehensive statistical research can be done in this manner with reasonable expense.

This prediction is not valid without limitation for wind situations whose wind components vary with path x-coordinates as for example in a thunderstorm downburst or in a frontal flow field. The wind speeds appearing alongside the aircraft are /116
dependent to a great extent on flight course. The energy level use calculated from the thrust control law permits only one approximation of the danger potential for one takeoff with a determined flight path. This state of affairs will be dealt with further in Section 5.3.

An estimation of the point of impact during landing with a fixed rudder from results of energy adjustment using the above-described method is possible if deviations from path and speed can be considered small. For the example in Section 5.3 of landing through a downburst the so-calculated value for x(H=0) is 9% larger than that for simulation calculations (surface contact 1635 meters before the theoretical touchdown point) with a maximum deviation from flight of DELTA V = -1.8 m/sec.

4.4.2 Comparison Between Energy Fitting and Data for Describing Windshear Strength

While in danger criteria won from energy considerations both horizontal and vertical wind influences are considered, in the

values "Severity Factor" and wind speed gradient only the wind speed u-component is considered. A comparison of the different methods thus only makes sense for wind situations such as boundary layer profiles and boundary layer "beam flow."

The values plotted together in Figure 4.11a for relative energy level error DELTA H_E (danger) and the factor s were determined from simulated landings. The wind curves originate from measurement data which were approximated by the boundary layer "beam flow" model of Eqns. 3.20 and 3.22. One recognizes the increasing tendency of the "Severity Factor" with increasing /117 energy level, even if considerable scatter appears.

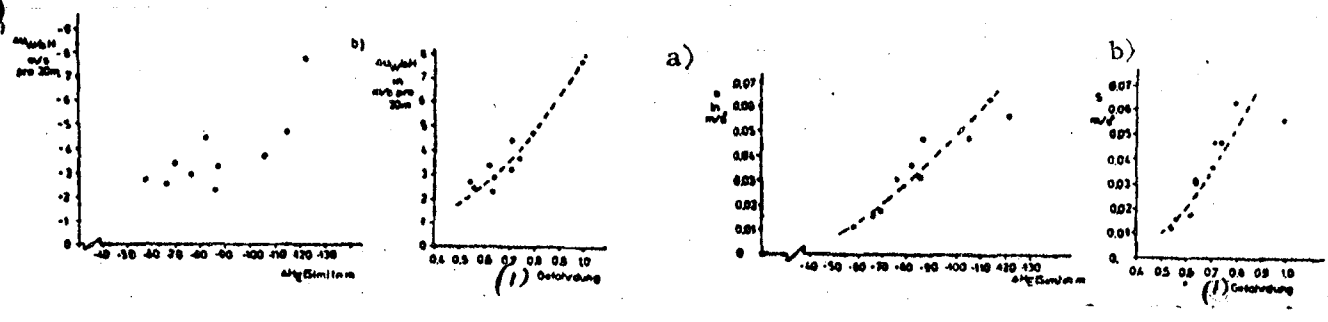

Figure 4.11: correlation between energy error, Severity Factor and vertical windshear gradient, 1-danger

If one compares definitions for thrust adjustment according to the thrust control law (u-component) and the Severity Factor it happens that with the exception of angle of position in both relationships the same parameters are used. The essential values in both cases are per unit time change in headwind components and the absolute change of u-components with respect to the reference point. It was already shown the the sign of DELTA u_{Wg} is

decisive in determining energy excess or defecit. For the factor s the sign has no effect on account of squaring the appearing term. A certain value for u_{Wg} leads then to a larger factor s if the magnitude of DELTA u_{Wg} is large; it thus considers spatial expansion of the shear layer. In contrast to vertical windshear gradients which alone describe headwind changes in an altitude /118
interval of 30m the Severity Factor represents a significant further development. If however no large fluctuations appear in the wind speed curve and the maximum value of u_{WH} is representative for the wind profile the vertical windshear gradient in the middle shows an increase with increasing energy error (Figure 4.11b). If the wind profile,shows effects of vortex or secondary squalls the vertical windshear gradient permits no immediate predictions about wind situation danger. This will be demonstrated by the example in Figure 4.12. At an altitude level of a few decameters vertical wind gradients of -2.9 to -3.6 m/sec per 30m appear. They have no effect on the aircraft's energy balance as the curve of relative energy level use makes clear. In contrast the lower diagram shows a wind situation which was recorded during a landing in a weather inversion in which wind gradients between -1.1 and -1.5 m/sec per 30m appeared. Via the longer effective period a significantly larger energy error appeared than in the case of the larger gradient. The vertical windshear gradient here has no power to predict the extent of danger.

For previous research the influence of flight speed (which entered into Severity Factor and thrust control law calculations

as the third value) was not considered. In pilot training at a few airlines it is recommended that landings under severe conditions should be performed while maintaining energy reserves with a guaranteed available excess of speed. In consideration of the Severity Factor, these recommendations can be supported. Certainly the per unit time derivatives of u-components increase with increasing flight speed but the quadratic influence of $1//V^2$ outweighs them. With the approximation: $\dot{u}_{Wg} \approx u_{WH}(V+u_{Wg})\tan\gamma$

/119

one obtains:

$$n \approx u_{WH}(V+u_{Wg}) \cdot r \cdot (\Delta u_{Wg}/V)^2 \qquad (4.15)$$

From energy considerations the opposite tendency is indicated. For this the relationship concerning thrust adjustment from the thrust control law will once again be considered for which the above named approximation for u_{Wg} will be used.

$$\Delta H_g \approx \int_{H_1}^{H_2} (u_{WH}(V+u_{Wg})/g + \Delta u_{Wg}/V) \cdot dH \qquad (4.16)$$

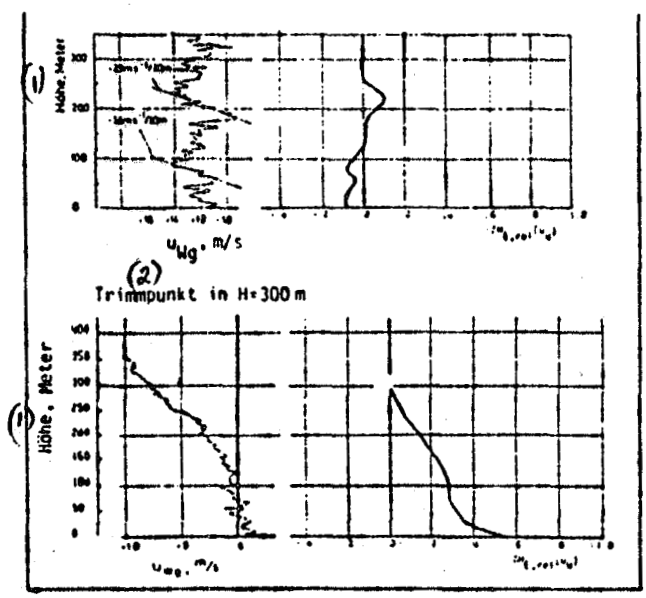

Figure 4.12: energy adjustment for different wind situations
1-altitude, meters, 2-trim point at H=300m

The variation result of V is represented in Figure 4.13. For a landing with decreasing headwind the significant first term (u_{Wg} component) gives an increasing energy use with decreasing speed. The DELTA u_{Wg} dependant component under the named conditions basically leads to an energy excess which is reduced with decreasing speed. Increasing flight speed produces a worsening of the aircraft's energy situation. This state was detected in a simulation with fixed rudder.

If a changing vertical wind appears, the integral leads from the expression DELTA u_{Wg} for increasing downdraft to a new energy requirement which is easily reducible with increasing speed. A speed-dependent compensation is only thinkable during extreme downdraft changes.

4.4.3 Danger Statistics from Measured Results

As far as the writer knows no danger statistics regarding windshear in the vicinity of airports have been published. This is certainly due to the absence of suited danger criteria, so that one has been limited to evaluation of vertical windshear gradients or the "Wind Shear Severity Factor" in the case of the RAE. The methods in this work based on energy considerations offer the possibility of predicting the danger to aircrft arising from windshear. In comparison with simulation calculations the computation expense is small so that this method is especially good for statistical analysis of measurement data.

/121

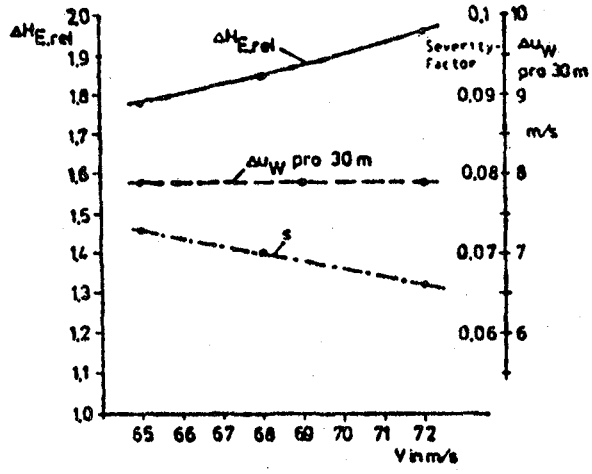

Figure 4.13: influence of flight speed on energy use and Severity Factor

For a data base there are 229 sets of data from the previously-mentioned windshear measurements using the LUFTHANSA Airbus /5, 6/. A direct determination of the energy error during landings was not realizable because some necessary information and data were not available for reasons of capacity and data storage. See /7/. The evaluation took place with the help of energy adjustment via the thrust control law as relates to the danger boundaries defined in /1/.

/122

To estimate the probability of over- or understepping a determined value the frequency summations for relative energy errors were calculated from random measurments and placed in a probability network. Thus there occurs along with a total representation a divided evaluation of components conditioned by the wind. Figure 4.14 shows the frequency summations for the maximum relative energy use resulting from the headwind components. The 0.5x value for the danger boundary is exceeded in 2.5% of cases with an average value of 0.1 and a maximum of 0.62.

The frequency distribution in Figure 4.15 shows that more than 50% of the maximum relative energy errors appear in lower altitudes (H<34m). Usually the landing takes place against the wind so that energy use during increasing wind speeds increases at the surface boundary layer with proximity to the ground (see the examples in Sections 4.4, 5.1 and 5.2).

Maximum energy use generated by vertical wind components is depicted in Figure 4.16 as a frequency summation. Here 5% of the random values exceed the 0.5x value for the danger boundary, that is, the w_W component gives higher danger values than the u_W component. It should be noted that calculation of energy use dependent on vertical wind is very sensitive to measurement imprecision as regards vertical speed of the measuring aircraft (or vertical components of airspeed) /51/. A drift in the H-signal of 0.007 m/sec per second (at an altitude of 300m) leads to an error in the energy level adjustment of more than 25 meters. Statistics for the vertical wind component as regards danger (and thus transferral to w and u components) in Figure 4.17 should be considered with some limitations.

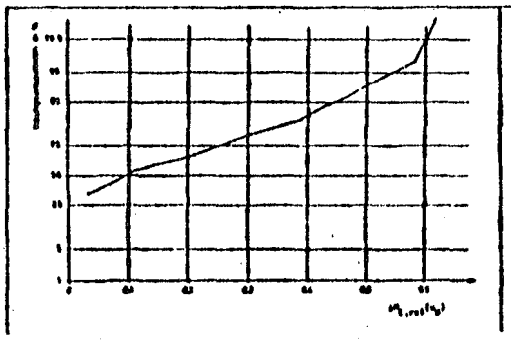

Figure 4.14: frequency summation for danger via influence of headwind

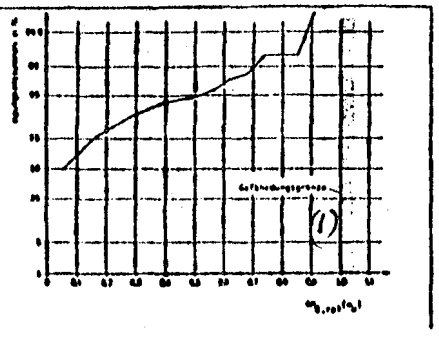

Figure 4.16: vertical wind component for danger
1-danger boundary

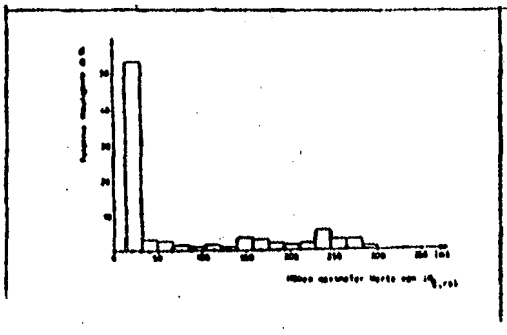

Figure 4.15: distribution of maximum danger through max. ceiling

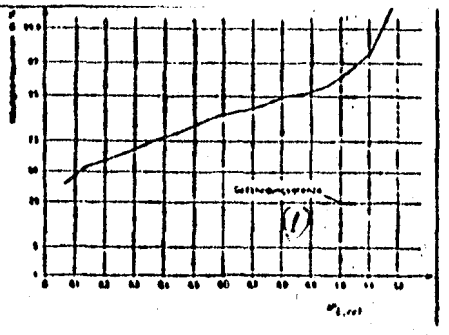

Figure 4.17: total danger from transferral of u_W and w_W
1-danger boundary

As already mentioned for the analysis of windshear gradients the influence of atmospheric stability on extent of danger will be researched. Figure 4.18 shows the frequency sums for headwind components, vertical wind components and superposition of both components of the relative energy level requirements. If one considers the values for 25% and 5% exceeding probability (75 or 5% summation frequency) an increase in energy level is seen as a tendency for the u-components and thus growing danger with increasing stability (Figure 4.19).

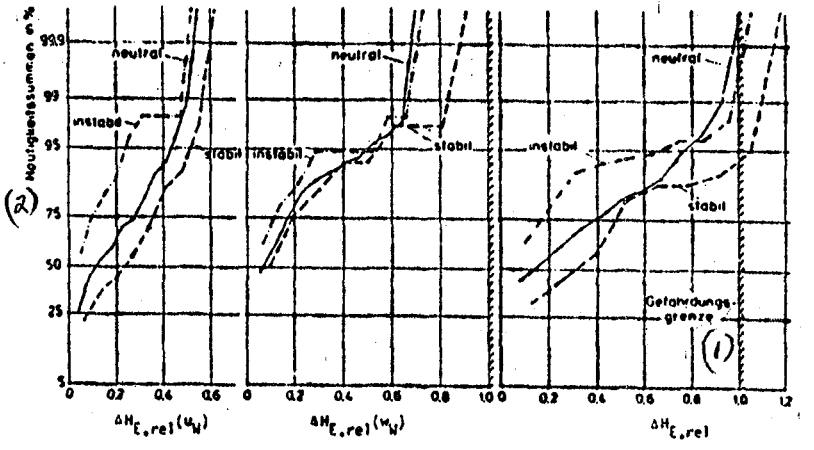

Figure 4.18: influence of atmospheric stability on danger
1-danger boundary, 2-frequency sum in percent

This result confirms the superposition described in Section 4.4.2 (see Figure 4.12). Vertical windshear gradients (for stable layers) of typical wind profiles generally indicate large values. However wind changes are effective over a great altitude range so that considerable energy errors can form.

According to windshear statistics in Section 2.2 large vertical gradients appear under neutral and unstable conditions.

Apparently in this case we are concerned with short-term wind changes as a result of squall fronts and influences of turbulence which have no effect on an aircraft's energy balance. The comparison between danger statistics and statistical research on windshear gradients underlines the result that the vertical windshear gradient alone does not allow any predictions regarding aircraft safety.

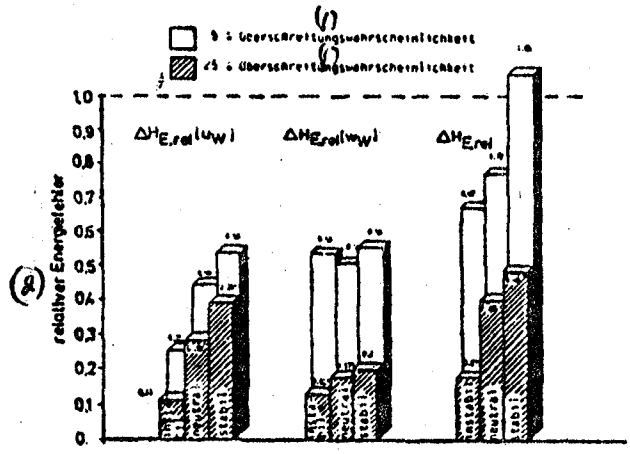

Figure 4.19: danger values for 25% and 5% exceeding frequency
1-exceeding probability, 2-relative energy error

In contrast to the u-component no clear tendency is visible for vertical wind influences. Certainly one would expect the largest vertical wind changes during unstable layering but downdrafts would be balanced by corresponding updraft errors. The assumption of increased energy use can thus not be derived herefrom.

/126

It was already mentioned that to avoid course errors, aircraft acceleration must take place with the wind. Thus an evaluation of per unit time changes in the headwind is of interest. Figure 4.20 shows the frequency summations for the maximum value of u_{Wg}, whence an average value of 0.19 m/sec^2 comes. The "exceeding probability" for a wind acceleration of

0.6 m/sec^2 is about 2% and has a maximum value of 1.0 m/sec^2. According to research in /16/ and /84/ one may presuppose typical acceleration capacity for a turbine-driven transport aircraft during landing to be about 1.5 m/sec^2. The required supplemental thrust can be estimated from Eqn. 4.9 and leads to an acceleration of 1.0 m/sec^2 and thus a thrust increase of $0.3F_{max}$ which corresponds to a total thrust of about $0.6F_{max}$. According to research in /41/ the required thrust change speeds have proven to be non-critical.

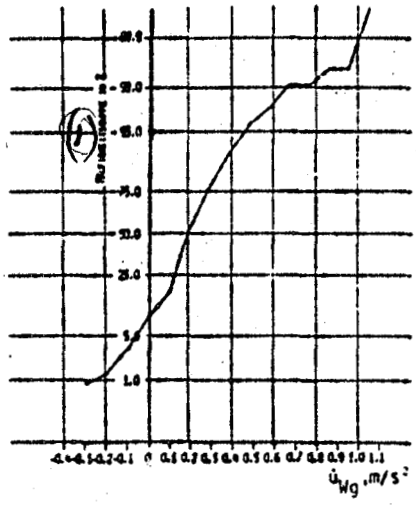

Figure 4.20: frequency summations for maximum wind acceleration
1-frequency summation in percent

5. Estimation of Aircraft Danger from Windshear during Landing

To estimate the danger to aircraft during landing in windshear phenomena, simulation calculations were performed using different wind models. Research by KONIG /1/ has shown that modern flight controllers (autopilot + thrust controller) are often in the position to prevent accidents in dangerous wind situations even when there is a significant potential for improvement. Because previously no satisfactory pilot models were available, experiments prescribed manual landings in a flight simulator (with visual system if possible) and required the use of many pilots for a sufficient statistical base. On the other hand, simulated landings with fixed rudder have shown that the appearing crash profiles didn't differ significantly from path profiles which were reconstructed from crash investigation data /36/. Thus the possibility is offered for doing preliminary research with significantly smaller expense of time, apparatus and personnel.

5.1 Landing under Normal Boundary Layer Conditions

Surface boundary layer profiles as they are represented and described in Section 3.1 depict the normal case of windshear during takeoffs and landings. According to surface roughness and atmospheric stability, there result differences in profile form. /128

With use of the exponential law according to Eqn. 3.7 this is expressed by choice of exponent m; this is depicted in Figure 5.1.

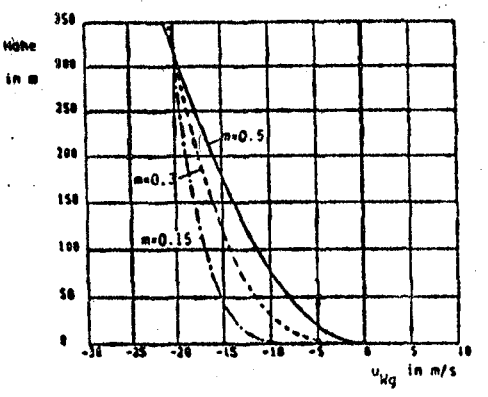

Figure 5.1: relationship between wind profile form and exponential law exponent

Moreover the wind speed level ($u_W(H_{ref})$) itself is significant. For a landing with constant air speed V=68 m/sec on a glide path of gamma = -3^o (trim point at H=314m, corresponding to 6000 meters before runway threshold)one obtains (from energy considerations with help of the ideal thrust control law) the energy level deficits represented in Figure 5.2 at 5m above the ground (aircraft thrust point at touchdown).

One recognizes an increase in required supplemental energy with increasing exponent. For m $\geq$0.5 the increase is only marginal. The maximum value is reached at m=0.7 where energy required is slightly above the value for wind increasing linearly with altitude (m=1). /129

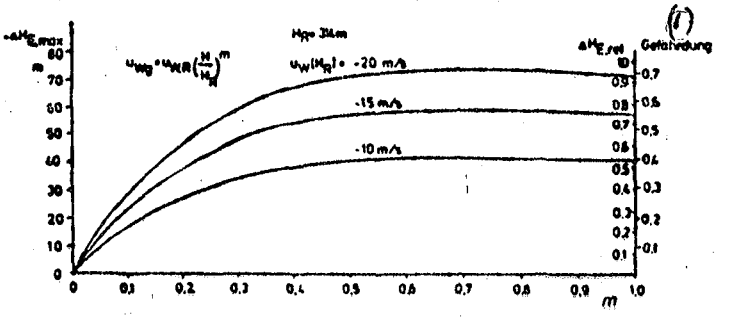

Figure 5.2: energy use as depends on exponent "m", 1-danger

Doubling wind speed at the 314m altitude reference point from 10 m/sec to 20 m/sec affects an energy defecit increase of about 70%.

Typical values for the exponent m lie between 0.1 and 0.4 (see Section 3.1). If one starts with the representative value 0.2 and V_W(H=10m) = 5 m/sec the maximum energy level defecit to be dealt with upon landing is 27 meters. That corresponds to a relative energy level error of 0.35 or 0.25 (recalculated for a takeoff with fixed rudder) which is considered unproblematic from experience. In a stable atmosphere, greater surface roughness and higher wind speeds, for example $V_{(H=314m)}$ = 20 m/sec and m=0.4 the energy level deficit can climb to 65% of the danger boundary value.

Superposed disturbances from squalls or vortexes (as they are depicted in the examples of Section 4.4, Figure 4.12) make their effects only slightly known on the aircraft's energy balance in /130
horizontal winds but can have effects as vertical wind changes.

5.2 Danger to Landing Aircraft by Boundary Layer "Beam Flow"

As was introduced in Section 3.2, boundary layer beam flow appears generally during weak wind conditions near the ground. If information from surface measurements alone is available for the pilot (typical altitude 10m), he can under normal boundary layer conditions expect wind speeds twice the reported ground surface values at a height of 200m above the runway. In the case of boundary layer beam flow the actual wind speed can have values 3 to 4x the surface value.

To understand the effects of the aircraft on flight trajectory it is understandably decisive that flight direction and wind direction remain together. If wind direction change is formed by altitude change, then unfavorable conditions appear for a landing into the wind. For large changes of direction which in Northern Germany have reached 90°, this is the case for a landing into the direction of flow at the altitude of maximum wind or thereabouts. This is illustrated in an example in Figure 5.3.

The approach directions deviating from this strongly affect wind changes on side wind components whose influence will not be further studied here.

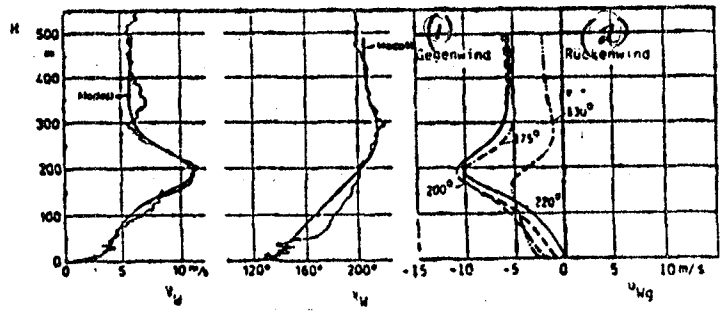

Figure 5.3: u-component profile for differing course angles
1-headwind, 2-tailwind

The following simulation calculations presuppose the energetically unfavorable case as regards runway and wind direction. The phenomena thus appearing will be examined in the example for boundary layer beam flow in Figure 5.4 whose model parameters were won from conditioning measurement results from the Institute for Meteoroogy and Climatology at the University of Hannover.

For a landing at the direction 145° there results the profile in Figure 4.4 for wind u-components oriented to the runway

direction.

In the upper diagram of Figure 5.5 there is a flight path curve, in the lower diagram the curve for wind speed as it resulted from simulations under different conditions (fixed rudder as well as autopilot with and without thrust controller). Next a landing with fixed rudder will be considered (coarse line).

Conditioned by a headwind increase, flight speed decreases for a short period before the plane slows via decrease of course or /132 ground surface speed (Figure 5.8)

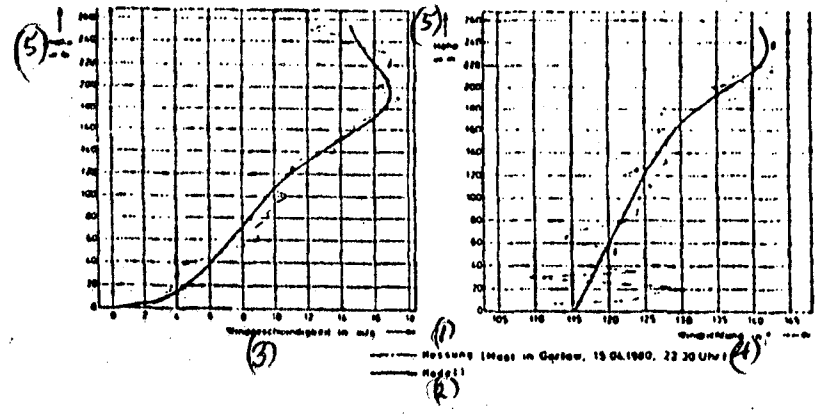

Figure 5.4: boundary layer beam flow from example calculations
1-measurement (mast at Gartow, April 15, 1980)
2-model, 3-wind speed in m/sec, 4-wind direction
5-altitude in m

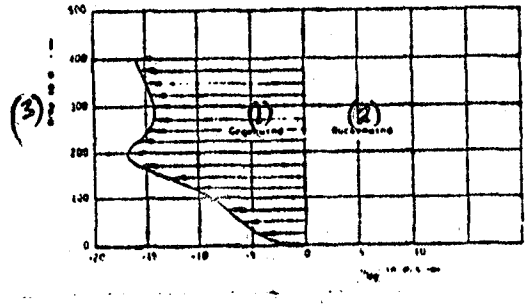

Figure 5.5: profile of components oriented to the direction of the runway, 1-headwind, 2-tailwind, 3-altitude in m

With an increase in flight speed there is associated an increase in lift - and to a small extent - resistance so that the aircraft climbs above the theoretical glide path. Excitation of phygoid oscillation is recognizable. The exchange of potential and kinetic energy associated therewith affects a decrease in flight speed during further climbing through/above the theoretical glide path.

/133

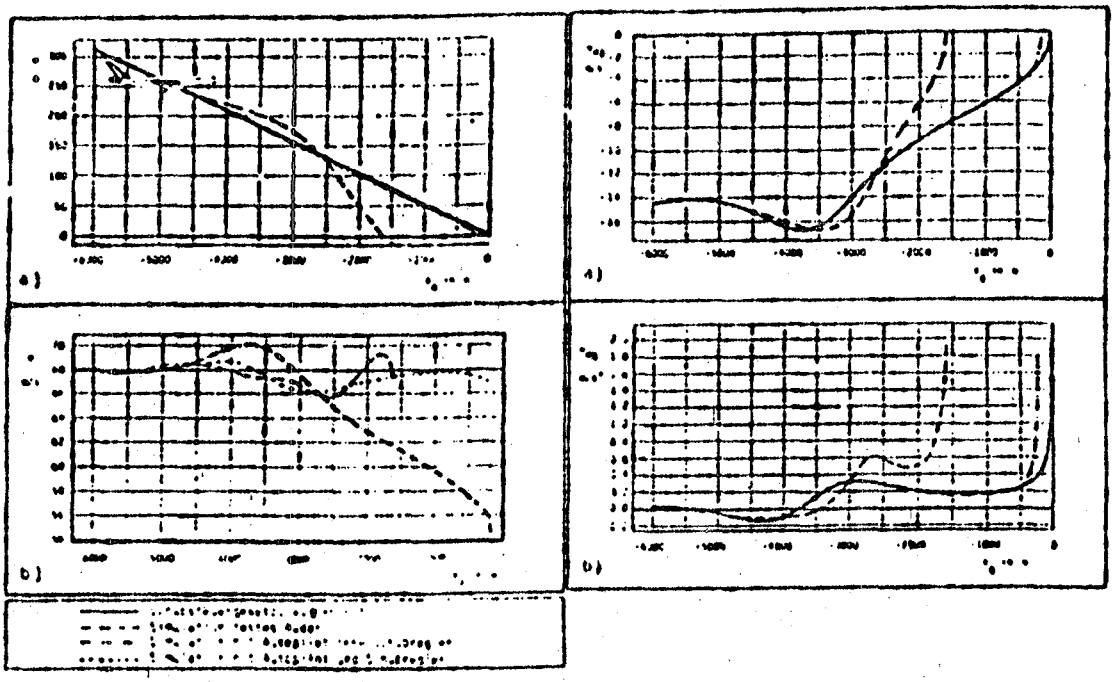

Figure 5.6: curves of flight path and speed
KEY ILLEGIBLE

Figure 5.7: curves of wind values

About 3400m in front of the runway threshold the wind speed maximum is throughflown and headwinds decrease sharply. Phygoid oscillation is excited in opposite phases, flight speed and lift decrease and lead to a steep flight path so that the aircraft prematurely sets down 1600m before the theoretial touchdown point. The angle of flight is -8.5^{o}. This qualitatively corresponds to the curve of state-of-flight values given by KRAUSPE /36/ for solutions and approximations for constant wind gradients u^{WH}.

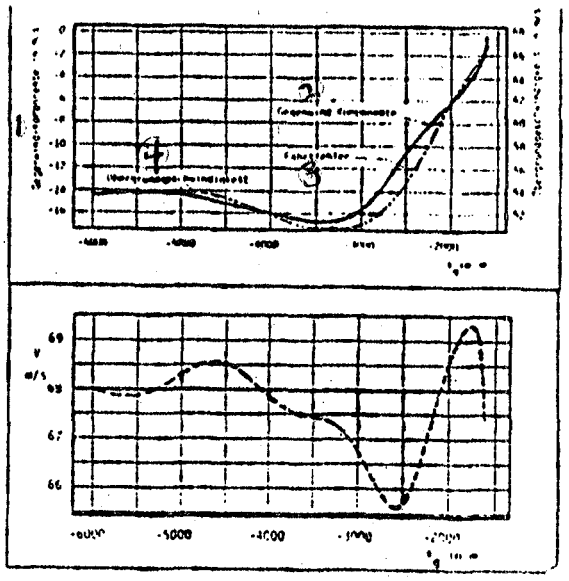

Figure 5.8: reconstruction of course errors, 1-headwind components, 2-headwind components, 3-course error, 4-surface wind speed

THIS PAGE INTENTIONALLY

LEFT BLANK

If one considers the energy-altitude error curve in Figure 5.9 which corresponds to Equation 4.4 an increasing energy "overshoot" up to attainment of the headwind maximum is recognizable which then steadily decreases and passes into an energy-altitude deficit. In the immediate vicinity of the ground surface the deficit has a value of $DELTAH_E$ = -90m, corresponding to a relative energy-altitude (or energy level) error of exactly 0.7. The attempt to maintain theoretical glide path alone by use of the elevators (as is done for example by an autopilot without thrust controller) forcedly leads to large deviations in flight. According to Figure 5.6b (dotted line), flight speed deviates between 70 and 54.5 m/sec, which corresponds to 1.34 or 1.04x of stall speed. The appearing energy excesses or deficits (Figure 5.8) are almost exclusively kinetic energy, which is seen in the course/speed graph.

If one compares the appearing energy-altitude errors with required energy adjustment according to the thrust control law, the comparatively good correlation in the case of simulation with fixed rudder is no longer valid, which above all is due to small deviations in values for V and C_W/C_A in the thrust control law. Because wind speed depends only on altitude it makes sense to plot absolute and relative energy-altitude errors as a function of altitude (Figure 5.9a and 5.9b).

Significant deviations between relative energy-altitude requirements for V and γ = const and relative energy-altitude errors in the case of the "fixed rudder" appear below a flying altitude of 50m where flight paths differ significantly from each

other. In the simulation case there resulted a premature touchdown 1200m before the runway threshold, while according to the thrust cntrol law, energy demand is calculated exactly on the glide path. About 950m in front of the theoretical setdown point there is an inflection in the danger curve boundary (see Section 4), which corresponds to a glide path of 3^{o} at an elevation of /136 50m.

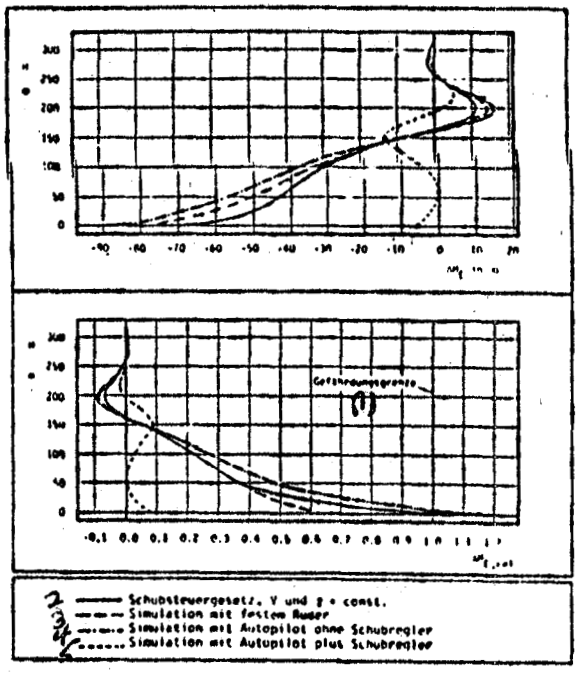
Schubsteuergesetz, V und γ = const.
Simulation mit festem Ruder
Simulation mit Autopilot ohne Schubregler
Simulation mit Autopilot plus Schubregler

Figure 5.9: absolute and relative energy-altitude error as a function of altitude, 1-danger boundary, 2-thrust control law - V and gamma const., 3-simulation with fixed rudder, 4-simulation with autopilot without thrust controller, 5-simulation with autopilot plus thrust controller

If for the lower section one uses the same relationship for danger boundaries as in the range for x< -950m there appears practically no difference between relative energy demand and relative energy error (fixed rudder).

An energy or thrust adjustment according to the thrust control law (Eqn. 4.8) is practically not realizable in its ideal form even when one does not consider the problem of thrust "rest." KONIG

/1/ attained good results with a method which superimposes appearing energy and performance errors onto thrust. But autopilots which appear in the future with thrust control systems (as they are realized today in modern transport craft) represent /137 sufficient margins of safety for landings in the windshear situations described here. Relative energy-altitude error remains below 10% of the danger boundary value (Figure 5.9). The problem area is apparently to be found earlier in a manual landing and the thus appearing danger does not depend on individual pilot behavior or pilot mistakes. If, for example, after the next appearing energy "overshoot" the aircraft is flown along the glide path at the altitude of the wind maximum and thrust is correspondingly cut back without immediately adjusting to the very strong headwind decrease with immediate thrust increase, this leads to a significant worsening of the situation. This will be demonstrated with the "worst case" scenario of a boundary layer "beam" flow whose model parameters were determined from mast measurements in KHABAROVSK (see Section 3.3). The wind speed maximum of 23 m/sec appears here at an altitude of 120m above the ground. If the aircraft is trimmed 6000m before the runway threshold (corresponding to H=314m) and stationary landing approach thrust set, it happens that the craft touches down prematurely about 750m before the threshold (with fixed rudder) at a maximum danger index of 0.9. If there is a trim and thrust adjustment on the glide path at the windspeed maximum and no subsequent rudder movement by the pilot, a crash course with ground contact 1310m in front of the runway threshold becomes apparent (Figure 5.10, upper section). The path slope angle

reaches a value of -15.8° and flight speed falls continuously to about 1.14x stall speed (Figure 5.10, lower). Near the ground the danger boundary is attained with an energy altitude error value of -122m. If the pilot undertakes thrust adjustment 6000m in front of the runway threshold, there results an energy deficit of -95m with a maximum energy "overshoot" at the altitude of wind /138
maximum (30m). The difference between the two values is -125m, about the adjustment value at H_m. The least favorable energy case can be approximated in this way (Figure 5.11).

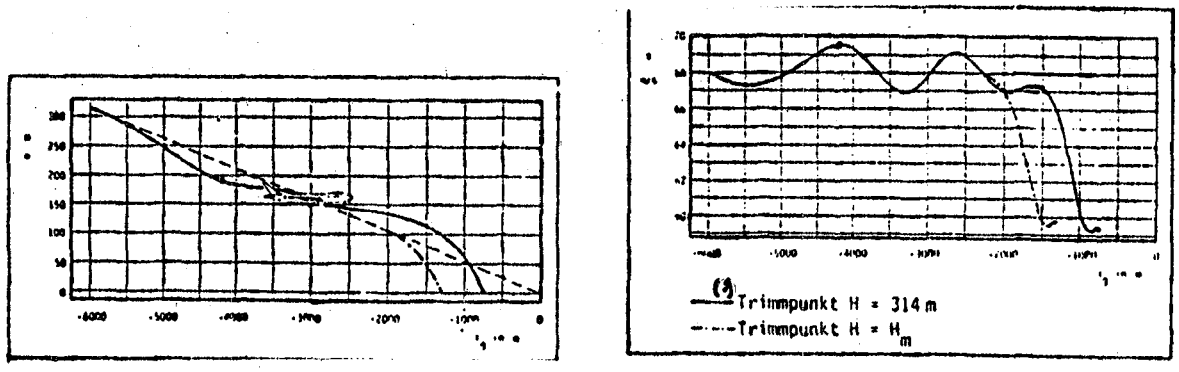

Figure 5.10: curves of flight path and speed for landings in a worst-case boundary layer "beam" flow, 1-trim point

A boundary layer "beam" flow this strong can represent significant danger for a landing aircraft.

It would certainly be desirable to be able to estimate danger from characteristic measured values of wind profiles which originate in a boundary layer beam flow process. From research on 24 measured boundary layer profiles, H_m the altitude of the wind speed maximum (V_{Wx}) and the decrease in headwind between /139
altitude of the maximum and reference altitudes H_R are considered

as having the most significant influences.

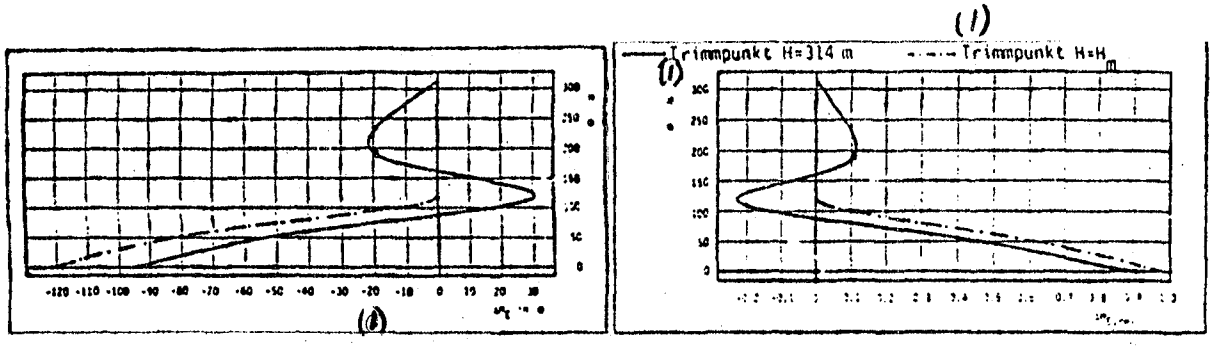

Figure 5.11: curves of absolute and relative energy-altitude errors, 1-trim point

The value of H_R should not be too small in order to detect influences of different profile forms (Figure 5.12). The usual measurement height of H_r=10m is a good choice. Research results are portrayed in Figure 5.13. Relative energy-altitude errors are plotted versus wind maximum altitude, with DELTAu as a parameter.

As an evaluation method (with regard for small expense), energy adjustment DELTA $H_{E,rel}$ from the thrust control law was chosen wherein a supplemental recalculation of danger for landing approach with fixed rudder was done. Because several regions were not supported by measurement results, model parameters (maximum wind jet speed) were varied in a few cases as well as interpolation and extrapolation.

/140

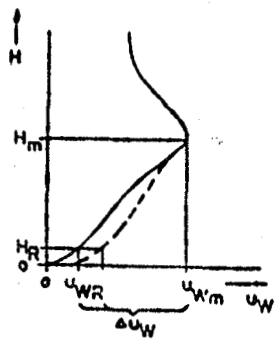

Figure 5.12: definition of magnitudes of influence

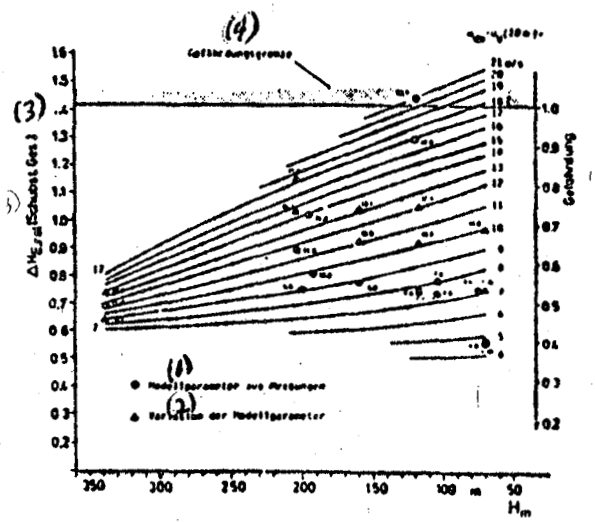

Figure 5.13: diagram for estimation of danger from boundary layer beam flow using easily measureable parameters, 1-model parameters from measurement, 2-variation of model parameters, 3-thrust control law, 4-danger boundary, 5-danger index

/141

An increase in danger is shown with decreasing wind-maximum altitude and increasing speed difference DELTA u_w. An energy level demand related to the the danger boundary of more than 1.0 is expected for wind maxima at 200-250m altitude for values of DELTAu_w between 14 and 16 m/sec. At H=70m the critical value is 10.5m/sec. If one recalculates the relative energy error for danger for a landing approach with fixed rudder, the boundary value for the measured wind curves exceeds the KHABAROVSK profile.

5.3 Landing in a Cloud/Thunderstorm Downdraft

In contrast to the previously considered wind situations, wind speed components change in thunderstorm downdrafts (downbursts, microbursts) as well as with altitude H. As a result, wind speeds appearing along a flight path and their per-unit-time derivatives are affected by the flight path itself and thus the appearing energy errors for the aircraft. Systematic research on landing approaches has shown that along with structure and intensity of a downdraft, takeoff speed, path slope and position of flight path in relation to thunderstorm core are all significant influences. For a better understanding of the phenomena appearing here the example of a landing through a thunderstorm will be closely examined (two-dimensional case). Thunderstorm flow is described as a model by superimposition of induced speeds of 9 vortex pairs. The downburst centrum lies 1700m in front of the runway threshold. At a distance of 6000m in front of the threshold the /142
aircraft is trimmed and stationary landing thrust is set for a glide path of gamma = -3^{o}.

Figure 5.14 shows a flight path curve from simulation calculations with a fixed rudder (solid line), autopilot without thrust controller (dotted line) and autopilot plus thrust controller (finely dotted line). In the last case, the flight path was not supported within the framework of sign precision with the theoretical glide path curve (dotted line) and was for reasons of clarity not drawn in.

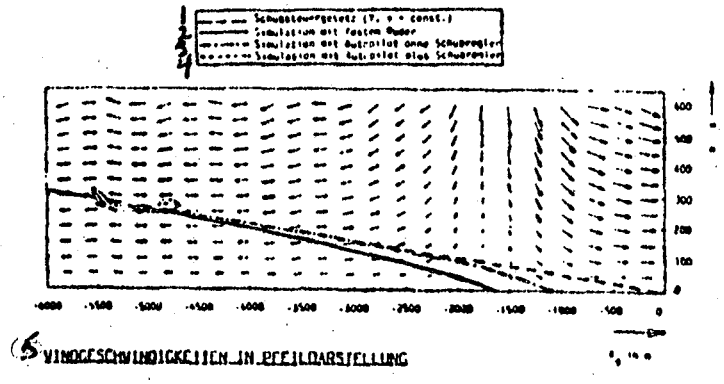

Figure 5.14: flight paths for simulated landings through a thunderstorm downburst, 1-thrust control law (V, γ constant), 2-simulation with fixed rudder, 3-simulation with autopilot without thrust controller, 4-simulation with autopilot plus thrust controller, 5-windspeeds in arrow-type description

The greatest flight deviation occurs in the "fixed rudder" case with touchdown 1650m before the theoretical setdown point. For an engaged autopilot without thrust controller one obtains better path control via steadily increasing speed/course error (Figure 5.16), so that 1800m in front of the theoretical setdown point the stall speed is attained. Below this boundary value the simulation does not give realistic results because the utilized mathematic model does not correctly reproduce aerodynamic relationships in this region.

/143

In the case of simulation with fixed rudder and for engaged autopilot plus thrust controller, the decrease in flight speed is comparatively small at between 2 and 4 m/sec.

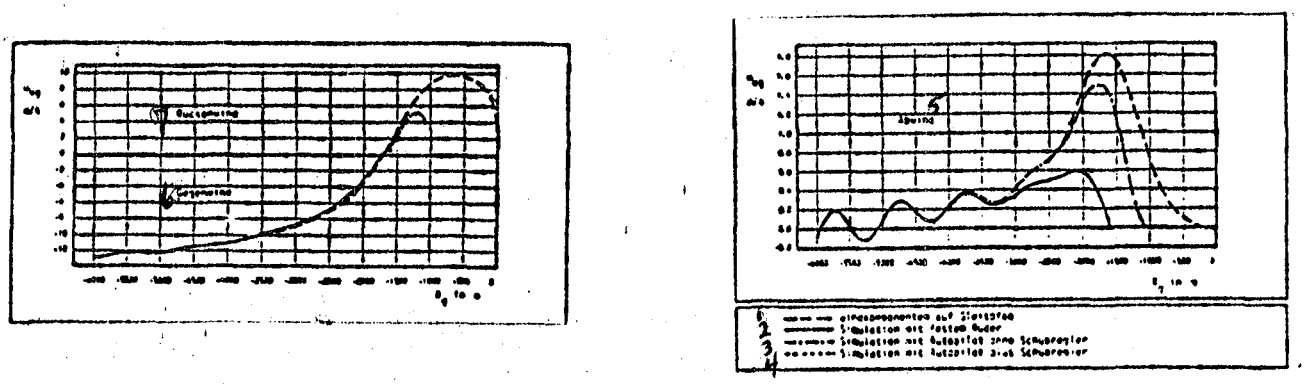

Figure 5.15: wind speed components along different flight paths 1-wind components along glide path, 2-simulation with fixed rudder, 3-simulation with autopilot without thrust controller, 4-simulation with autopilot plus thrust controller, 5-downdraft, 6-headwind, 7-tailwind

In order to localize the influence of different flight courses on wind speed components along the flight path, wind components are plotted in Figure 5.15 versus the coordinate x. It is thus shown that u-components (oriented to runway direction) in all cases approximate nearly the same curves, if one disregards different setdown points. This indicates that the u-component (like the stagnation point model and the vortex model) is predominantly a function of path x. In contrast to this, different flight courses /144 decisively affect vertical winds which have effects on the aircraft.

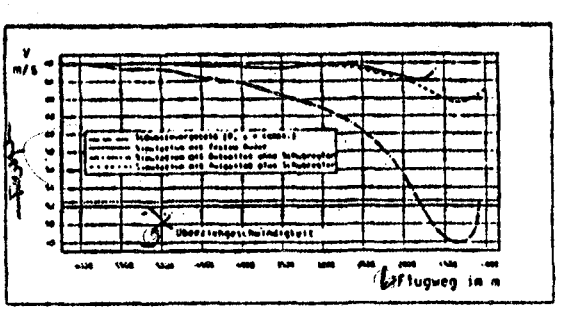

Figure 5.16: curves for flight speeds, 1-thrust control law (V, γ constant), 2-simulation with fixed rudder, 3-simulation with autopilot without thrust controller, 4-simulation with autopilot plus thrust controller, 5-stall speed, 6-flight path in m

The thunderstorm core is flown through in different cases at different distances from the ground so that maximum downdraft lies between 0.6 m/sec for the lowest flight (fixed rudder) and 1.8 m/sec for through-flight in the glide path. This correspondingly influences the appearing energy-altitude error along the flight path (Figure 5.17). The smallest energy deficit appears during landing with fixed rudder because the craft did not fly into the area of increasing tailwind due to premature touchdown and vertical winds attained their smallest values. The greatest flight deviations appear to be related to phygoid excitation.

In the case of landing with autopilot (without thrust control) there appear significantly greater energy errors as a result of larger downdrafts and increasing headwinds. The danger boundary is reached 1600m before the runway threshold but we must mention the limitations associated with falling below stall speed. By use of the autopilot and thrust controller, energy-altitude errors can be limited to +30m. Supplemental energy use according to the thrust control law attains at 180m a comparatively high /145 value which lies far below the danger boundary. This case represents the danger potential for landing at a glide path of $\gamma = -3^{o}$.

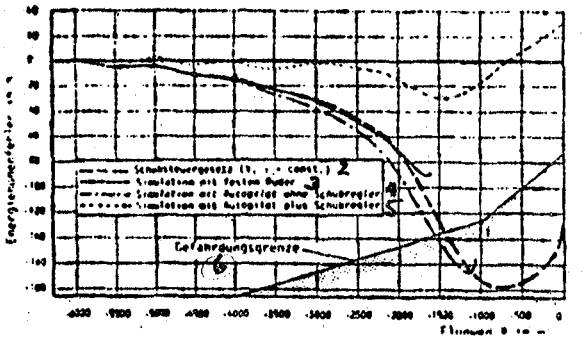

Figure 5.17: energy-altitude errors for landing in a thunderstorm downburst, 1-energy-altitude error in m, 2-thrust control law (V, γ = constant), 3-simulation with fixed rudder, 4-simulation with autopilot without thrust controller, 5-simulation with autopilot plus thrust controller, 6-danger boundary

According to position of flight path in relation to thunderstorm core, different values can be expected as was already clearly shown in the example. The results in Figure 5.18 for a variation of path slope angle and thunderstorm core position in front of the runway threshold can be qualitatively predicted from previously won information. The greater the distance from the ground during storm through-flight, the larger the downdraft wind speed and thus the expected energy error. That means the steeper the path angle and the greater the distance of the downburst from the theoretical setdown point, the less favorable will be the aircraft's energy situation. Above all, danger limits are likewise a function of distance from the theoretical setdown point, so that the relative energy-altitude error (which is evaluated as a measure of danger) can in certain cases decrease in spite of increasing absolute value.

/146

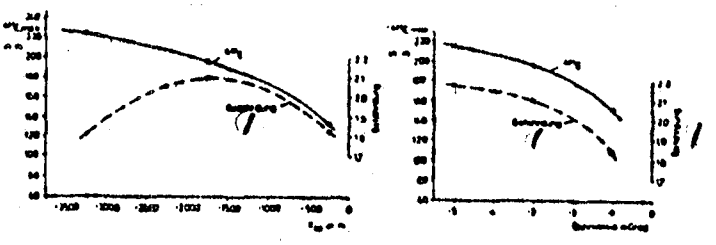

Figure 5.18: influence of thunderstorm core position and path slope angle on energy error, 1-danger

5.4 Landing in A Flow Field in a Front

The flow field in a front is shaped by a directional reverse of the wind in front of and behind the front and by an outwardly directed air flow in the area of the frontal plane. For a landing through such a wind field there are sudden changes in tail and head winds and to some extent very intense updrafts. Both affect an energy surplus whenever by recession of thrust and if necessary by supplemental resistance increase a balance is created. The order of magnitude of the energy surplus was calculated according to the thrust control law for one landing at a -3^{o} glide path. Figure 5.19 shows the wind speed field, wind components and energy use which results when flying through a frontal flow (flow surface branching model - see Eqn. 3.32). Via the sharp change in horizontal wind from 13 m/sec tailwind into a headwind of -12 m/sec and an updraft field of maximum -2.4 m/sec there forms an energy-altitude surplus of 170m. In order to hold /147
course constant, the thrust had to be reduced 32% from F_{max}, which for a stationary landing thrust of 29% of F_{max} is practically not realizable. Here there are additional steps to be considered for increasing resistance via airbrakes and spoilers.

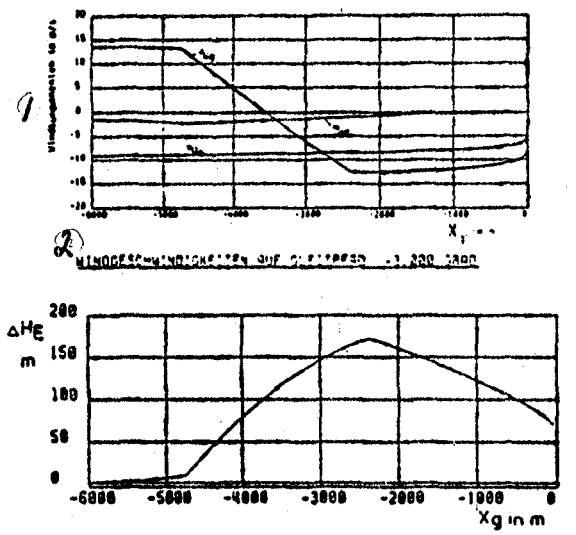

Figure 5.19: wind speeds and energy surpluses on a -3^{o} glide path in a front (flow surface branching model) 1-wind components in m/sec, 2-wind speeds on a glide path of -3^{o}

Results of a simulated landing with fixed rudder can be seen in the following Figures where the flow field was subjected to superposition by viscous vortex pairs. Speed changes and vertical wind are not so strongly shaped as in the above example. Figure 5.20 shows the curve for wind components on a -3^{o} glide path while Figure 5.21 shows flight path in the flow field. One recognizes an exceeding of the theoretical flight path at altitudes above 120m, which for speed deviations of +3 m/sec and /148 -4.5 m/sec has the result of an energy-altitude surplus of 105m. The necessary energy surplus according to the thrust control law is smaller at 95%, because in the simulation the frontal plane is flown through at a greater altitude where large updraft speeds appear (-2.1 m/sec). For engaged autopilots the same energy surplus appeared with a speed increase of 12.5 m/sec with especially good adherence to theoretical flight path. With the help of the autopilot plus thrust controller system, appearing energy surpluses or deficits can be limited to +25m or -15m even

if the required propulsion system throttling to 12% of maximum thrust is problematic.

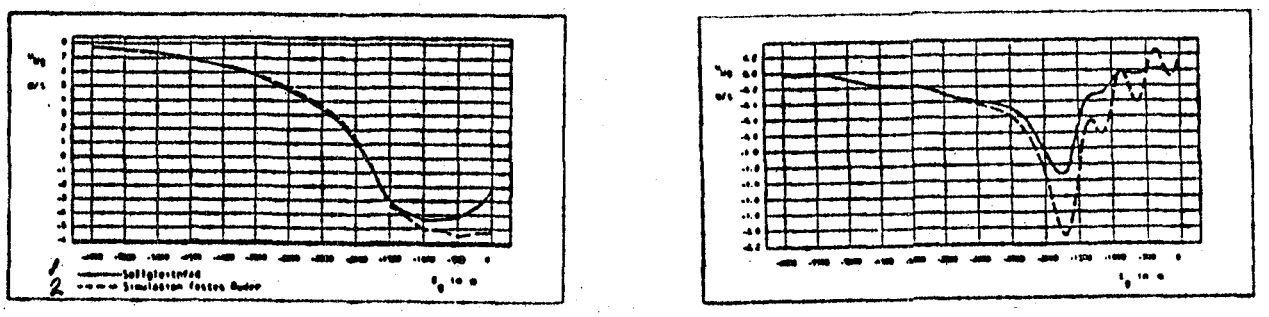

Figure 5.20: curves for wind speed components on the glide path (vortex model) 1-theoretical flight path, 2-simulation with fixed rudder

It is thus shown that during a landing in the area of a weather front, danger to an aircraft can arise via significant energy /149 surpluses in contrast to other windshear phenomena.

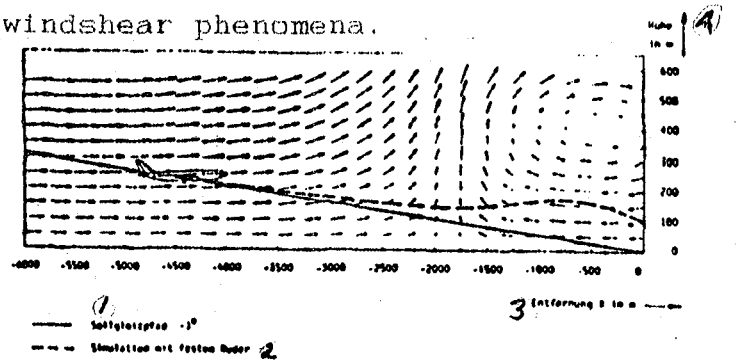

Figure 5.21: flight path position in a flow field, 1-theoretical glide path -3°, 2-simulation with fixed rudder, 3-distance x in m, 4-altitude in m

There exists the danger of touching down too late on the runway if the situation is not properly recognized by the pilot and if necessary alleviated by a quick takeoff. A thrust or energy adjustment according to the thrust control law is only possible with limitations.

/150

6. Conclusion and Views

Research on endangerment to aircraft via windshear requires suited wind models which describe the typical curves for flow speeds for dangerous wind situations with sufficient resolution. Thus ,for applications in flight simulation there often results the requirement for a simple mathematic model construction for reasons of computation time limitations,so that one must limit oneself to simplified quasistationary approximation solutions.

The results represented in this work show that development of suitable analytical half-empirical engineering models is realizable via application or combination of known solutions from flow mechanics. Thus,solutions and potential flows as well as frictionally loaded flows can find application. For simulation of takeoff and landing procedures the range of validity of models as a rule can be limited to cross-sections 10km long and 500m high.

For tasks in flight technology,there are four different wind situations of significance which are described with models: thunderstorm downburst, windshear in weather fronts, boundary layer beam (laminar?) flow and ground boundary layer shear and their deviations.

To depict speed curves in weather fronts and thunderstorm downbursts, superposition of wind speed components (which are induced by a number of viscous vortex pairs) is well suited. According to the particular problem and existing data, an

expanded stagnation point flow in the case of downburst or flow /151
surface branching gives good results for frontal flow.

A simple half-empirical engineering model for boundary layer beam flow is obtained by superposing speed distributions from one planar free jet and one ground boundary layer profile, wherein for describing the boundary layer profile the commonly known exponential law finds application. A comparison of the model with a number of results from mast and aircraft measurements shows that with this supposition a quite good approximation of measured wind curves can be had.

These four wind models form the basis for research regarding endangerment of aircraft during landing procedures. Herein one can comprehend the danger criteria that were obtained by KONIG from energy considerations. If one expresses appearing deviations from theoretical values of flight speed and the path angle (glide path) as an error in the aerokinetic and potential energy one obtains - oriented to flight weight - energy level deficits or surpluses along the flight path. This can be related to danger limits/boundaries which KONIG formulated as a function of stall speed (relative danger "speed") and distance from theoretical touchdown (landing) point. Thus a measure of danger emanating from different windshear situations can be determined from simulated landings.

A somewhat simpler method which produces a direct relationship between wind situation parameters and energy values originates with the consideration that energy errors from a corresponding

adjustment of propulsion unit thrust are avoidable. During a stationary landing with constant wind, landing thrust is set constant which trims the aircraft to a constant decrease in /152 potential energy and thus with V=const the total energy. If wind changes appear along the flight path a corresponding energy addition or reduction is performed with the help of thrust if speed and path angle do not change. The measure for necessary thrust adjustment is determined by the ideal thrust control law which is transformed into an energy control law by integration along the path. In this law, headwind and vertical wind enter as wind values as well as their per-unit-time derivatives, while as an aircraft-oriented parameter the theoretical values of speed and path angle enter into consideration. If one starts from the simplified assumption that while omitting energy adjustment, energy errors of the same magnitude are present, the above-named danger boundaries are applied. Because path angle and speed and thus aerodynamic state (C_W/C_A) during simulated landings are subjected to more or less strong deviations but are in contrast presumed to be constant in the thrust control law, the named predictions are not exactly met with.

Comparative experiments between both danger criteria have shown that energy errors appearing in simulation with a fixed rudder and the values resulting from energy adjustment according to the thrust control law basically coincide. It should be differentiated whether wind speed is a function of altitude alone as one can assume for boundary layer beam flow and frequently for ground boundary layer profiles or whether it also varies with the

path coordinate. In the first case wind speeds affecting the aircraft during landing are independent of flight path. The per-unit-time change in wind components is certainly dependent on the aircraft's vertical speed; however, this effect is compensated for by an opposing sinking speed tendency when flying through the /153 shear layer. Deviations from the required energy levels which appear along simulated flight paths during landing on the glide path with constant speed are thus speed errors and point back to the associated change in aerodynamic state and can be considered via correction factors. Thus maximum energy error and extent of danger can be estimated for a fixed rudder landing from simple computations with the thrust control law.

In the second case, in which (like during a thunderstorm downburst or frontal flow) path and altitude dependent wind speeds appear, wind components affecting the aircraft as well as their per-unit-time derivatives are dependent on light path and the position of the flight path in the wind field. Values computed from thrust or energy adjustment for relative energy level requirements thus represent the danger potential for a landing on a defined glide path.

A comparison of danger criteria resulting from energy considerations and characteristics for describing windshear strength (as they are expressed by local windshear gradients and the Wind Shear Severity Factor [RAE]) shows a recognizable relationship if the maximum windshear gradient is representative for the entire wind profile. If wind gradients are generated by secondary squall fronts or other non-homogeneities they are

generally of short duration and have little effect on the aircraft's energy balance. This prediction is confirmed by statistical analyses of over 200 wind curves obtained by a LUFTHANSA Airbus. For this frequency, summations of maximum windshear gradient as well as maximum relative energy-altitude adjustment are calculated and evaluated. During discrimination or distinction of atmospheric stability a tendency towards increasing maximum energy use and thus danger with increasing /154
stability is shown, although larger vertical windshear gradients u_{WH} appear during stable layering with less frequency. The typical wind profile for stable conditions generally exhibits comparably small vertical gradients which however have an effect over a great altitude range. Thereby considerable energy errors can build during a landing.

Experimental results concerning danger which originates from the described model windshear situations for landings can be understood as follows.

As existing accident statistics would lead one to expect, the greatest danger during landing in windshear conditions is in thunderstorm downbursts because the effects here are a combination of tailwind shears and downdrafts. Neglecting intensity of wind changes the extent of danger is greatly dependant on path angle with which the downdraft is flown through and on the position of the thunderstorm core with respect to the theoretical touchdown point. The greater the magnitude of the flight path angle and the further the storm core is from the landing runway threshold the less favorable the energy

relationships for the aircraft whenever trimming thrust to the wind situation takes place outside the core flow.

In contrast to the thunderstorm situation, a significant energy surplus can form during a landing through the flow field for reasons of headwind shear and the outwards-directed flow. There thus arises the danger of overshooting the runway if the situation is not quickly recognized by the pilot and avoided if necessary by a quick pull-up.

/155

During boundary layer beam flow the danger situation in a landing is comparatively well controllable because one can start with approximation methods from horizontal wind field homogeneity and the energy error can be had from a few parameters. Throughflight direction, distance to the ground from the headwind speed maximum as well as decrease in headwind between maximum value and a reference value near the ground are considered significant influences. For one wind curve measured in Northern Germany, nightly boundary layer beam flow reached 70 to 75% of the danger boundary value (as relates to simulation with fixed rudder). In the case of the "worst case profile" used in the USSR, the danger boundary is absolutely exceeded.

Normal ground boundary layer shears give - as day-to-day experience in aviation shows - no safety problems. Relative energy errors of more than 50% of the danger value are mostly for wind profiles as they appear during stable layering and great surface roughness and are expected in combination with strong winds.

It should be strongly stated that windshear conditions can lead to critical situations and premature ground contact even if danger limits are not yet attained or exceeded. This along with the influence of wind changes is part of aircraft dynamics which can lead to loss of phygoid oscillation damping in the aircraft /36/ and not the least affect pilot behavior. This factor can scarcely be considered without a realistic pilot model for energy considerations. So during phygoidal oscillation one can start with a good approximation for the exchange of potential and kinetic energy without the total energy changing significantly. If the pilot recognizes too late or not at all (for reasons of high loading/stress during landing) vertical deviation from his /156
glide path, he cannot use the resulting portion from the speed surplus (as kinetic energy) to balance the deficit of potential energy. A crash results although a critical total energy error was not attained. Further research should include investigation of pilot behavior and factors in supplemental pilot stress during landings under windshear conditions. I mention here switching from instrument to visual flight in the final stages of landing, the influence of variable side winds and not the least influences of turbulence which have special significance in thunderstorms and fronts. There are good prospects for obtaining the missing measurement data in an international frontal experiment planned for 1987.

7. Literature

/1/ König, R.

Erhöhung der Flugsicherheit bei Scherwindanflügen durch Modifikation von Schubregelungssystemen und bestehender Cockpit-Instrumentierung.
Jahrestagung der DGLR, Stuttgart.
5. - 7. Oktober 1982 Vortrag Nr. 82 - 033
und Wissenschaftliche Berichte 1982, SFB 58 'Flugführung' TU Braunschweig u. DFVLR

/2/ Schanzer, G.

Influence of Windshear on Flight Safety.
AGARD, 42nd Symposium of the Flight Mechanics Panel Athens, Greece,
10. - 13. May 1983, Paper No 12

/3/ Schanzer, G.

Einführung in die Flugphysik.
Vorlesungsmanuskript zur Vorlesung an Institut für Flugführung der TU Braunschweig, 1983

/4/ Reichardt, H.

Impuls- und Wärmeaustausch in freier Turbulenz.
ZAMM 24, 268 (1944)

/5/ Krousse, P.
Swolinsky, M.
Voremann, P.

Windmessungen bei Start und Landung zur Analyse von Scherwindsituationen.
DGLR-Jahrestagg, Aachen 1981
Vortrag Nr. 81-062

/6/ Krousse, P.
Swolinsky, M.
Voremann, P.

Wind Determination and Wind Shear Detection from Flight test and Airline Flight Data.
International Conference on Aviation Weather System, American Meteorological Society, Montreal, Que, May 1981

/7/ Swolinsky, M.
Krousse, P.

Windbestimmung aus Flugmeßdaten eines Linienflugzeugs.
Meteorologische Rundschau 37, 77-81,
Juni 1984

/8/ Jacob, H.G.

Fortran-Programm zur Erstellung eines lokalen Optimums einer beschränkten multivariablen Funktion ohne Kenntnis ihrer Ableitungen.
Bericht Nr. KFK-PDV 36, Kernforschungszentrum Karlsruhe, 1975

/9/ Reichardt, H.

Gesetzmäßigkeiten der freien Turbulenz,
VDI-Forschungsheft 414 (1942), 2.Aufl.1951

/10/ Gertler

Berechnung von Aufgaben der freien Turbulenz auf Grund eines neuen Näherungsansatzes.
ZAMM 632, 244 - 256 (1942)

/11/ Ville, A.
Fernholz, H.

Report on the first European Mechanics Colloquium on Coanda effect
J. Fluid Mech. Vol. 23, part 4,
801 - 819, (1965)

/12/ Glauert, M.B.

The wall jet.
J. Fluid Mech. 1, 625 - 643 (1956)

/13/ König, R.
Krousse, P.
Schanzer, G.

Procedures to Improve Flight Safety in Wind Shear Conditions.
in: Proceedings of the 12th Congress of the Aeronautical Sciences.
Munich, FRG, Oct. 1980
ICAS - 80 - 22.3.

/14/ König, R.

Kompensation von Scherwind durch Eingriff in den Energiehaushalt.
Sonderforschungsbereich 58 'Flugführung'
Bericht Nr. 69, Dez. 1982

/15/ Bodner, J.

Low-Level Wind Shear: A Critical Review.
NOAA Techn. Memorandum NWS FCST - 23.
National Oceanic and Atmospheric Administration,
Silver Spring, Md., Apr. 1979.

/16/ Woodfield, A.E.
Wood, J.F.

Worldwide Occurrence of Wind Shear During 1981-1982.
AGARD CP No. 347
Athens, 10. - 13. May 1983

/17/ Haanes, A.

Description of a Program Developed for the Analysis of Windshears Experienced During Aircraft Approach to Landing.
Royal Aircraft Establishment
Techn. MEMO FS 321, March 1983

/18/ Heverdings, H.

On the use of AIDS-data for a statistical analysis of wind shear during the approach.
10. Symposium 'Bordintegrierte Flugdatenprozesse', Aachen, März 1980
DFVLR-Mitt. 80-09

Note: Foreign references are illegible.

/19/ Hoverdings, H.

AIDS-Derived Wind Shear Statistics for Approach and Landing.
NLR TR 81066 L, Mai 1981

/20/ Roth, R.

Ansätze einer Theorie der Grundschicht. Projekt 4.
Heft 1, 1974, S. 3 - 6

/21/ Bradshaw, P.
Gee, M.T.

Turbulent wall jets with and without an external stream.
A.R.C. R _n 3252, 2 - 48 (1962)

/22/ Prandtl, L.
Tollmien, W.

Die Windverteilung über dem Erdboden, errechnet aus den Gesetzen der Rohrströmung.
Zeitschrift f. Geophysik, 1.Jg. (1924), S. 47 - 55
und L. Prandtl, Gesammelte Abhandlungen.
Dritter Teil. Springer Verlag 1961.

/23/ Monin, A.S.
Obuchow, A. M.

Fundamentale Gesetzmäßigkeit der turbulenten Vermischung in der bodennahen Schicht der Atmosphäre.
in: Statistische Theorie der Turbulenz
Akademieverlag, Berlin 1958, S. 199-226

/24/ Plate, E. J.

Aerodynamic Characteristics of Atmospheric Boundary Layers.
Atomic Energy Commission
Division of Technical Information, 1971

/25/ Frost, R.

The Velocity Profile in the Lowest 400 ft.
Meteorol. Magazin, 76, S. 14 (1947)

/26/ Homel, G.

Seitaförmige Bewegung zäher Flüssigkeiten.
Jahresberichte der Dt.Mathematiker-Vereinigung 25, S. 38 - 60 (1916)

/27/ Ekman, V.

Dynamische Gesetze der Meeresströmungen.
Innsbrucker Vorträge 1922, S. 99.

/28/ Prandtl, L.

Strömungslehre.
Vieweg-Verlag, Braunschweig, 1965

/29/ Hunt, J.C.R.
Snyder, W.H.
Lawson, R.

Flow Structure and turbulent Diffusion around a three-dimensional hill.
Part I, Flow Structure,C.E.R.A. Report

/30/ Hornung, H.
Perry, A.E.

Some Aspects of Three-Dimensional Separation. Part I : Streamsurface Bifurcations
Z. Flugwiss. Weltraumforsch. 8 (1984), H. 2

/31/ Roth, R.

Der nächtliche Grenzschichtstrahlstrom.
Symposium 'Nächtliche Grenzschichtstrahlströme',
18.-19.6.1980, Traben-Trarbach.

/32/ Kottmeier, C.

Die Vertikalstruktur nächtlicher Grenzschichtstrahlströme.
Dissertation am Institut für Meteorologie und Klimatologie der Universität Hannover, 1982

/33/ Roth, R.
Kottmeier, C.
Lege, U.

Die lokale Feinstruktur eines Grenzschichtstrahlstroms.
Meteorol. Rdsch. 32, 65-72 (Juni 1979)

/34/ Albring, W.

Angewandte Strömungslehre.
Verlag Theodor Steinkopff.
Dresden, 1978

/35/ Shelkownikow, M.S.

Struinye techenia na sklonakh vozdushnykh (Strahlströme in geringer Höhe).
Meteorologie i gidrologie, 1941,
Nr. 11, Moskau, S. 48 - 56

/36/ Krause, P.

Beiträge zur Längsbewegung von Flugzeugen in Windscherungen.
Dissertation, Fakultät für Maschinenbau und Elektrotechnik der TU Braunschweig, 1983

/37/ Ellis, O.W.
Keenan, M.G.

Development of Wind Shear Models and Determination of Wind Shear Hazards.
FAA-Report No. FAA-RD-79-119
January 1978.

/38/ Sinclair

A Simple Model of Frontal Surface Windshear.
National Research Concil of Canada
Internar Bericht

/39/ Heintsch, B

Untersuchungen zur Gefährdung eines Verkehrsflugzeuges beim Durchfliegen von Gewitterstürmen.
Diplomarbeit am Institut für Flugführung der TU Braunschweig
März 1984

/40/ Shangxiang Zhu
Ethin, B.

Fluid-Dynamic Model of a Downburst.
UTIAS-Report Nr. 271, April 1983

/41/ Krauspe, P.
Schänzer, G.

Einfaches Triebwerksmodell zur Simulation nichtlinearer dynamischer Schubänderungen.
Z. Flugwiss.Weltraumforsch. Bd.2, Heft 3, 1978

/42/ Lee, J.T.
Stotus, J.
Seeaki, Y.
Bowker, T.

Thunderstorm Gust Front-Observation and Modeling.
FAA-Report Nr. FAA-RD-78-145
December 1978

/43/ Goff, R.C.

Thunderstorm-Outflow Kinematics and Dynamics.
NOAA IM ERL NSSL-75, Dec. 1975.

/44/ Goff, R.C.
Lee, J.T.
Brandes, E.A.

Gust Front Analytical Study.
FAA-Report No. FAA-RD-77-119

/45/ Pritchard, F.E.
Colvin, C.E.
Mc Vehil, G.E.

Spectral and Exceedance Probability Models of Atmospheric Turbulence for use in Aircraft Design and Operation.
AFFDL-TR-65-122, November 1965.

/46/ Mc Carthy, J.
Black, E.F.
Bowsch, R.D.

A Spectral Analysis of Thunderstorm Turbulence and Jet Transport Landing Performance.
Conference on Atmospheric Environments of Aerospace Systems and Applied Meteorology.
New York, November 1978

/47/ Barr, N.M. et.al.

Wind models for Flight Simulator Certification of Landing and Approach Guidance and Control Systems.
FAA-RD-74-206, Dec. 1974

/48/ -

Procedures for Air Navigation Services Aircraft Operations.
PANS-OPS Volume I, 1980, ICAO

/49/ Vorsmann, P.

Ein Beitrag zur bordautonomen Windmessung.
Dissertation, Fakultät für Maschinenbau und Elektrotechnik der TU Braunschweig.
1984

/50/ Svatinsky, M.

Abschlußbericht zum Forschungsvorhaben DFG/Schä 338/3-1 'Windmessungen während der Start- und Landephase eines Linienflugzeuges zur statistischen Scherwindanalyse'.
Institut für Flugführung der TU Braunschweig, April 1985

/51/ Svatinsky, M.

Windmessungen während der Start- und Landephase eines Linienflugzeugen zur statistischen Scherwindanalyse.
Wissenschaftliche Berichte 1982
Sonderforschungsbereich 58 'Flugführung'

/52/ Counihan, J.

Adiabatic Atmospheric Boundary Layers A Review and Analysis of Data from the Period 1880-1972.
Atmosph. Environment, Vol 9, S. 871-905
Pergamon Press 1975

/53/ Fiedler, F.

Die Grenzschicht der Atmosphäre: Struktureller Aufbau.
in: Promet 6, Heft 1, 1976, S. 1-3

/54/ Blackadar, A.K.

Boundary Layer wind maxima and their significance for the growth of nocturnal inversions. Bull.Am. Meteorol. Soc. 38, 283 - 290, 1957

/55/ England, J.
Ulbricht, W.

Flugmeteorologie.
Transpress VEB Verlag für Verkehrswesen Berlin 1980

/56/ Weber, F.

Windscherungen und Inversionen im Bereich der planetaren Grenzschicht.
Z. Flugwiss. Weltraumforsch. 2 (1978), Heft 3, S. 175 - 180

/57/ Wilson, J.W.
Roberts, R.D.
Kessinger, C.
Mc Carthy, J.

Microburst Wind Structure and Evaluation of Doppler Radar for Airport Wind Shear Detection.
Journal of Climate and Applied Meteorology Vol 23, Juni 1984, S. 898 - 915

/58/ Eichenberger, W.

Fluguetterkunde. Handbuch für die Fliegerei. Schweizer Druck- und Verlagshaus AG, Zurich 1962

/59/ Soua, O.F.

Low-Level Wind Shear - Its Effects on Approach and Climbout.
IDC Flight Approach No. 20/1974, pp. 10-17
Mc Donnell Douglas Aircraft Comp., St.Louis,Miss.

/60/ Krauspe, P.
Konig, R.

The Influence of Wind Shear and Vertical Winds on Takeoffs and Go-Arounds.
Airport Forum, Vol.XI, Heft 5, Oct.1981

/61/ Archibald, W.

An account of some preliminary experiments with Dirona anemometers,attached to kite strings.
Nature 31 (1883), 66.

/62/ -

Circulation of Proposed Wind Model Appendix for Project 412 Based on UK ARB Regulatory Document.
Airlines Electronic Engineering Committee Letter No. 70-2-40, July 17, 1970.

/63/ Davenport, A.G.

Rationale for Determining Design Wind Velocities.
Journal of the Proceedings of the American Society of Civil Engineers, Structural Division, May 1960.

/64/ Shelton, G.B.

Investigation of Gusts on V/STOL Craft in Transition on Hover.
AFFDL-TR-68-89.

/65/ Hunt, J.C.R.
Simpson, J.E.

Atmospheric Boundary Layers over Non-Homogeneous Terrain.
int Engineering Meteorology (Hrsg. Plate), Kap. 7, S. 269 ff

/66/ -

Windmessungen an der Weidacher Höhe.
Zwischenbericht zum Forschungs- und Entwicklungsauftrag BMV-FE-L-4784
Institut für Flugführung der TU Braunschweig, 1985

/67/ Schanzer, G.

Untersuchung über die Hindernisfreiheit beim Durchstart von Verkehrsflugzeugen in Landebahnrichtung 26.
Gutachten für das Land Baden-Württemberg Braunschweig, 1978

/68/ Thorpe, A.J.
Miller, M.J.
Moncrieff

Dynamic Models of Two-Dimensional Downdraughts.
Quart. J. R. Met. Soc.(1980), 106, 463-484

/69/ Schlichting, H.

Grenzschicht-Theorie.
Verlag G. Braun, Karlsruhe 1982.

/70/ Fortak, H.

Meteorologie.
Dietrich Reimer Verlag, Berlin 1983

/71/ -

Bericht der Europäischen Gemeinschaft zur Sicherheit im Luftverkehr (1983) (vergl. auch Flug Revue 6 (1983), 6-7

/72/ Bray, R.S.

A Method for Three-Dimensional Modelling of Wind-Shear Environments for Flight Simulator Applications.
NASA TM 85969, 1985

/73/ Bedard, A.J.

Optimizing the Use of Surface Sensors for Wind Shear Detection.
J. Aircraft, Vol. 21, No.12, Dec. 1984

/74/ Brost, R.A.
Wyngaard, J.C.

A Model Study of Stable Stratified Planetary Boundary Layer.
J. Atm. Sc. 35,(1978), 1427-1440

/75/ Deleage, Y.

A Numerical Study of the Nocturnal Atmospheric Boundary Layer.
Quart. J. R. Met. Soc. 100 (1974), 351-364

/76/ Thorpe, A.J.
Guyner, T.H.

The Nocturnal Jet.
Quart.J.Roy.Met.Soc. 103 (1977), 633-653

/77/ Etling, D.

Zur Modellierung des Grenzschichtstrahlstromes.
Symposium 'Nächtliche Grenzschichtstrahlströme', 18. - 19.6.1980, Freiburg-Frarbach

/78/ Lucas, J.K.
Reeves, J.B.

Effects of Shear on Aircraft Landing.
NASA CR-2087, Nov. 1972

/79/ Snyder, C.T.

Analog Study of the Longitudinal Response of a Swept-wing Transport Airplane to Wind Shear on Sustained Gusts during Landing Approach.
NASA TN D-6477, Apr. 1960

/80/ Bera, J.

The Influence of Vertical Wind Gradients on the Longitudinal Motion of Airplanes.
NASA TN D-6430, Sept. 1971

/81/ Shorenn, V.L.

Theoretical Analysis of Airplane Longitudinal Stability and Control as Affected by Wind Shear.
NASA TN D-8496, July 1977

/82/ Shorenn, V.L.

Theoretical Study of the Effects of Wind Velocity Gradients on Longitudinal Stability and Control in Climbing and Level Flight.
NASA TP 1332, dec. 1978

/83/ Kuchemann, D.
Weber, J.

Aerodynamics of Propulsion.
Mc Graw-Hill Book Company, INC.
New York, Toronto, London, 1953

/84/ Brousse, P.

Die Gefährdung der Flugsicherheit durch Scherwind.
Sonderforschungsbereich 58 'Flugführung' der TU Braunschweig, Berichte Nr.62.
Sept. 1977
auch DGLR-Jahrbuch 1977, Bd.I, Bau.29

/85/ Konig, R.
Teegen, U.

Experimentelle Untersuchung von Anzeigevorschlagen zur Kompensation von Scherwindeinflussen.
Institutsbericht IB 112 - 81/01, Institut für Flugführung der DFVLR, Oct. 1981.
Braunschweig

/86/ Peterson, E.W.

Modification of Mean Flow and Turbulent Energy by Change of Surface Roughness Under Conditions of Neutral Stability.
Quart. J. R. Met. Soc.(1969), 95, 561-575

/86/ Vörsmann, P.
Swolinsky, M.

Wind Shear Detection from PCM-Recorded MLS-Flight Data.
12th ICAS Congress, Oct.12-17, Munchen 1980

/87/ Swolinsky, M.

Digitale Filterung von PCM-Flugmeßdaten zur Windbestimmung.
10. GIDS-Symposium, Aachen 1980
DFVLR-Mitt.80-09

/88/ Lahl, N.

Vermessung und Modellierung der Flugzeugbewegung sowie deren Auswirkung auf die Navigationsgenauigkeit eines Strapdown Systems.
Dissertation an der TU Braunschweig.
1.November 1981

/89/ Hase, B.

Bestimmung des Schiebewinkels mit Hilfe herkömmlicher Sensoren eines Linienflugzeuges.
Studienarbeit am Institut für Flugführung der TU Braunschweig, Nov. 1983

/90/ Swolinsky, M.
Vörsmann, P.

Windmessungen an Bord des Forschungsflugzeuges Do 28 Skyservant für das MERKUR-Experiment.
Bericht des Institute für Flugführung.
1982

/91/ Lewellen, W.S.

Modeling the Lowest 1 km of the Atmosphere
AGARDograph No. 267, 1981

8. Appendices

A1 Determination Equations for Model Parameters in the LOG-LIN Law

A2 Wind Speed curves of Different Models of the Surface Boundary Layer

A3 Comparison Between Measured Results and Model Description for Boundary Layer Beam Flow

A4 Relationship Between Speed and Temperature Profiles in Free Jets

A5 Model Parameters for Depicted Examples

A6 Measured Results from Thunderstorms and Secondary Squall Fronts

A7 Derivation and Simplification of the Ideal Thrust Control Law

A8 Measurement Concept, Data Preparation and Error Balancing for Wind Determinations in Airline Aircraft Operation

A.1 Determination Equations for Model Parameters in the LOG-LIN Law

Determination of model parameters in the LOG-LIN law (Eqn. 3.6) from measured wind profiles can generally be performed without using linear regression analyses. As a rule, consideration of three measured values (V_{W1}, V_{W2}, V_{W3}) at points H_1, H_2 and H_3 leads to a satisfactory approximation of the measured profile (see sketch below). The determination equations for model parameters are listed below wherein the longitudinal scale L_* is determined from Eqn. 3.4a.

a.

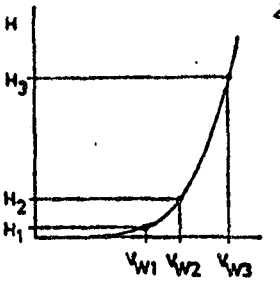

b.

$$\frac{\alpha_\phi}{L_*} = \frac{\ln\frac{H_2}{H_3} - \frac{V_{W2}-V_{W3}}{V_{W1}-V_{W2}}\ln\frac{H_1}{H_2}}{\frac{V_{W2}-V_{W3}}{V_{W1}-V_{W2}}(H_1-H_2)+H_3-H_2}$$

$$u_* = \frac{(V_{W2}-V_{W3})\cdot k}{\ln(\frac{H_2}{H_3}) + \frac{\alpha_\phi}{L_*}(H_2-H_3)}$$

$$H_0 = H_1 \cdot e^{(\frac{\alpha_\phi}{L_*}H_1 - \frac{V_{W1}\cdot k}{u_*})}$$

A.2 Wind Speed Curves of Different Models of the Surface Boundary Layer

To compare ground boundary layer models according to the LOG-LIN law (Eqn. 3.6), the DYER-BUSINGER relationship (Eqns. 3.8 a and b) and the exponential law (Eqn. 3.9) wind profiles are depicted for different atmospheric stability conditions in the diagrams below.

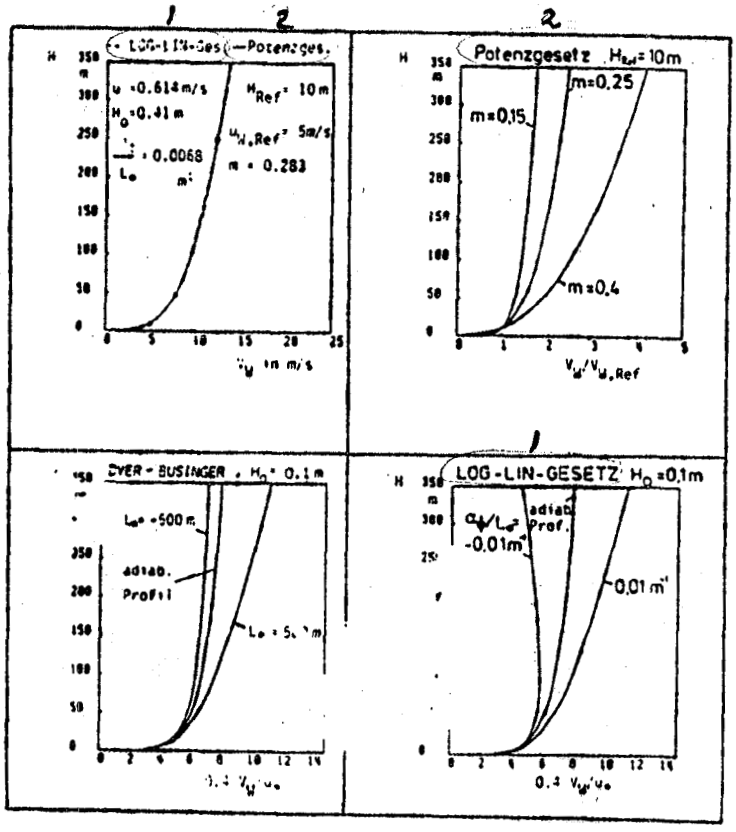

1-LOG-LIN law, 2-exponential law,

A.3 Comparison Between Measured Results and Model Description for Boundary Layer Beam Flow

To determine model parameters during approximation of boundary layer beam flow application of optimization methods based on least squares seems to be the best choice. In this method, the sum of the squared deviation is minimized between the corresponding model and measured value (DELTA $V_W(n)$) by variation of model parameters ($a_1, \ldots a_i$) (with n as number of measured points and i as the number of model parameters.

The following is valid:

$$Q = \sum_{1}^{n} (\Delta V_W(m))^2 \longrightarrow \text{Minimum} \quad (1)$$

with:

$$\Delta V_W(m) = V_{W,Mod}(a_1, a_2 \ldots a_i, n) - V_{W,Mess}(n) \quad (2)$$

For the example shown below, optimum fitting of model parameters occurs with the help of the EXTREM program /8/ which is used at the Institute for Aviation at the Technical University of Braunschweig for several tasks in parameter identification and flight simulation.

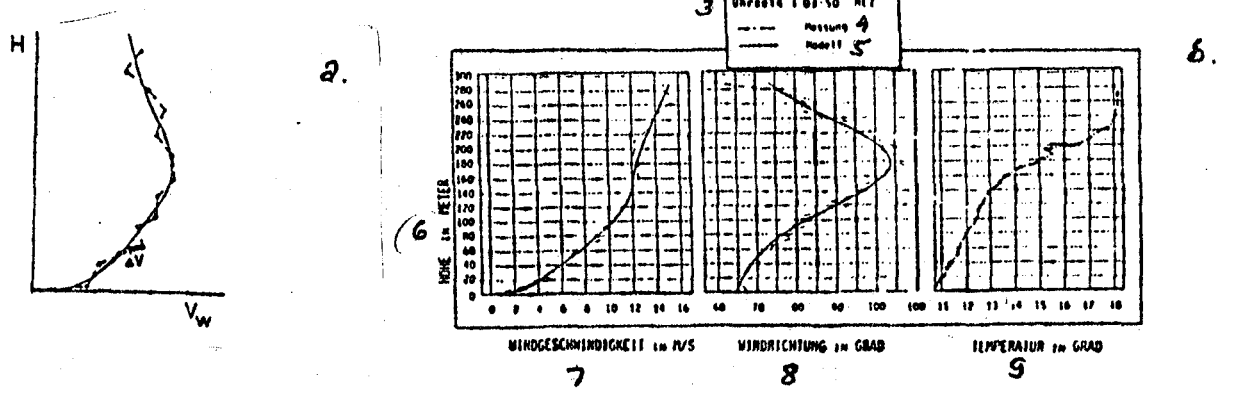

1-measurement site, 2-date, 3-clock time, 4-measurement, 5-model, 6-altitude in m, 7-wind speed in m/sec, 8-wind direction in degrees, 9-temperature in degrees

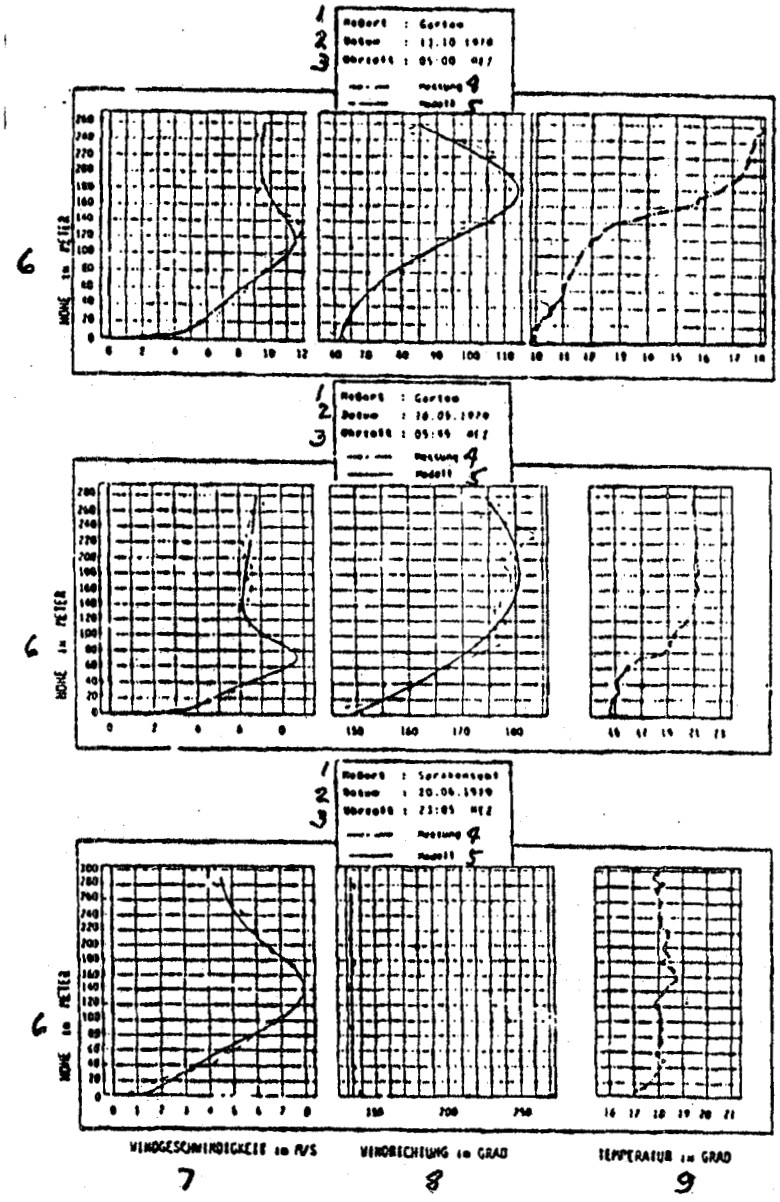

1-measurement site/location, 2-date, 3-clock time, 4-measurement 5-model, 6-altitude in m, 7-wind speed in m/sec, 8-wind direction in degrees, 9-temperature in degrees

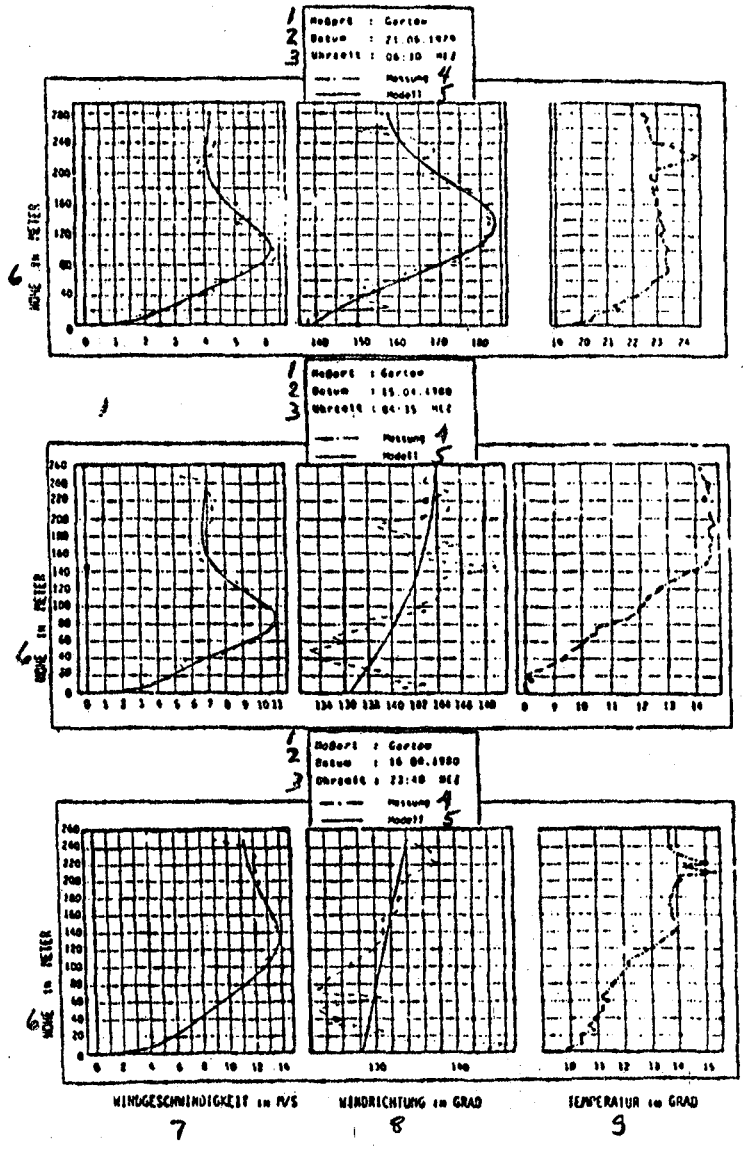

1-measurement site/location, 2-date, 3-clock time, 4-measurement 5-model, 6-altitude in m, 7-wind speed in m/sec, 8-wind direction in degrees, 9-temperature in degrees

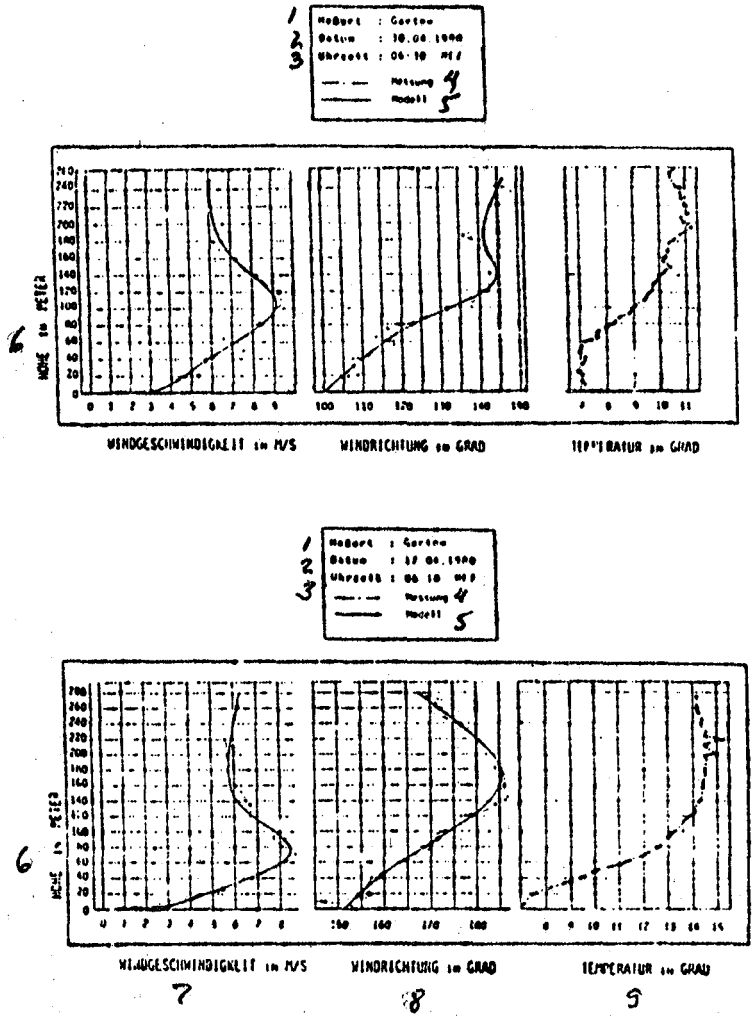

1-measurement site/location, 2-date, 3-clock time, 4-measurement 5-model, 6-altitude in m, 7-wind speed in m/sec, 8-wind direction in degrees, 9-temperature in degrees

/A8

A.4 Relationship Between Speed and Temperature Profiles in Free Jets

Turbulent flow processes are so characterized that average flow is subjected to irregular deviation in movement which intimately mixes the flowing medium. Thus, properties of the medium are exchanged transverse to the main direction of flow. Along with turbulent exchange of suspended particles there is also exchange of impulse and heat. Density of the turbulent impulse transverse flow (τ, identical to turbulent shear stress) and heat (q) are coupled via the exchange value A_τ or A_q with the changes of average speed (u) or average temperature (T) appearing transverse to the direction of expansion /4/:

$$\tau = A_\tau \, d\bar{u}/dz \qquad (A4.1) \qquad q = c_p A_q \, d\bar{T}/dz \qquad (A4.2)$$

For the case that the ratio A_τ / A_q can be considered to be sufficiently constant, REICHARDT /4, 9/ advanced approximations for the relationship between speed and temperature curves transverse to the direction of expansion (Eqn. (A4.3)) wherein normalization occurs with the corresponding maximum value u or T:

$$(\bar{u}/\bar{u}_0) = (\bar{T}/\bar{T}_0)^{A_\tau/A_q} \qquad (A4.3)$$

While for frictional layers (as for example in heated pipes) equally large values for A_q and A_τ were assumed, later experiments showed a ratio of 1.4 or 1.5. For exchange processes in free turbulence (e.g. the area protected from prevailing winds on heated poles in planar free flow) REICHARDT /4/ determined /A9
with a good approximation a fairly constant value of 2. In Figure A4.1 the dimensionless profile of speed and temperature are plotted as a function of transverse distance $\nu = z/B$ where B

is the beam width.

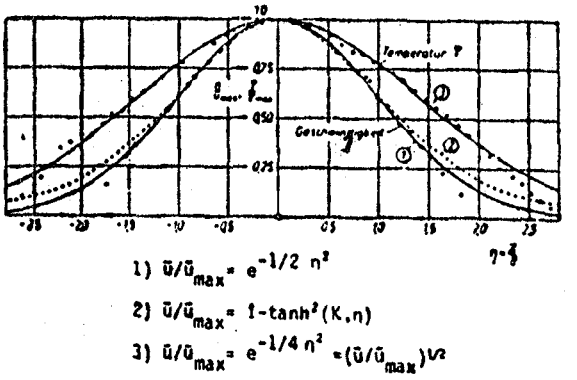

Figure A4.1: temperature and speed distribution in planar free flow from /4, 69/, 1-speed

One would expect only limited transferability of these results to relationships in boundary layer beam flow for reasons of different mechanisms of origin and boundary conditions (no transverse flow, expansion and rotating Earth, wind direction change, etc.). In spite of these limitations similarities in wind and temperature curves are recognizable in a number of measured boundary layer beam flows if one considers the temperature profile (arising from heat flux from the ground surface) as being made up of a flow component which increases linearly with altitude and a flow component which behaves according to Eqn. A4.3.

A.5 Model Parameters for Depicted Examples

A.5.1 Ground Boundary Layer Profile

Model Equations (3.9) and (3.21)

1 Meßort	2 Datum	3 GMT	$V_{W,R}$ m/s	H_R m	m	χ_W(H=10m) Grad 4	χ_{WG} Grad 4	H_0 m	H_G m
Bremen	25.10.80	21:20	3.82	10	0.270	265	36.0	10	300
Hannover	14.11.80	16:50	5.55	10	0.315	210	7.0	10	300
Düsseld.	07.02.81	12:54	6.80	10	0.135	253	10.7	10	300
Frankf.	07.02.81	14:28	5.60	10	0.213	216.5	26.0	10	300
Wien	07.02.81	16:46	9.33	50	0.177	286.0	6.0	10	300
Düsseld.	08.02.81	16:35	5.70	10	0.190	220	16.6	10	300
Frankf.	31.10.80	18:42	4.50	10	0.240				

6.

1-measurement location, 2-date, 3-clock time, 4-degrees

A.5.2 Boundary Layer Beam Flow

Model Equations: wind speed, Eqns. (3.26) and (3.28)

wind direction, Eqn. (3.27)

temperature, under consideration of Eqn. (3.31)

$$T = T_0 + T_H H + \frac{T_m}{\cosh\left(C_T \frac{H - H_T}{H_T}\right)}$$

with $T_0 = T(H=0)$,

$T_H = dT/dH$ (linear component)

T_m = maximum temperature in the flow component at altitude H_T

Boundary Layer Beam Flow and Inversion Shear

Grenzschichtstrahlströme und Inversionsscherungen

6 Flugzeugmessungen

1 Meßort	2 Datum	3 GMT	$V_{W,R}$ m/s	H_R m	m	V_{Ws} m/s	H_s m	C_s	4 X_{Wo} Grad	X_{WG} Grad	H_o m	H_G m	X_{WL} Grad	H_L m	C_L	T_o °C	T_H °C	T_m °C	C_T	H_T m
Bremen	21.10.80	21:20	6.80	500	.532	11.8	135	.85	194.0	33.0	10	500	12.8	240	1.50					
Bremen	22.10.80	06:22	3.00	10	.179	6.0	190	3.04	130.0	70.0	0	500	20.7	250	2.18					
Bremen	23.10.80	06:15	4.79	50	.406	3.4	330	5.28	179.0	28.5	0	500	0.0	-	-					
Frankfurt	23.10.80	07:11	5.65	50	.360	3.4	225	2.00	189.0	18.0	0	500	13.0	445	3.35					
Frankfurt	11.11.80	07:07	4.00	50	.267	5.1	233	2.28	212.0	-4.2	0	500	42.7	550	4.37					
Hamburg	13.11.80	07:55	12.00	500	.430	2.4	275	2.66	210.0	47.0	10	500	27.7	250	2.18					
Frankfurt	14.11.80	10:14	3.74	10	.360	4.0	200	3.64	200.0	22.0	0	350	0.0	-	-					

5 Mastmessungen

Meßort	2 Datum	3 MEZ	$V_{W,R}$ m/s	H_R m	m	V_{Ws} m/s	H_s m	C_s	X_{Wo} Grad	X_{WG} Grad	H_o m	H_G m	X_{WL} Grad	H_L m	C_L	T_o °C	T_H °C	T_m °C	C_T	H_T m
Khabarovsk	23.01.75	?	13.5	200	.750	13.8	114	2.20	-	-	-	-	-	-	-					
Khabarovsk	27.01.75	?	0.5	10	1.00	12.9	193	1.36	-	-	-	-	-	-	-					
Gartow	12.10.78	22:30	3.0	10	.422	5.0	100	1.52	61.5	0.0	10	200	37.4	143	1.47	14	.0017	2.1	3.5	130
Gartow	13.10 78	03:50	2.7	10	.516	1.6	114	2.08	61.7	0.0	10	200	42.1	178	2.02					
Gartow	13.10.78	05:00	4.4	10	.236	3.6	113	2.16	57.2	0.0	10	200	56.7	179	2.00					
Sprakensehl	08.05.79	23:35	2.7	10	.384	4.8	145	1.48	112.3	14.9	10	200	66.9	80	0.14	115	.0065	2.2	2.4	150
Sprakensehl	15.05.79	22:45	2.2	10	.403	5.4	98	1.39	176.0	3.6	0	240	7.9	150	2.00	19	.0150	2.5	2.0	100
Gartow	16.05.79	05:45	3.6	10	.190	3.4	70	2.20	49.9	35.6	10	80	105.9	80	0.22					
Sprakensehl	20.06.79	23:05	0.7	10	.505	5.3	134	1.53	90.6	0.0	10	200	-	-	0.00					
Gartow	21.06.79	06.30	1.3	10	.351	3.3	96	1.59	131.2	15.6	10	200	42.4	127	1.45					
Gartow	15.04.80	04:35	2.9	10	.281	5.8	83	1.84	60.5	0.0	10	200	83.3	255	0.31					
Gartow	15.04.80	22:30	3.4	10	.419	5.4	188	3.54	116.0	15.0	10	200	8.7	228	5.49	115	.0095	1.8	6.3	220
Gartow	16.04.80	23:40	3.0	10	.369	5.6	125	1.54	128.3	4.7	0	200	-	-	0.00					
Gartow	17.04.80	06:10	2.3	10	.302	4.3	71	1.37	142.3	4.6	10	200	39.1	167	1.35					
Gartow	30.04.80	06:30	3.3	10	.182	4.0	101	1.76	102.1	37.5	10	200	15.8	128	3.03					
Sprakensehl	10.06.83	05:47	1.8	40	.466	3.1	70	1.50	15.0	31.0	0	350	70.0	115	1.08					

1-measurement site, 2-date, 3-clock time, 4-degrees, 5-mast measurements, 6-aircraft measurements

A.5.3 Thunderstorm Downdrafts

A.5.3.1 Stagnation Point Flow

Model Equation (3.34), example Figure 3.32

$a = 0.02\ sec^{-1}$, $b = 0.08\ sec^{-1}$, $c = 0.1\ sec^{-1}$

A.5.3.2 Superimposition of Viscous Vortex

Circumferential speed U_τ in a viscous vortex can be described in dependence of a radius r and time t (age of the vortex) with the following equation /69/:

$$u_T(r,t) = \frac{\Gamma_0}{2\pi r}\left(1 - e^{\frac{-r^2}{4\nu t}}\right) \qquad \text{(A5.1)}$$

Herein, $GAMMA_o$ is the vortex filament circulation at time t=0 and ν is apparent kinematic viscosity. Vertical and horizontal components from several superimposed vortexes give the following:

$$u_{Wg} = \sum_i^n \frac{\Gamma_{o,i}}{2\pi}\frac{\tilde{H}_i}{r_i^2}\left(1 - e^{-(r_i^2/(4\nu t))}\right)$$

$$w_{Wg} = \sum_i^n \frac{\Gamma_{o,i}}{2\pi}\frac{\tilde{X}_i}{r_i^2}\left(1 - e^{-(r_i^2/(4\nu t))}\right) \qquad \text{(A5.2)} \qquad \text{(A5.2)}$$

mit $\tilde{H}_i = H - H_{io}$ and $\tilde{X}_i = x_g - X_{io}$, $r^2 = \tilde{X}_i^2 + \tilde{H}_i^2$

The principal method as well as definition of a few utilized values can be taken from Figure A5.1.

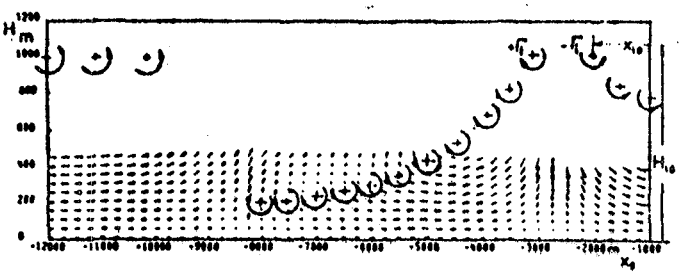

Figure A5.1: principal of superposition of vortexes for wind modeling

Example in Figure 3.36 and 5.14

Number of vortex pairs: 9

Wirbel-Nr.	x_{i0}, m	H_{i0}, m	Γ_{i0}, m^2/s
1	-8000	±1000	±18000
2	-7000	±1000	±18000
3	-6000	±1000	±18000
4	-5000	±1000	±18000
5	-4000	±1000	±18000
6	-3000	±1000	±18000
7	-2000	±1000	±30000
8	-1000	±1000	±45000
9	0	±1000	±45000

1-vortex number

nu - apparent kinematic viscosity: 15.0 m^2/s
t - vortex "age" : 900.0 y
m - boundary layer equation exponent: 0.21
H_{Ref} - reference altitude : 500.0m

Example in Figure 3.37

Number of vortex pairs: 24

	X_{io}, m	H_{io}, m	Γ_{io}, m^2/s
1. WIRBELP	-13000.0	±1200.0	∓18 0000
2. WIRBELP	-12000.0	±1200.0	∓18 0000
3. WIRBELP	-11000.0	±1200.0	∓18 0000
4. WIRBELP	-10000.0	±1200.0	∓18 0000
5. WIRBELP	-8000.0	± 200.0	±14 0000
6. WIRBELP	-7500.0	± 210.0	±14 0000
7. WIRBELP	-7000.0	± 230.0	±14 0000
8. WIRBELP	-6500.0	± 260.0	±14 0000
9. WIRBELP	-6000.0	± 300.0	±14 0000
10. WIRBELP	-5500.0	± 350.0	±16 0000
11. WIRBELP	-5000.0	± 440.0	±18 0000
12. WIRBELP	-4500.0	± 550.0	±18 0000
13. WIRBELP	-4000.0	± 670.0	±18 0000
14. WIRBELP	-3500.0	± 830.0	±18 0000
15. WIRBELP	-3000.0	±1000.0	±18 0000
16. WIRBELP	-3000.0	±1200.0	±18 0000
17. WIRBELP	-2000.0	±1200.0	∓10 0000
18. WIRBELP	-2000.0	±1000.0	∓10 0000
19. WIRBELP	-1500.0	±1000.0	∓10 0000
20. WIRBELP	-1000.0	±1000.0	∓10 0000
21. WIRBELP	-750.0	±1000.0	∓10 0000
22. WIRBELP	-500.0	±1000.0	∓10 0000
23. WIRBELP	-250.0	±1000.0	∓10 0000
24. WIRBELP	0.0	±1000.0	∓10 0000

1--vortex pair

ν	- apparent kinematic viscosity	15.0 m^2/sec
t	- vortex age	900.0 sec
m	- boundary layer equation exponent	0.21
H_{Ref}	- reference altitude	500m
u_{wo}	- superimposed translated speed	8.0 m/sec

A.5.4 Flow Relationships in Fronts

A.5.4.1 Flow Surface Branching Model

Modellparameter für Glg.(3.41)

(1) Beispiel	e, s^{-1}	f, s^{-1}	(2) Begrenzung u_{max}	(3) Grenzschicht m	H_R	(4) Querkompon. $v_{wq,R}$
(5) Bild 3.40	-0.01	0.05	15 m/s	0.08	1000 m	-5 m/s
Bild 3.41	-0.01	0.08	15 m/s	0.08	1000 m	-5 m/s

1-example, 2-limit, 3-boundary layer, 4-xverse component, 5-figure

A.5.4.2 Superposition of Viscous Vortex

Number of vortex pairs: 9

Example from Figure 3.41:

(1)	X_{io}, m	H_{io}, m	Γ_{io}, m^2/s
1. WIRBELP.	-8000.0	±1500.0	∓10.0000
2. WIRBELP.	-6500.0	±1500.0	∓10.0000
3. WIRBELP.	-5000.0	±1500.0	∓10.0000
4. WIRBELP.	-3500.0	±1500.0	∓10.0000
5. WIRBELP.	-1500.0	± 300.0	± 6.0000
6. WIRBELP.	-1000.0	± 300.0	± 6.0000
7. WIRBELP.	-500.0	± 300.0	± 6.0000
8. WIRBELP.	000.0	± 300.0	± 6.0000
9. WIRBELP.	500.0	± 300.0	± 6.0000

1-vortex pair

Example from Figure 5.21

(1)			
1. WIRBELP.	-8000.0	±1500.0	∓10.0000
2. WIRBELP.	-6500.0	±1500.0	∓10.0000
3. WIRBELP.	-5000.0	±1500.0	∓10.0000
4. WIRBELP.	-3500.0	±1500.0	∓10.0000
5. WIRBELP.	-1500.0	± 400.0	± 8.0000
6. WIRBELP.	-1000.0	± 400.0	± 8.0000
7. WIRBELP.	-500.0	± 400.0	± 8.0000
8. WIRBELP.	000.0	± 400.0	± 8.0000
9. WIRBELP.	500.0	± 400.0	± 8.0000

1-vortex pair (#)

τ	- apparent kinematic viscosity	15.0 m^2/sec
t	- vortex age	900 sec
m	- boundary layer equation exponent	0.21
H_{Ref}	- reference altitude	500m
u_{wo}	- superposed translated speed	4.0 m/sec

A.6 Measured Results from Thunderstorms and Secondary Squall Fronts

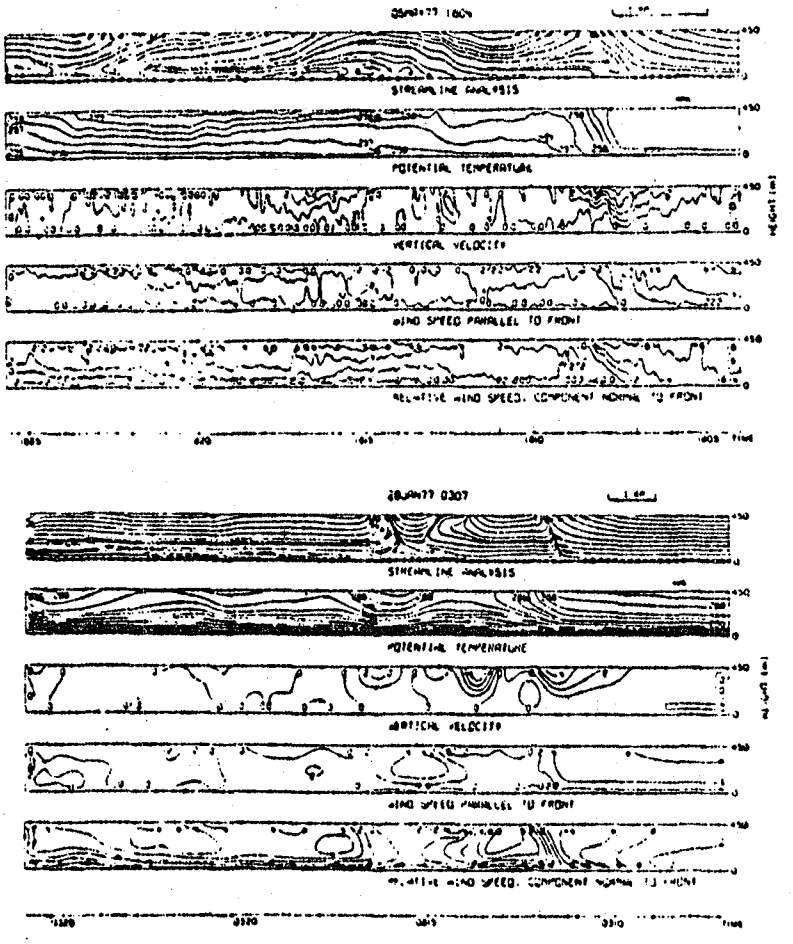

Figure A 6.1 and A 6.2: measured results from /42/

A.7 Derivation and Simplification of the Ideal Thrust Control Law

The starting point of the ideal thrust control law is formed by lift and resistance equations for aircraft longitudinal motion as they were described in Section 4.3.2 with Eqn. 4.5. Under the conditions occurring in landings at low angles the following simplifications can be made:

$$\cos\gamma \approx 1 \qquad \cos\alpha_g \approx 1 \qquad \cos(\alpha-\alpha_g) \approx 1$$
$$\sin\gamma \approx \gamma \qquad \sin\alpha_g \approx \alpha_g$$

Furthermore, thrust and resistance can be omitted in the lift equation because they are an order of magnitude smaller than lift. Thus Equation 4.5 can be expressed by the following approximation :

$$X_k: \quad \dot{V}_k/g = -\gamma + F/G - W/G + A/G\,\alpha_g$$
$$Z_k: \quad n\,G = A \qquad \text{(A7.1)}$$

For a safe landing it is necessary that flight speed and path angle are constant, that is τ and V are equal to zero.

Thus there results for the load factor:

$$n = \cos\gamma \approx 1 \quad \text{and thus} \quad A \approx G$$

Used in the resistance equation and solved using the ratio of thrust to weight one obtains:

$$F/G = \dot{V}_k/g + \gamma + C_w/C_A - \alpha_g \qquad \text{(A7.2)}$$

For thrust adjustment the necessary change in thrust is of interest compared to stationary landing thrust:

$$\Delta F/G = F/G - (F/G)_0 \qquad \text{(A7.3)}$$

1-stationary component $= \dot{V}_K/g + \gamma + C_W/C_A - \alpha_W - \underbrace{\gamma_0 + (C_W/C_A)_0 - \alpha_{W0}}_{\text{stationärer Anteil}}$ /

With the consideration of constant values for path angle and speed and thus also for the ratio of resistance to lift there results:

$$\Delta F/G = \dot{V}_K/g - (\alpha_W - \alpha_{W0}) \qquad \text{(A7.4)}$$

As the accompanying sketch shows, the magnitude of path speed can be expressed by flight speed and wind components. For small angles the following is valid:

$$V_K = V + u_{Wg} - u_{Wg}*(\gamma \quad .)$$

and thus for the per-unit-time derivation

$$\dot{V}_K = \dot{u}_{Wg} - \dot{u}_{Wg}.$$

Further, the angle of wind incidence can be expresses via the wind components (see sketch).

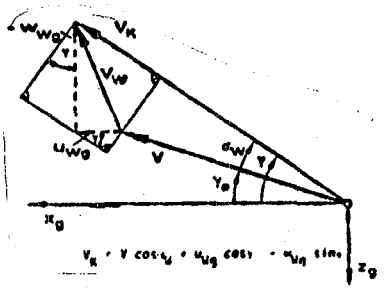

$$\alpha_W = -1/V\,(u_{Wg}\,\gamma + w_{Wg})$$

$$\Delta\alpha_W = -1/V\,(\Delta u_{Wg}\,\gamma + \Delta w_{Wg})$$

Used in Eqn. A7.4 one finally obtains for relative thrust change:

$$\Delta F/G = \dot{u}_{Wg}/g - \dot{w}_{Wg}\,\gamma/g + 1/V\,(\Delta u_{Wg}\,\gamma + \Delta w_{Wg}) \qquad \text{(A7.5)}$$

As research has shown the term ($\dot{u}_{Wg}$ γ /g) is permissibly small in comparison with the remaining components. It is thus not used in further computations.

A.8 Measurement Concept, Data Preparation and Error Balancing for Wind Determinations in Airline Aircraft Operation

A.8.1 Measurement Concept

A.8.1.1 Basis for Automatic Onboard Wind Determination

To determine the wind vector $\underline{V}_W$ along an aircraft's path the vectorial difference between path speed $\underline{V}_K$ and flight speed $\underline{V}$ is formed:

$$\underline{V}_W = \underline{V}_K - \underline{V} \qquad \text{(A8.1)}$$

For this, inertial data and air data for the aircraft must be known. Inertial data are obtained in modern aircraft with automatic onboard inertial platforms. These give among other things aircraft speed above the ground with the associated path azimuth or speed components in geodetic coordinates. On the other hand, air data describe speed, angle of incidence and displacement angles for flight speed vectors. From this, there arises the necessity of coordinate transformation for determining wind vector components in selected axis systems. Thus, the following values must be recorded:

Air Data	Inertial Data
angle of incidence - α	path azimuth - x
displacement angle - β	above ground speed V_{GS}
magnitude of flight speed V	vertical acceleration z_g
	barometric altitude H_{baro}
	course angle - ψ
	pitch angle - θ
	banking angle - ϕ

This list and axis system is the basis of definition for Aviation Norm (Luftfahrtnorm) LN 9300.

For a description of wind components in geodetic coordinates a simplified notation results from Eqn. A8.1:

$$\begin{aligned} u_{Wg} &= u_{Kg} - V \cdot \cos\nu_a \cos\chi_a \\ v_{Wg} &= v_{Kg} - V \cdot \cos\nu_a \cdot \sin\chi_a \\ w_{Wg} &= -\dot{H} + V \cdot \sin\nu_a \end{aligned} \qquad \text{(A8.2)}$$

For reasons of clarity the angles ν_s and χ_a are introduced here which are functions of position and flow angle. Details for this can be found in VORSMANN /49/.

If a sensor is not at the center of gravity of the aircraft, supplemental speeds are induced at the sensor site by yaw, pitch and rolling movement. To recompute wind components at the center gravity of the aircraft, correction factors are necessary /49/.

A.8.1.2 Construction of the Measurement Unit in the AIRBUS A300

In the Airbus A300 inertial navigation computer information about wind direction and speed are determined and displayed to the pilot on demand. However, the precision of this data is not sufficient for the task at hand. Thus, the above-mentioned raw data have to be recorded which can later be rerecorded for further processing at a computer center at the TU Braunschweig.

Problems occurred when recording inertial values of state because they were not detected like air data and angle of position by the automatic onboard data system (Aircraft Integrated Data System) in the Airbus A300.

Because these values exist as digital values (32 bit) at the output of the inertial platform (INS) they can be reprocessed with a supplemental interface. For reasons of safety the AIDS unit (consisting of FDAU and PMR segments) was practically doubled in size. Figure A8.1 shows the entire equipment package.

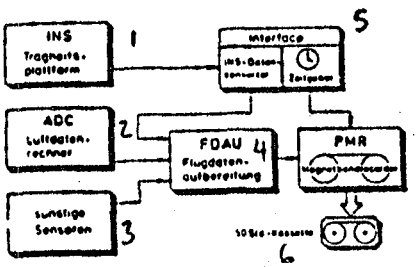

1-inertial platform
2-air data computer
3-other sensors
4-flight data preparation
5-data (illeg),time generator
6- hrs. cassette ?

Figure A8.1: construction of the Airbus A300 measurement unit

The measurement unit developed especially for the measurement project (Interface Data Converter) had the task of fitting inertial platform data structure to that in the FDAU (flight data preparation unit). It additionally contains a timer with logic circuitry for on and off switching of the recorder according to certain criteria. The circuitry was so designed that the PMR (tape recorder) was automatically in operation for:

- landing from the time the landing gear is extended (or below 300m altitude until the nose wheel touches the ground,
- takeoff after leaving the ground
- for an eventual hurried takeoff (waveoff)

} for 4 minutes after switch on

In this manner, it was managed to record only the data needed during takeoffs and landings and a series of progressive landings and takeoffs was available.

The named on/off criteria limit wind determination to the following regions:

Takeoff: from about 5m flight elevation to about 3000m over a stretch of about 10 NM (18.5km).

Landing: from a flight elevation of 300-500m to the ground. The distance flown through corresponds to the distance from the "outer markers" to the touchdown point (4 NM ~ 7.2km).

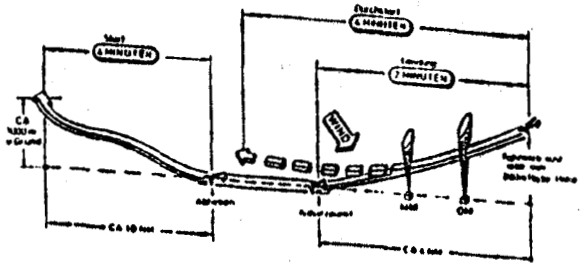

Figure A8.2: space and time boundary conditions for wind determinations (key illegible)

A.8.2 Data Preparation and Error Balancing

The measurement sensors in LUFTHANSA'S Airbus certainly meet specifications for the airline but there are no calibration curves for the sensor-aircraft measurement system available for use. Thus one asks the question whether sensor precision for a precise wind determination is sufficient.

Research showed the necessity for unexpectedly high amounts of data preparation and error balancing. The necessary steps which were attempted with the help of the Do 28 research craft are described as follows:

Elimination of disturbance signals:

Filtration: use of nonrecursive digital filters /87/ to eliminate weakly damped signal oscillation for vertical speed and flight speed signals (probably caused by filter oscillation in the Air Data Computer, Figure A8.3).

Outlier Elimination: use of a special program to eliminate data skips or outliers in the INS data for above-ground speed, path azimuth and azimuth (Figure A8.4)

Correction of Installation Errors, Signal Fallout and Systematic Errors

Because during selection of recorded data, redundant points are considered, a determination was possible in most cases for missing values or signals which had fallen out by coupling other suited parameters (for example, by using complementary or collector filters).

Barometric altitude and vertical speed: the occasional missing signal for barometric altitude must be determined via numeric integration of vertical speed. In proximity to the ground there is an adulteration of static pressure and its per-unit-time derivative due to ground effects and thus there is inaccuracy in barometric altitude H_b (Figure A8.5) and vertical aircraft speed $\dot{H}_b$.

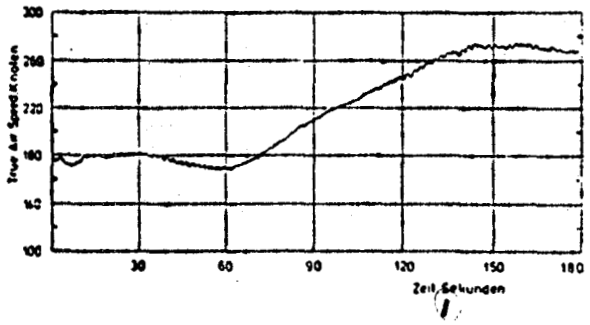

Figure A8.3: erroneous signal for flight speed, 1-time in sec

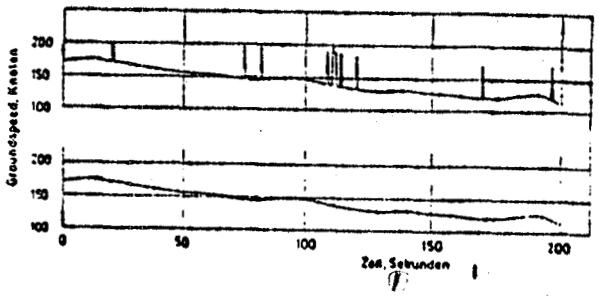

Figure A8.4: elimination of data "outliers", 1-time in sec

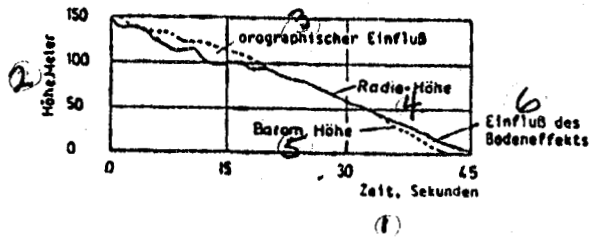

Figure A8.5: influence of ground effects on barometric altitude 1-time in sec, 2-altitude in m, 3-orographic influence, 4-radio altitude, 5-barometric altitude, 6-influence of ground effects

More precise altitude information can be attained by coupling the barometric altitude signal with the radio altitude. To increase vertical speed precision, complementary and collector filters were used in which information about the aircraft's altitude and vertical speed were coupled (Figure A8.6).

Determination of sideslip angle

The Airbus A300 used was not equipped with a sensor to detect sideslip. Later re-instrumentation did not give satisfactory results because significant adulteration of data occurred due to flow around the fuselage. A method was thus developed in which the sideslip angle was determined via coupling with suited measured values /89/. For certain flying conditions which are characterized by small aircraft rotation speeds and rudder deflection the sideslip angle β can be computed from transverse acceleration $\ddot{y}_f$, angle of incidence alpha and load factor n for known derivatives of $C_{Q,\beta}$ and $C_{A,\alpha}$:

$$\beta = n \frac{1}{C_{Q\beta}} \frac{\ddot{y}_f}{g} (C_{A_0} + C_{A\alpha}\alpha) \quad \text{(A8.3)}$$

The method was tried with the Do28 research aircraft and gave good results /89/.

Error models: to research the influence of static measurement errors on wind determination precision and error balancing, an error model was developed for three wind components /49/. The error equations for horizontal wind components show periodic dependence on the controlled course error.

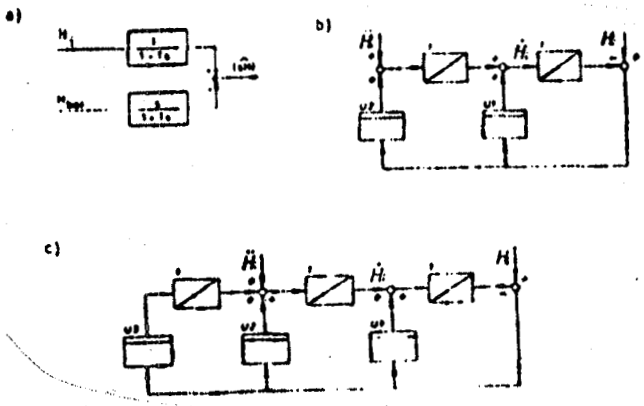

Figure A8.6a: principles of the different filters, a-complementary filter, b-collector filter, 2nd order, c-collector filter, 3rd order

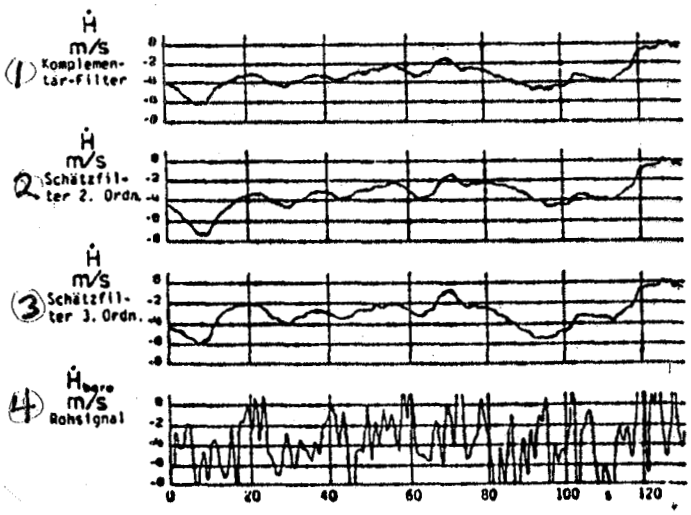

Figure A8.6b: output signals for different filters, 1-complementary filter, 2-collector filter, 2nd order, 3-collector filter, 3rd order, 4-raw signal

Precision of flight speed values has a tremendous influence. Above-ground speed, sideslip angle path azimuth and azimuth

Calculation error in vertical wind determinations is by contrast not dependent on course angle and is significantly influenced by measurement errors in vertical speed, angle of incidence and longitudinal position angle.

On the basis of production data and specifications for sensors, data detectors, etc, an estimation of errors in wind determinations was performed. From that, the horizontal wind component has an error of +/- 2.1 m/sec; the vertical wind component an error of +/- 1.1 m/sec (landing configuration). An improvement in precision is possible by using the error model /49/. One obtains the approximately corrected components from the following relationship:

$$\begin{aligned} u_{Wg,kor} &= u_{Wg} - C\cdot\sin\psi + D\cdot\cos\psi \\ v_{Wg,kor} &= v_{Wg} - D\cdot\sin\psi - C\cdot\cos\psi \end{aligned} \qquad \text{(A8.4)}$$

Coefficients C and D which are functions of sensor error and state of flight at the reference point as well as the corrected wind components $u_{Wg,cor}$ and $v_{Wg,cor}$ can be determined if at least two different courses psi_1 and psi_2 are measured. A requirement is the existence of a homogenous wind field and sufficiently small change in state of flight during the measurement. Figure A8.7 shows a result which was gotten during a trial of the method in the Do28 (Dornier) in stationary curved flight. Because in the Airbus trials in stationary landing flight only minimal changes in flight took place (ψ = const.), reference

measurements were necessary to solve Eqn. A8.4). These can be taken from Meteorological Air Reports METAR (for H=10m) in most cases. They are offered by the Deutschen Wetterdienst (German /A28 Weather Service) in Offenbach.

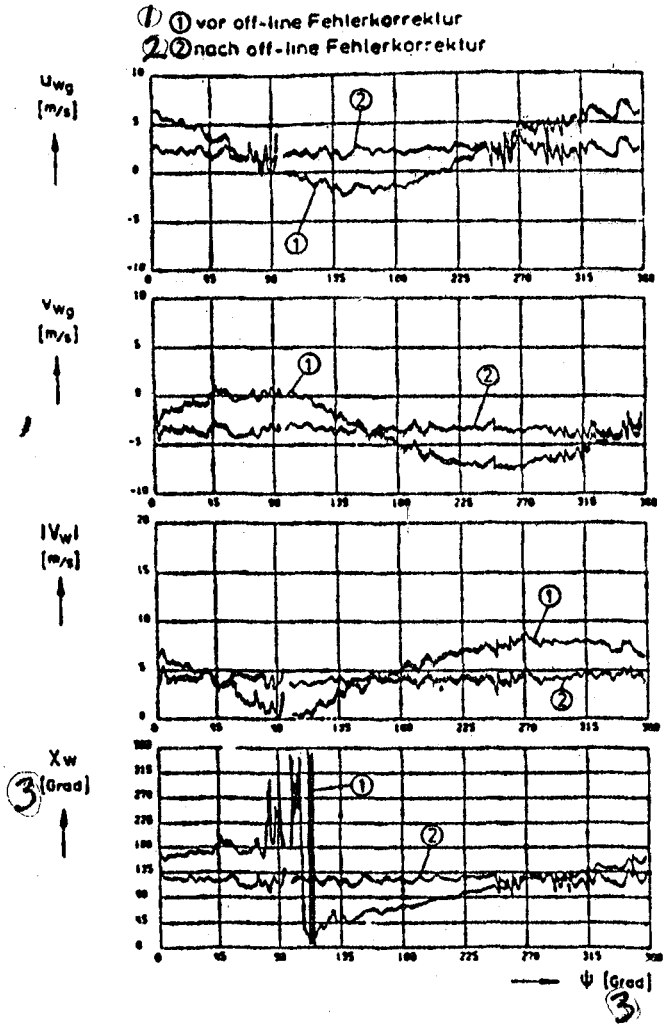

Figure A8.7: wind determination in curved flight before and after error correction /90/, 1-before off-line error correction, 2-after off-line error correction, 3-degrees

LANGLEY RESEARCH CENTER
3 1176 01327 0914